COMPARISON OF THEORY AND EXPERIMENT FOR FLEXURAL - TORSIONAL BUCKLING OF LAMINATED COMPOSITE COLUMNS.

by

Patrick Kar-Leung Lo

Thesis submitted to the Faculty of the

Virginia Polytechnic Institute and State University

in partial fulfillment of the requirements for the degree of

Master of Science

in

Aerospace and Ocean Engineering

APPROVED:

Dr. Eric R. Johnson, Chairman

Dr. Raphael T. Haftka

Dr. Robert M. Jones

December 1985

Blacksburg, Virginia

COMPARISON OF THEORY AND EXPERIMENT FOR FLEXURAL - TORSIONAL BUCKLING OF LAMINATED COMPOSITE COLUMNS.

by

Patrick Kar-Leung Lo

Dr. Eric R. Johnson, Chairman

Aerospace and Ocean Engineering

(ABSTRACT)

Vlasov's one-dimensional structural theory for thin-walled open section bars was originally developed and used for metallic elements. The theory was recently extended to laminated bars fabricated from advanced composite materials. The purpose of this research is to provide a study and assessment of the extended theory. The focus is on flexural and torsional-flexural buckling of thin-walled, open section, laminated composite columns. Buckling loads are computed from the theory using a linear bifurcation analysis, and are compared to available experimental data. Also, a geometrically nonlinear beam column analysis by the finite element method is developed from the theory. Results from the nonlinear compression response analysis are compared to limited available test data. The merits of the theory and its implementation are discussed.

ACKNOWLEDGEMENTS

This thesis is dedicated to my parents, for their unbounded support. Many thanks are due to Dr. Haftka and Dr. Jones. Most of all, I would like to express my graditude towards my advisor, Dr. Johnson. Without his patience and his guidance, this research would not have been possible.

I would also like to mention a few people whose dedication and enthusiasm in search for knowledge have inspired me

TABLE OF CONTENTS

LIST OF ILLUSTRATIONS

LIST OF TABLES

Nomenclature

(x,y,z)	Cartesian coordinate system
(n,s,z)	Curvilinear coordinate system
(s)	Contour coordinate, along the contour
(X,Y,Z)	Principal Cartesian coordinate system
(n*,s*,z*)	Convected curvilinear coordinate system
W (z)	Bar axial displacement of the centroid
U (z), V (z)	Bar lateral displacements of the pole
ϕ (z)	Bar rotation about the pole
r (s)	Distance between a generic point and the pole along the normal direction
q (s)	Distance between a generic point and the pole along the tangential direction
θ (s)	Angle between the Cartesian x-axis and the tangent at a generic point
$\bar{\omega}$ (s)	Sectorial area
P	Pole
C	Centroid
A	Generic point in the cross-section on the contour
(x_p, y_p)	coordinates of the pole P

$\bar{\varepsilon}_z$, $\bar{\gamma}_{zs}$	Shell strains at middle surface
$\bar{\kappa}_z$, $\bar{\kappa}_{zs}$	Shell curvatures at middle surface
p_n, p_s, p_z	Distributed shell loads
T_x, T_y, T_z	Line shell loads
m_x, m_y, m_ω	Equivalent bar loads
N	Axial compressive force through the centroid
M_x, M_y	Bending moment about the x-axis, y-axis
T,	Twisting moment about the z-axis
T_s, T_ω, M_ω	Saint Venant twisting moment, warping torque, warping moment
V_x, V_y	Transverse shear force in the x-direction, y-direction
S_x, S_y, S_ω	Moduli-weighted first moments of area
I_{xy}, I_{xx}, I_{yy}	Moduli-weighted second moments of area
$I_{\omega x}$, $I_{\omega y}$	Moduli-weighted cross moment of sectorial area
$I_{\omega\omega}$	Moduli-weighted second moment of sectorial area
H_s, H_c, H_q	Material coupling due to bending and twisting
JG	Moduli-weighted torsional stiffness
R_p	Radius of gyration of the cross-section about the polar axis represents coupling between bar resultants
K_x, K_y	Radius of curvature about the x-axis, y-axis; represents coupling between bar resultants
K_ω	A dimensionless parameter, represents coupling between the bar resultants

1.0 INTRODUCTION AND HISTORICAL REVIEW

1.1 MOTIVATION

In space and flight vehicles, composite materials are used extensively because of high strength and stiffness to weight ratio. These composite structures are very effective in weight-saving; the most commonly used structural elements are bars, panels, and cylindrical shells. It has been recorded in the literature [1] that the one-dimensional bars are the most under-investigated, and under-developed area in the field of composite structures. By comparison, research work on composite plates, panels and shells is extensive. Such apparent inbalance is related to the concept that laminated composites are basically multi-dimensional, and their properties can only be utilized in multi-dimensional structures. For example, composite I-sections are often analyzed as assemblages of laminated plates. This is particularly true in local effect problems, such as local buckling.

As demand for thin-walled structures has increased, demand on analysis has grown as well. Analytical solutions by elasticity are by no means accessible. Mathematically two-dimensional theories offer less accurate but workable solutions for plates and shells. For built-up structures, however, applications of two-dimensional theories are complex, thus high in computational cost. They can be justified in detailed investigations for critical design. One-dimensional analysis, on the

other hand, offers a cruder but simpler mathematical model and analysis when it is possible. Potentially, it is beneficial for preliminary design.

Vlasov's theory, developed in the middle of the century by the late V. Z. Vlasov [2, 3, 4], is a modified bar theory for thin-walled open sections. An extended Vlasov's theory has been developed for thin-walled laminated composite open-section bars, by Bauld and Tzeng [5]. The purpose of this research is to implement this one-dimensional theory for global buckling problems. The general buckling equations, derived from the extended theory, are presented but not solved in the original paper. Finite element models are developed to solve the buckling equations. Results of the analysis are compared with available experimental data. Merits of the extended theory and the analytical model are then assessed.

Global buckling is taken to be elastic. Loading on the structure is restricted to a compressive end load, passing through the centroid. The composite bars under investigation are assumed to have stresses lower than the failure stress of the material system. The overall material behavior of the beam column is therefore linear elastic. In the topics on buckling, the bar will be referred to as a beam column where appropriate.

Later in this chapter, the historical review will be presented. The first part will be on the isotropic bar theories. Materials are selected in relevance to recognition of the problem of flexural torsional coupled instability and investigations on this problem. Emphasis will be on the development of relevant structural theories, specifically Vlasov's theory. The second part of the historical review is on laminated composite bar theory, the extended Vlasov's theory. The composite structural theories on plates and shells will be mentioned for completeness. The overview

of these composite structural theories is a topic in its own right, and will not be attempted here.

In Chapter 2, Vlasov's theory and the extended theory will be formally presented. Chapter 3 will contain linear bifurcation analysis, and Chapter 4 nonlinear analysis. In Chapter 5, available experimental data will be compared to the nonlinear anaylsis results, which will be followed by a discussion section. Chapter 6 will be made up of conclusions and recommendations for further research.

1.2 HISTORICAL REVIEW

Thin-walled open section bars have been historically developed as weight-saving structural members. They are used to provide additional flexural rigidity to the structural assembly. The geometric characteristic of these bars is that the cross-sectional dimension is much smaller than the longitudinal dimension, and the thickness is in turn small compared to the cross-sectional dimension of the bar. Beams, columns, and beam columns are bars subjected to flexural loading, compressive loading, and a combination of flexural and compressive loading, respectively. When a thin-walled structure is compared to a solid structure with both structures having the same flexural rigidities, the thin-walled structure employs much less material per unit length. Thus, thin-walled structures are cost effective. The open section configurations, however, have small torsional stiffnesses.

As the aerospace industry expanded early in this century, thin-walled open-section bars have played a great part. Very early in airplane

design, thin-walled bars have been used to strengthen and stiffen skin panels. In additional to the weight saving and cost saving factors, the open section allows easy access for inspection. The most widely used thin-walled open sections are prismatic because of ease of manufacturing.

Anisotropic materials, specifically fiber-reinforced plastics, were being used in structural applications around the middle of the century. The mechanics of these composite structures are much more complicated than their metallic counterparts. While techniques for the analysis of metallic thin-walled open section bars were relatively well developed by then, there were no specialized theories to include the complex nature of the material properties of composite bars until much later.

1.2.1 ISOTROPIC THIN-WALLED BAR THEORY

The one-dimensional bar theory was developed along two separate paths, flexure and torsion. The engineering theory of flexure of beams was developed in the middle to late eighteenth century by D. Bernoulli, L. Euler, and C. A. Coulomb [6]. The essence of the theory is the approximation that cross sections remain plane in bending and the Bernoulli-Eulerian approximation of proportionality of the curvature to the bending moment. That is, the resistance to flexure is entirely due to the extension and contraction of the longitudinal filaments.

Using the general equations of elasticity developed in the 1820's by Navier, Cauchy, Poisson, etc., Saint-Venant (1855-6) presented solutions to torsion and flexure of beams. He solved the pure torsion problem by the semi-inverse method. In Saint-Venant's torsion solution the state

of strain consists of a simple twist about the axis of the rod combined with an axial displacement that varies over the cross section but is uniform along the axis. The variable axial displacement causes the section to warp.

Saint-Venant torsion and Euler-Bernoulli beam theory are inadequate when there is flexural deformation as well as torsional deformation. As the coupled deformations were studied at the turn of the century, the need for special bar theories became apparent. Potentially, the state of pure flexural buckling and pure torsional buckling should be recovered as special cases. Related research works were primarily conducted in the area of lateral stability, which differs from flexural torsional stability by the way of loading. While lateral instability is caused by end moments, flexural torsional instability is caused by a compressive axial force.

In general beam theory, the flexural rigidity of a beam cross section depends on the engineering properties of the material as well as the geometry of the section. The second moments of area, the geometric factors, are evaluated for principal axes through a characteristic point, the centroid, of the section. Special bar theories require higher moments of the area and identify more characteristic points in the cross section. The characteristic points are the centroid, the shear center (referred to as the pole by Vlasov), and the torsion center. The definitions of these characteristic points will be given in the following text. Realization of these characteristic points are of prime importance in the development. In the following historical review, attempts are made to

point out the major research that is relevant to Vlasov's bar theory for thin-walled open sections.

Instability of bars of thin-walled open sections was first recognized by Michell [7] and Prandtl [8] in 1899, who independently solved for the lateral stability of rectangular section. The warping effects were not considered in either of their solutions. In 1906, Timoshenko [9] experimentally studied I-beam sections subject to torsion in which axial normal stresses arise as well as shear stresses due to axial constraint at the fixed end. A third-order differential equation for the angle of twist was derived. The formulation was the first of its kind to include the out-of-plane deformation of the section in the context of lateral buckling.

The work of Timoshenko did not conclude the research in this area, because the solution was not for general cross sections. The second stage of the related research was highlighted by the effort to define the characteristic points in general cross sections. Efforts were made to isolate flexural response from torsional response. In 1909, Bach [10] carried out a series of experiments on channel sections. The compressive axial load which passed through the centroid caused torsional deformation in addition to bending. Consequently, it was proposed that such a phenomenon was associated with the asymmetric nature of the section. Twelve years later, Eggensschwyler [11] and Maillart [12], in 1921, pointed out that the centroid was not the only characteristic point of the section. The shear center was defined, a point through which the load passes to cause flexure but no torsional deformation, and methods were derived to determine such point in a cross section. This definition was by no means

generally accepted until much later. In 1926, Weber [13] developed an energy method to find the location of the shear center. A method of determining the normal stresses arising from torsion was presented for various simple sections. He further proved that the shear center and the torsion center coincide in cases where lateral displacements were accompanied by twisting deformation. The torsion center was defined as the point about which the whole cross section rotated. It was not until 1933 when Duncan [14] derived an exact formula for the coordinates of the shear center for very thin-walled cross sections. In 1927, Bernshtein [15] studied the out-of-plane deformation in cross sections of open bridge trusses, and called such phenomenon "deplanation". This term remains the standard Russian term for warping.

The first studies of torsional buckling are due to Wagner [16] in 1929. They were followed by a series of research efforts to study and quantify the torsional behavior. Equations were derived to determine the critical forces for torsional instability of bars. In the same text, the idea of the law of sectorial area was introduced. Wagner assumed that at instability, the shear center coincides with the torsion center. Ostenfeld [17] in 1931 noted that the assumption pursued by Wagner is true only for bars with double symmetry. In 1936, Bleichs [18] used the energy method to derive a set of differential equations for instability. In the same year, Vlasov [2] presented a similar law of sectorial area. In the following year, Kappus [19] proposed additional equilibrium conditions to amplify Wagner's analysis. Meanwhile, Lundquist and Fligg [20] determined the position of the center for rotation for the critical load. The theories developed up to that period were criticized by Vlasov [4, p. 466]:

> ...(the theories so developed for thin-walled sections) started from the law of plane sections and replaced the normal stresses in the cross section by their resultant, taken as a concentrated force applied at the centroid. As a result of this substitution the last term in one of the equations, the equilibrium of the beam under rotation about the longitudinal axis does not contain the longitudinal force. This led to the loss of one of the three roots of the corresponding solving equation and gave for the two other incorrect results.....

Vlasov went on to publish his collection of work which, according to the following statement by Nowinski [21], has had profound influence:

> In 1940, Vlasov published his book containing a comprehensive study of the equilibrium, stability, and vibration of open sections, and which, basically, determined the development of the Russian school on the subject.....

Vlasov's equations were derived by variational principles by Dzanelidze [22] three years later. In 1945, Timoshenko [23] unified the engineering theories of bending, torsion, and stability of open bars prior to that year.

Vlasov was credited for the first complete solution for thin-walled bars with arbitrary open section [24, p. v; 25, p. 26]. The fundamental differential equations and the derivations are also associated with Bleich [18], Chwalla [27], Goodier [28,29], Kappus [19], Kindem [30], Timoshenko [23, 31], Umanski [32, 33] and others. The development of special bar theories for thin-walled sections did not end with Vlasov's theory by any means, but for the relevance in this review it is not necessary to cover these readers are referred to various research papers on the history of this subject [21, 34, 35].

1.2.2 LAMINATED COMPOSITE BAR THEORY

The development of a special theory for thin-walled laminated composite bars is not so clear-cut as its isotropic counterpart. The research is compounded by lack of understanding of the nature of advanced fiber-reinforced composites. The stress-strain constitutive equation for laminated composites are considerably more complex than Hooke's Law. A bending moment applied to a bar does not necessarily lead to pure flexure. Likewise, a compressive end load may give rise to bending and twisting in addition to compression. The studies of micromechanics, in which the material system is treated as anisotropic and non-homogeneous, relates the engineering properties of the components in the system to the averaged properties of the system. The geometry of the unit cell is a dominant factor. In macromechnics, the material system is considered to be anisotropic but homogeneous. The derivation of the stress-strain constitutive equations is often dependent on the type of structural theories used. Plate and shell analyses are most frequently employed [36].

Flat laminates were initially examined because of their geometric simplicity. A basic set of constitutive relations so developed, known as classical lamination theory [37, 38], allows some insight into the effects of anisotropy on the stress-strain constitutive equations. Classical lamination theory serves not only as a structural theory for a special case of flat laminates, it is often used as the basis for more complicated plate analyses. There are three assumptions in classical lamination theory, and they are listed here for completeness. The laminate is assumed to be thin and consist of perfectly bonded laminae; the bonds

are assumed to be infinitesimally thin and shear rigid; and it is assumed that normals to the middle surface remain normal to the deformed middle surface (Kirchhoff assumption). Also, the through-thickness strain is assumed to be zero. For more general analyses of laminated plates, readers are referred to Ambartsumyan [39], Ashton and Whitney [40], and Lekhnitskii [41].

The first analyses of laminated shells are credited to Dong and et al [42], Reissner and Stavsky [38], and Ambartsumyan [43]. These composite shell theories contain coupling terms that are complex. Kinematic coupling due to the general curved geometry is well studied in the general shell theory for isotropic material systems. Different approximations to the kinematic coupling terms lead to a variety of shell theories. Such shell theories are often extended to include material coupling of laminated composites. The latter adds onto the already complicated analyses. Bert and Francis [1] present a very detailed historical review on composite structural theories.

In general, materials with multi-dimensional properties are best utilized in multi-dimensional structures. The development of composite bar theories has been hindered by common interpretation of the above concept. In the paper by Bauld and Tzeng [5], the extended Vlasov's theory is presented. The extended theory embeds the classical lamination theory in the analysis, hence it includes the two-dimensional properties of laminated composite to some extent.

2.0 EXTENDED VLASOV'S THEORY

2.1 INTRODUCTION

Vlasov's theory encompasses a great amount of detail, and the overall view of the theory is complex [24, p. v]. Historically, the theory was developed for the purpose of solving buckling problems. There are linear formulations for stress, deflection analysis, and a nonlinear formulation for bifurcation point and limit point buckling analyses. In terms of applications, Vlasov's theory has been adopted for elastic bars, plastic bars, open cross section bars, and closed cross section bars.

The extended Vlasov's theory by Bauld and Tzeng [5] deals with open cross section laminated composite bars. As in the isotropic Vlasov's theory, there are linear and nonlinear formulations.

In this chapter, the essential features of the extended Vlasov's theory are presented. The emphasis, as stated in the previous chapter, is on elastic buckling of prismatic open section laminated composite bars. The contrast between Vlasov's and the extended theory will be addressed in context. As an intermediate step to solve the buckling problem, cross-sectional properties have to be known. Computer codes developed to compute these quantities will be presented later in this chapter.

The main difference between Vlasov's theory and the general Euler-Bernoulli beam theory is that the former employs more general kinematic assumptions, which are summed up in the law of sectorial area. Vlasov's theory accounts for contribution of warping to stresses as well as out-

of-plane displacement.[1] These assumptions will be discussed in the following text. Vlasov [2] showed that pure bending and pure torsion of thin-walled bars are special cases of the more general theory, and the assumption the plane sections remain plane is a special case of the law of sectorial area [4, pp. 21-26].

2.2 LINEAR THEORY

A prismatic bar with a thin-walled cross section is considered a cylindrical shell whose generator is parallel to the longitudinal axis of the bar. The z-axis is taken to be parallel to the longitudinal axis of the bar. The intersection of the shell middle surface and the z=constant cross-sectional plane defines the contour of the cross section. The contour is a curve in the cross section of the bar which may or may not be smooth. There can be sharp corners and junctions along the contour. A section of the contour that lies between two junctions or between a junction and an end (a free edge) is called a branch. Thus, a branch is a segment of the contour in which the contour is a smooth curve. The cylindrical shell segment defined by the branch and the length of the bar is called an element of the bar. The thickness of the bar can be different for each element, and it can indeed be a function of the contour within a branch. When the cross section is divided into branches, the

---

[1] "...a thin-walled beam with an open section is closely allied to the warping of its sections. For these thin-walled beams cannot be studied by the methods of the elementary bending theory of beams, since these methods are based on the hypothesis of plane sections,.....",Vlasov [4, p. 466].

discretization is based on the contour lines. If the thicknesses of these branches are included, there will be areas of overlapping at the merging junctions. This geometric inaccuracy is small and can be disregarded [24, p. 5].

In Figure 1 on page 14 a thin-walled open section prismatic bar is shown. The bar is represented by traces of the middle surface, and the thickness of the bar is not shown explicitly. The contour at a constant value of z is marked, and the curvilinear coordinate system at a generic point on the contour is shown.

The essence of the linear theory is to relate bar forces to bar displacements through the governing constitutive equations. The theory treats a thin-walled open section bar at two levels: a two-dimensional cylindrical shell theory for the individual elements, and a one-dimensional bar theory for the collection of elements. In the extended theory [5], elements are modelled as plates. In the following text, elements will be referred to as shells or plates where appropriate. The duality allows a simple analysis of arbitrary prismatic open-sections in one dimension and, at the same time, retains the capability of detailed stress analysis. The schematic description of the analysis can be found in Figure 2 on page 15. The governing constitutive equations that relate bar forces and bar displacements can be regarded as the theme of Vlasov's theory. They are obtained through a series of steps: namely, kinematic considerations, shell resultant - bar displacement equations, and equivalent bar forces. The presentation of Vlasov's theory in this chapter will follow the above sequence.

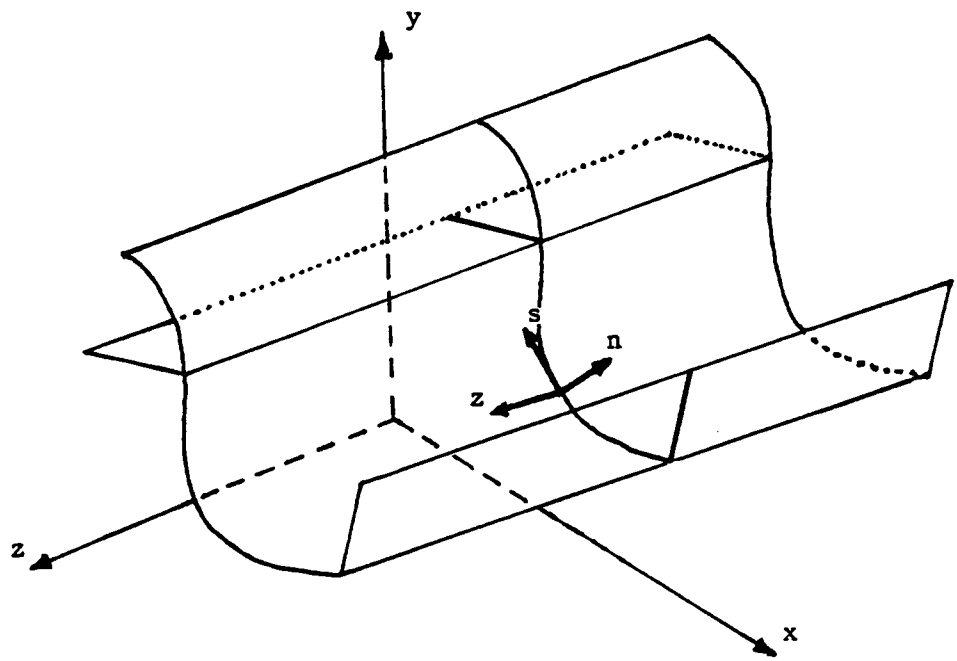

Figure 1. General form of a thin-walled open section prismatic bar

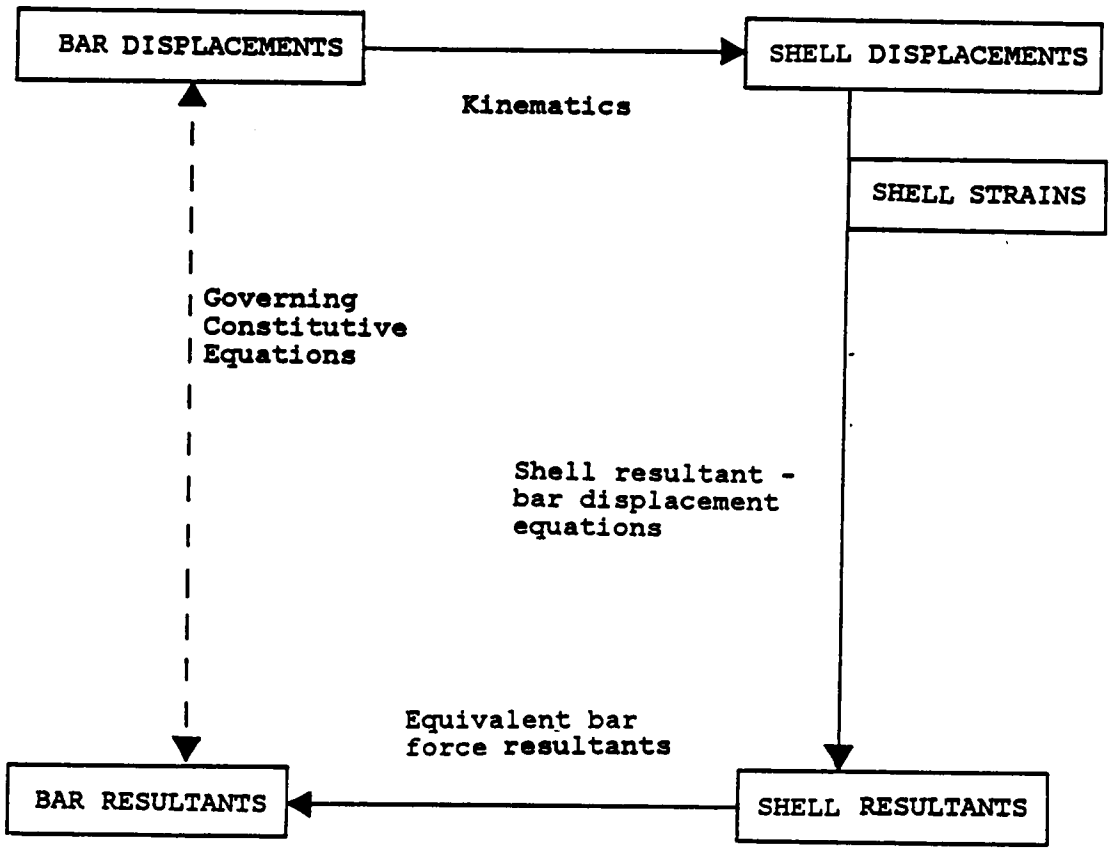

Figure 2. Schematic description of the extended Vlasov's theory

The stress-strain relationship for composite material element can be very involved if curvature effects are included. In the extended theory, elements of the cross section are modelled as plates so that classical lamination theory can be used. In the following presentation, the treatment of thin shell elements is adopted. Curvature effects in the kinematics and other areas are fully accounted for, except in the shell constitutive relationships. The curvature effects are assumed to have negligible influence on the latter so that classical lamination theory can be used.

In general, the governing constitutive equations are rather cumbersome to be used directly. The principal form, the simplest form of the governing constitutive equations, is associated with two principal coordinate systems and three characteristic points in the cross section. The principal coordinate systems consist of a principal Cartesian and a principal contour coordinate system. The three characteristic points are the centroid, the principal pole, and the principal contour origin. They will be discussed at the end of the chapter.

2.2.1 KINEMATICS

A cross section is shown in Figure 3 on page 17. The profile of the section is shown as contour C in the figure. The general outline denotes the plane in which the contour lies. The contour coordinate system is defined within a typical cross section by s, the arc length along the contour, the pole P, and coordinates r(s) and q(s) of a generic point A at s on the contour C. The origin of s (s=0) is called the contour origin

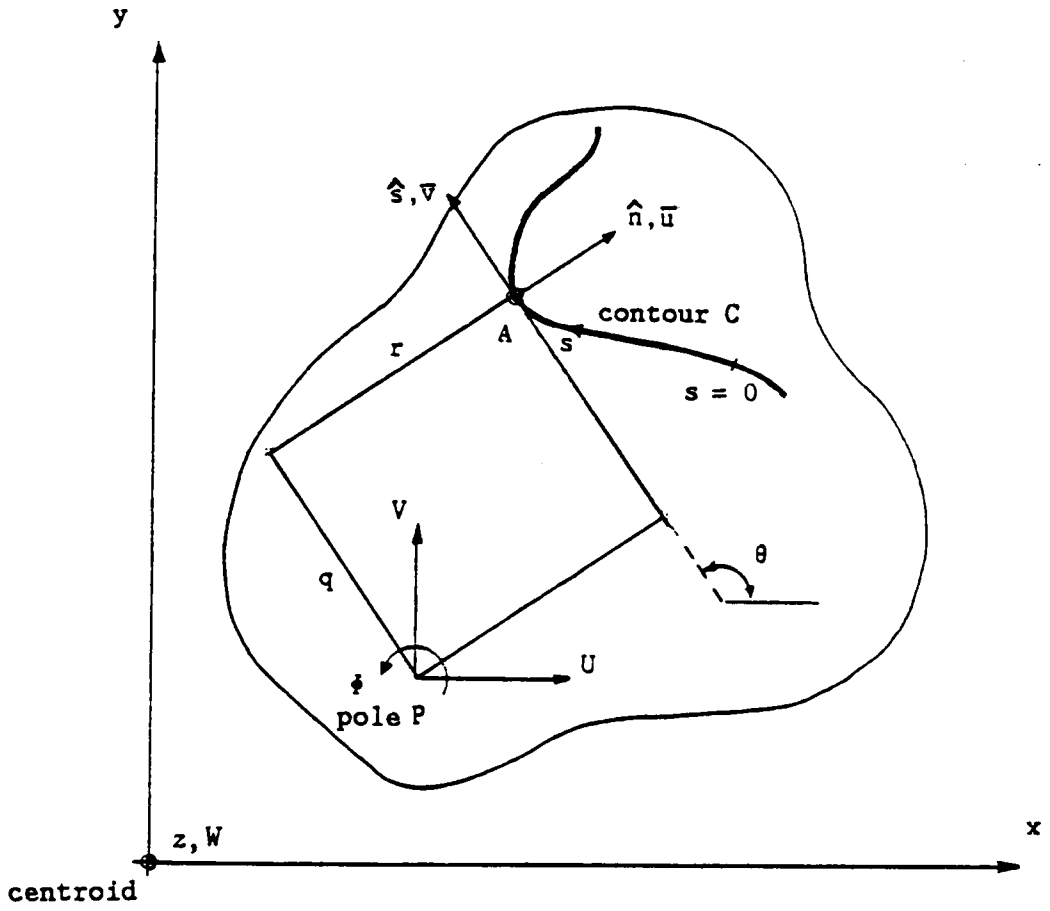

Figure 3. Coordinate systems in a cross section

and the positive sense for s along the contour can be arbitrarily selected. The position of the point (x_p, y_p) for the pole may also be arbitrarily selected. Let $\hat{s}$ denote a unit vector tangent to the contour at A with a positive sense in the direction of increasing s. Let $\hat{n}$ be a unit normal vector to C at A such that $(\hat{n},\hat{s},z)$ constitutes a right-handed orthogonal system. The angle between the positive x-direction and s is denoted by θ. The position of point A on the contour is given by $\bar{x}(s)$ and $\bar{y}(s)$ in Cartesian coordinates. In the contour coordinates, position of point A on the contour relative to the pole is given by r(s) along the $\hat{n}$-direction and by q(s) along the $\hat{s}$-direction. It is shown by Gjelsvik [24, pp. 8-9] that the contour coordinates satisfy the following kinematic relations:

$$q \frac{d\theta}{ds} = \frac{dr}{ds} \tag{2.1}$$

$$r \frac{d\theta}{ds} + \frac{dq}{ds} = 1 \tag{2.2}$$

$$a \frac{d\theta}{ds} = 1 \tag{2.3}$$

$$\frac{d\bar{x}}{ds} = \cos\theta \tag{2.4}$$

$$\frac{d\bar{y}}{ds} = \sin\theta \tag{2.5}$$

in which "a" denotes the radius of curvature of the contour at A.

Bar displacements are designated by U(z), V(z), and W(z) in the x-, y-, and z-direction, respectively. Displacements U and V refer to lateral displacements of the pole and W is the longitudinal displacement of the centroid. Rotation of the bar about the z-axis through the pole is denoted by $\phi(z)$, where ϕ is positive counterclockwise when viewed down the positive z-axis. These bar displacements are shown in Figure 3 on page 17. Shell displacements of the middle surface in the $\hat{n}$-, $\hat{s}$-, and z-directions

are denoted by $\bar{u}(s,z)$, $\bar{v}(s,z)$, and $\bar{w}(s,z)$, respectively. In general, shell variables with an overbar designate middle surface quantities.

There are three characteristic points in the cross section associated with principal coordinate systems. The first point is the centroid which is taken as the origin of the Cartesian coordinate system. The second point is the principal pole, or shear center. The third point is the principal contour origin. These three points, along with the principal directions for the x- and y-axes, result in the simplest form for the governing constitutive equations for the bar. More detail on principal coordinates will be presented later in this chapter.

Four basic kinematic assumptions are cited in the original paper by Vlasov [2]:

- The thin-walled bar of open section can be considered as a shell of rigid section. The contour is allowed to deform out of the plane, but the projection of the contour onto the plane remains the same during deformation.

- The shear strain, $\bar{\gamma}_{sz}$, of the middle surface is zero in each element.

- Each element behaves as a thin plate following Kirchhoff's assumption of straight lines normal to the middle surface remaining normal during deformation.

- The normal stress σ_{ss} is assumed small compared to the axial stress σ_{zz}.

The first assumption is complementary to the plane sections remain plane assumption in Euler-Bernoulli beam theory, but a relaxation of the latter. This assumption allows the out-of-plane deformation to be taken into account. The second assumption is known as the Vlasov assumption, and is the cornerstone for this formulation. The concept of sectorial area, the warping function, which is associated with the out-of-plane deformation, is derived from this assumption. Kirchhoff's assumption from the plate and shell theory is invoked, so that the through-thickness strain, ε_n, vanishes. At the same time, the through-thickness normal stress σ_{nn} is considered small compared to the axial normal stress, σ_{zz}. Although the two conditions are contradictory, they are generally accepted. The last of the four assumptions is similar to beam theory where all transverse stresses are assumed negligible with respect to the axial normal stress. Again, assuming σ_{ss} and ε_s both vanish is contradictory in Hooke's Law.

Consider a rigid body displacement of a generic cross section of the bar given by the components U(z) and V(z) of the pole plus a rotation $\Phi(z)$ about the pole axis. For a small rotation angle Φ, the middle surface shell displacements $\bar{u}(s,z)$ and $\bar{v}(s,z)$ are related to the bar displacements and rotation by (see Figure 3 on page 17),

$$\bar{u}\ (z,s) = U \sin\theta - V \cos\theta - \Phi\ q \tag{2.6}$$

$$\bar{v}\ (z,s) = U \cos\theta + V \sin\theta + \Phi\ r \tag{2.7}$$

Under the Vlasov assumption, the shear strain at middle surface is zero,

$$\bar{\gamma}_{zs} = \frac{\partial \bar{v}}{\partial z} + \frac{\partial \bar{w}}{\partial s} = 0 \tag{2.8}$$

The displacement $\bar{v}$ in Equation (2.7) is substituted in the Vlasov's assumption (Equation 2.8), and the latter is integrated with respect to s using Equations (2.4) and (2.5) to get

$$\bar{w}\ (z,s) = W(z) - U'(z)\ \bar{x} - V'(z)\ \bar{y} - \Phi'(z)\ \bar{\omega} \qquad (2.9)$$

where the prime means differentiation with respect to z and

$$\bar{\omega} = \int_C r(s)\ ds \qquad (2.10)$$

The last term on the right-hand side of the equation for $\bar{w}$ is the out-of-plane warping contribution to the axial displacement. The quantity $\bar{\omega}$ is called the sectorial area because it can be interpreted as twice the area swept by a vector with one end fixed at the pole and whose opposite end moves along the contour. In Figure 4 on page 22 a vector $\overrightarrow{PA}$ is shown to move a distance ds along the contour C. The contribution to the sectorial area by the small contour segment ds is equal to twice the area, dA, swept out by $\overrightarrow{PA}$. For a complicated section with multiple branches, the sectorial area is continuous at a junction, but may not be continuous as a function of the global monotonic increasing contour coordinate (s). An example section is shown in Figure 5 on page 23. In the upper diagram, the sectorial area at the generic point A is plotted along the contour. In the lower diagram, the sectorial area is plotted as a function of the global monotonic increasing contour coordinate (s). The number shown next to each branch is used to indicate the order in which s covers the contour. The quantity $\bar{\omega}$ is also called the contour warping function, since the product of $\bar{\omega}$ and the twist per unit length Φ' determines the out-of-plane component of the axial displacement.

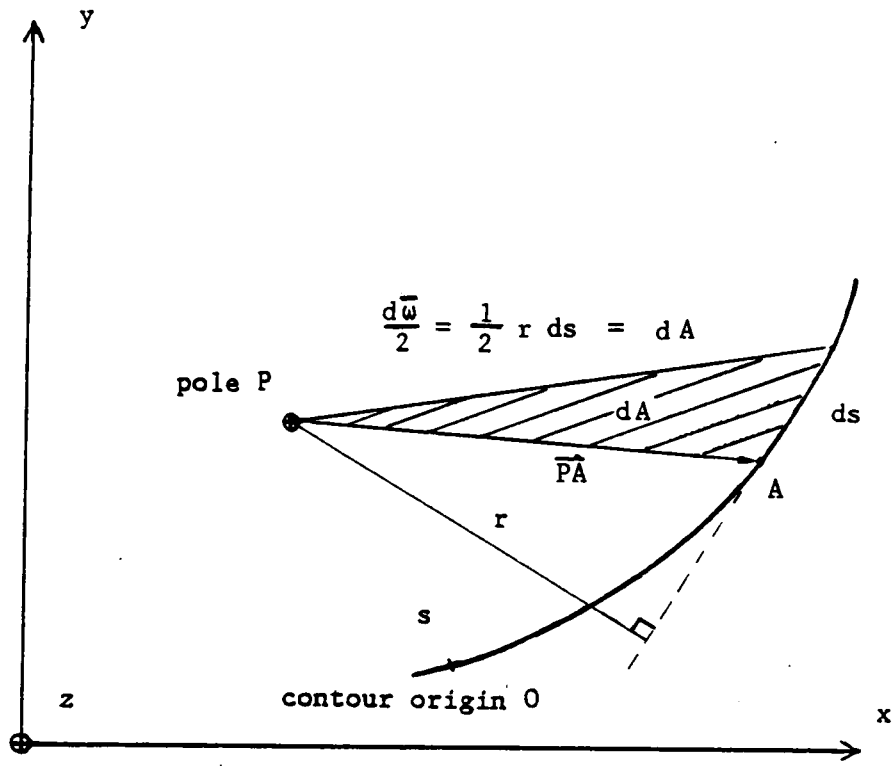

Figure 4. Graphical representation of sectorial area

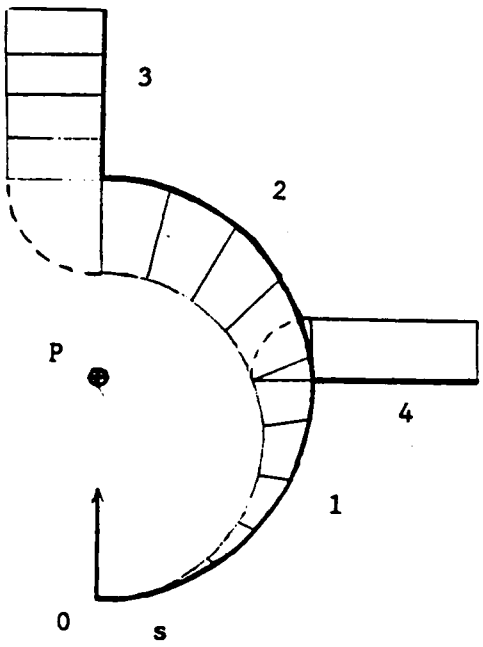

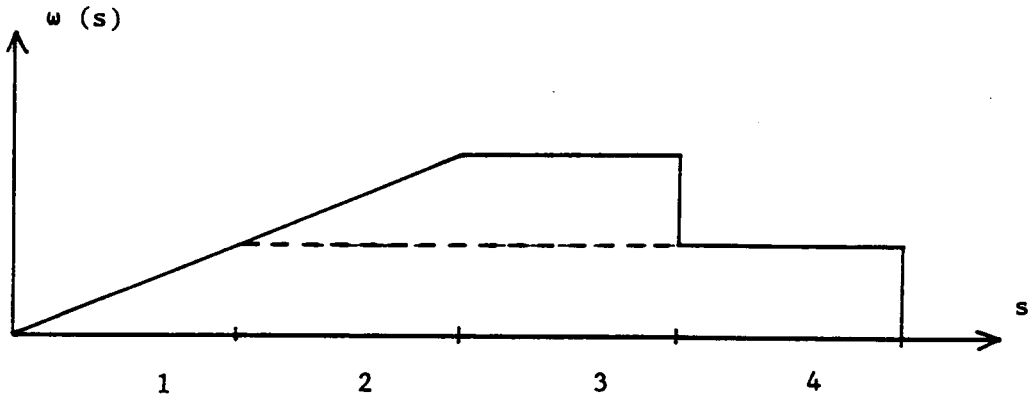

Figure 5. Sectorial area distribution of an example section

2.2.2 SHELL RESULTANT - BAR DISPLACEMENT EQUATIONS

From Flugge's cylindrical shell theory [46, pp. 122, 211, 212], the middle surface strain-displacement relations are

$$\begin{aligned}
\bar{\varepsilon}_z &= \frac{\partial \bar{w}}{\partial z} & \bar{\kappa}_z &= \frac{\partial^2 \bar{u}}{\partial z^2} \\
\bar{\varepsilon}_s &= \frac{\partial \bar{v}}{\partial s} + \frac{1}{a}\,\bar{u} & \bar{\kappa}_s &= \frac{\partial^2 \bar{u}}{\partial s^2} - \frac{1}{a}\,\frac{\partial \bar{v}}{\partial s} \\
\bar{\gamma}_{zs} &= \frac{\partial \bar{v}}{\partial z} + \frac{\partial \bar{w}}{\partial s} & \bar{\kappa}_{sz} &= \frac{\partial^2 \bar{u}}{\partial z\,\partial s} - \frac{1}{2a}\left(\frac{\partial \bar{w}}{\partial s} - \frac{\partial \bar{v}}{\partial z}\right) \\
& & \bar{\kappa}_{zs} &= \bar{\kappa}_{sz} - \frac{1}{2a}\,\bar{\gamma}_{sz}
\end{aligned} \tag{2.11}$$

If Equations (2.6), (2.7), and (2.9) for the shell displacements in terms of the bar displacements are substituted in the relations for $\bar{\varepsilon}_s$, $\bar{\gamma}_{zs}$, and $\bar{\kappa}_s$ above, it will be seen that these strain measures vanish. Thus, the two twist curvatures $\bar{\kappa}_{sz}$ and $\bar{\kappa}_{zs}$ are the same. The non-zero shell strains in terms of bar displacements are

$$\bar{\varepsilon}_z = W' - U''\,\bar{x} - V''\,\bar{y} - \Phi''\,\bar{\omega} \tag{2.12}$$

$$\bar{\kappa}_z = U''\sin\theta - V''\cos\theta - \Phi''\,q \tag{2.13}$$

$$\bar{\kappa}_{zs} = \bar{\kappa}_{sz} = -\Phi' \tag{2.14}$$

The stress-strain relationship is simply Hooke's law for elastic isotropic Vlasov's theory. Laminated plates with general lay-ups allow coupling between bending and extension. Analysis of such composite laminates is complex. If the composite lay-up is restricted to a mid-plane symmetric type, coupling between bending and extension is eliminated. The justification of this restriction is not academic, but practical. Also, for a thin cylindrical shell, the factor n/a in Flugge's theory is neg-

lected with respect to unity in the definitions of the shell resultants in terms of the stresses, and in the parallel surface strain measures. Consequently, the constitutive equations for flat laminates and thin shells are the same. The notations for classical lamination theory are adopted from Jones [44, pp. 147-172]. The simplified equations are as follows:

$$\begin{bmatrix} N_z \\ N_s \\ N_{zs} \end{bmatrix} = \begin{bmatrix} A_{11} & A_{12} & A_{16} \\ A_{21} & A_{22} & A_{26} \\ A_{61} & A_{62} & A_{66} \end{bmatrix} \begin{bmatrix} \bar{\varepsilon}_z \\ \bar{\varepsilon}_s \\ \bar{\gamma}_{zs} \end{bmatrix} \tag{2.15}$$

$$\begin{bmatrix} M_z \\ M_s \\ M_{zs} \end{bmatrix} = \begin{bmatrix} D_{11} & D_{12} & D_{16} \\ D_{21} & D_{22} & D_{26} \\ D_{61} & D_{62} & D_{66} \end{bmatrix} \begin{bmatrix} \bar{\kappa}_z \\ \bar{\kappa}_s \\ 2\bar{\kappa}_{zs} \end{bmatrix} \tag{2.16}$$

Of the above six plate resulants, three of them (N_s, N_{zs}, M_s) are reactive. By definition, there are no deformations associated with reactive resultants. The deformations corresponding to reactive plate resultants are denied through the kinematic assumptions. Thus, they do not appear in the strain energy. The values for the resultants, N_s, N_{zs}, and M_s, are not determined from the consitutive equations. Rather, the reactive forces must be determined from the equilibrium equations.[2] They have

---

[2] Alternatively, the linear theory can be derived from the variational principle. The generalized reactive forces will appear in the boundary conditions.

to be known in the stress and deflection analysis. Readers are referred to Gjelsvik [24, p. 18] for detailed discussion on the reactive forces.

Through the classical lamination theory constitutive equations, the active laminate force resultants N_z, M_z, M_{zs} can be expressed directly in terms of laminate properties A_{ij}, D_{ij} and derivatives of the plate displacements.

At this point, the active shell resultants can also be expressed in terms of bar displacements through the kinematics. Hence, the shell resultant - bar displacement equations are

$$N_z = A_{11} (W' - U'' \bar{x} - V'' \bar{y} - \Phi'' \bar{\omega}) \tag{2.17}$$

$$M_z = D_{11} (U'' \sin\theta - V'' \cos\theta - \Phi'' q) - 2 D_{16} \Phi' \tag{2.18}$$

$$M_{zs} = D_{61} (U'' \sin\theta - V'' \cos\theta - \Phi'' q) - 2 D_{66} \Phi' \tag{2.19}$$

These shell resultants, active and reactive, are related through the general shell equilibrium equations [46, pp. 204-206]. The shell equilibrium equations are as follows,

$$\begin{aligned}
\frac{\partial Q_s}{\partial s} + \frac{\partial Q_z}{\partial z} + \frac{N_s}{a} - p_n &= 0 \\
\frac{\partial N_s}{\partial s} + \frac{\partial N_{zs}}{\partial z} - \frac{Q_s}{a} + p_s &= 0 \\
\frac{\partial N_z}{\partial z} + \frac{\partial N_{sz}}{\partial s} + p_z &= 0 \\
N_{zs} - N_{sz} + \frac{M_{sz}}{a} &= 0 \\
\frac{\partial M_z}{\partial z} + \frac{\partial M_{sz}}{\partial s} - Q_z &= 0 \\
\frac{\partial M_s}{\partial s} + \frac{\partial M_{zs}}{\partial z} - Q_s &= 0
\end{aligned} \tag{2.20}$$

in which p_n, p_s and p_z are external loads per unit middle surface area of the shell acting in the $\hat{n}$-, $\hat{s}$-, and z-directions, respectively. These equilibrium equations can be integrated to determine the reactive shell resultants if active shell resultants N_s, M_s, M_{sz} are known functions of s and z. There are basically two types of external loads acting on the bar, the distributed traction, and concentrated line load acting along junctions. The concentrated point load is a special case of the latter, and is not discussed separately. In Vlasov's theory, there are no body forces. In Figure 6 on page 28, a finite segment of the bar is shown. Both the reactive shell resultants and external loads are shown. The quantities T_x, T_y, and T_z denote x-, y-, and z-direction external force intensities, respectively, that are distributed along a junction.

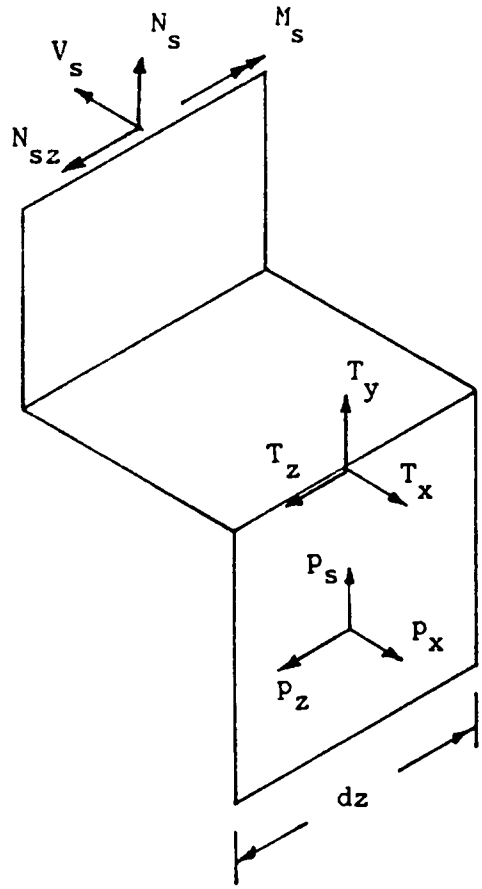

Figure 6. Reactive shell resultants and external loads acting on a finite segment of a bar

2.2.3 EQUIVALENT BAR RESULTANTS

The relationships between bar forces and shell resultants are obtained by computing the virtual work of shell resultants acting on the cross section. The virtual work expression is an integral over the contour of the shell resultants times their conjugate virtual displacements. To achieve the equivalency, virtual shell displacements are written in terms of virtual bar displacements and then substituted into the virtual work expression. The virtual work expression can then be interpreted as bar forces times virtual bar displacements. In this manner Gjelsvik [24, pp. 23-24, 29] shows the bar forces are given by

$$
\begin{aligned}
N &= \int N_z \, ds \\
V_x &= \int \left(\bar{x} \frac{\partial N}{\partial z} z - \frac{\partial M}{\partial z} z \sin\theta\right) ds - m_y \\
V_y &= \int \left(\bar{y} \frac{\partial N}{\partial z} z + \frac{\partial M}{\partial z} z \cos\theta\right) ds + m_x \\
M_x &= \int \left(N_z \bar{y} + M_z \cos\theta\right) ds \\
M_y &= - \int \left(N_z \bar{x} - M_z \sin\theta\right) ds \\
T &= \int \left(\bar{\omega} \frac{\partial N}{\partial z} z + q \frac{\partial M}{\partial z} z\right) ds - m_\omega - \int \left(M_{sz} + M_{zs}\right) ds \\
M_\omega &= - \int \left(N_z \bar{\omega} + M_z q\right) ds
\end{aligned}
\tag{2.21}
$$

The shell resultants and the bar forces are shown in Figure 7 on page 30. The quantity M_ω, shown by a three-headed arrow in the figure, is called the bimoment or warping moment. This warping moment is statically equivalent to zero force and moment; it has no point of application [24, pp. 25, 36]. It is an additional bar force unique to thin-walled bars. It has dimensions of force times length square.

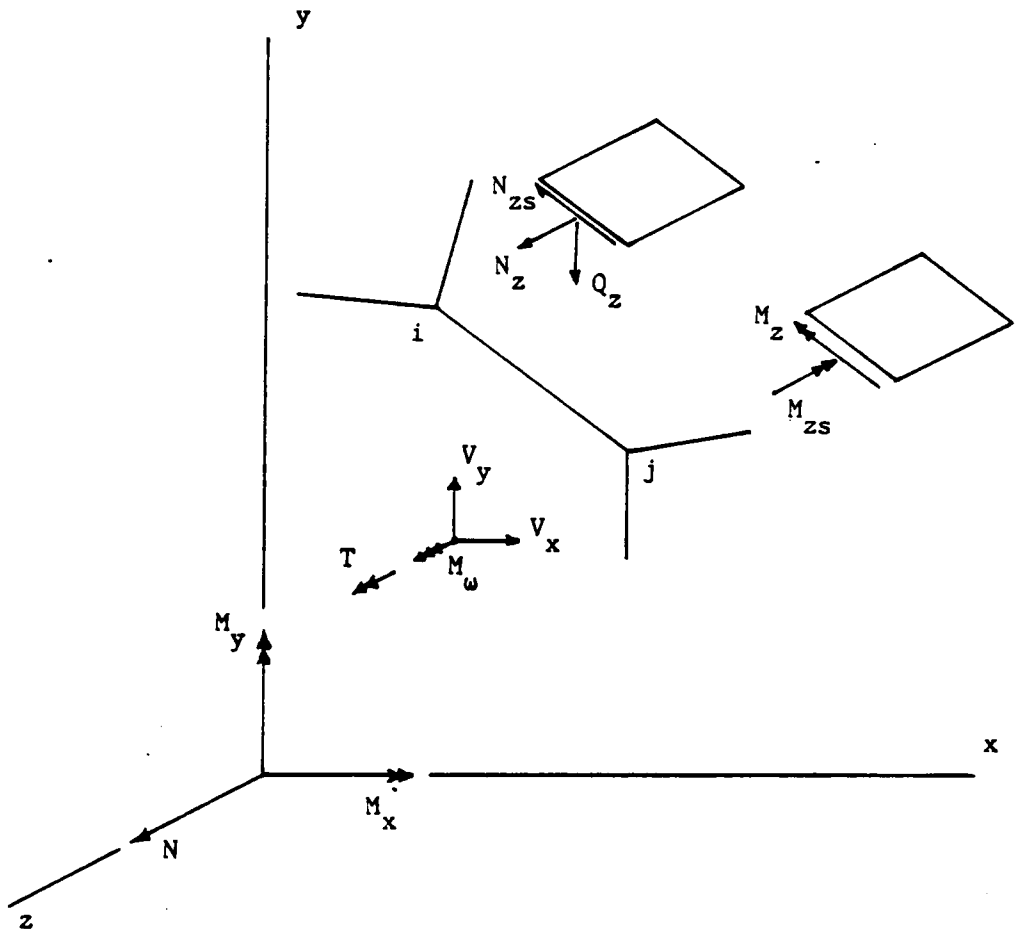

Figure 7. Equivalent bar forces

The external shell loads can also be replaced by equivalent external bar loads. The external shell loads and external bar loads are shown in Figure 8 on page 32, respectively. Equivalency between these two sets of load distributions is accomplished through the principle of virtual work.

2.2.4 BAR RESULTANT - BAR DISPLACEMENT RELATIONS

The strain energy per unit axial length of the bar is U_s, where

$$2\,U_s = \int_c (N_z\,\bar{\varepsilon}_z + M_z\,\bar{\kappa}_z + M_{zs}\,\bar{\kappa}_{zs} + M_{sz}\,\bar{\kappa}_{sz})\,ds \qquad (2.22)$$

When the shell strain - bar displacement relations (Eq. 2.12-2.14) are substituted in this equation, the strain energy becomes

$$2\,U_s = N\,W' + M_y\,U'' - M_x\,V'' + M_\omega\,\Phi'' + T_s\,\Phi' \qquad (2.23)$$

in which the bar forces N, M_x,M_y, and M_ω are as defined in Section 2.2.3, and

$$T_s = -\int_c (M_{zs} + M_{sz})\,ds \qquad (2.24)$$

The quantity T_s is called the Saint Venant torque. It is a portion of the total torque T. The total torque T is written as the sum of T_s and T_ω, where T_ω is called the warping torque. The strain energy expression shows that bar force N, bending moments M_x and M_y, the bimoment, M_ω, and the Saint-Venant torque T_s are active bar forces. Bar shear forces V_x and V_y and the warping torque T_ω are reactive bar forces. The active bar forces are functions of the active shell resultants. The active shell resultant - bar displacement Equations (2.17-2.19) are substituted in the bar force - shell resultant Equations (2.21, 2.24) to get the governing constitutive

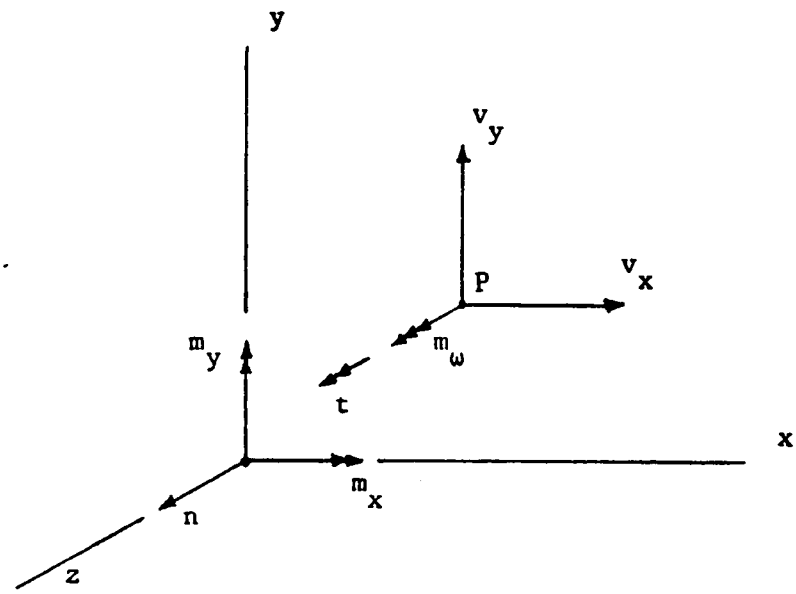

Figure 8. External bar load resultants

equations for the bar. Written in matrix form, these governing constitutive equations are

$$\begin{bmatrix} N \\ -M_x \\ M_y \\ M_\omega \\ T_s \end{bmatrix} = \begin{bmatrix} A & -S_x & -S_y & -S_\omega & 0 \\ -S_x & I_{xx} & I_{xy} & I_{x\omega} & H_c \\ -S_y & I_{yx} & I_{yy} & I_{y\omega} & -H_s \\ -S_\omega & I_{\omega x} & I_{\omega y} & I_{\omega\omega} & H_q \\ 0 & H_c & -H_s & H_q & GJ \end{bmatrix} \begin{bmatrix} W' \\ V'' \\ U'' \\ \Phi'' \\ \Phi' \end{bmatrix} \tag{2.25}$$

Coefficients in the matrix are defined by contour integrals. They are

$$\begin{aligned} A &= \int A_{11}\, ds \\ S_x &= \int A_{11}\, \bar{y}\, ds \\ S_y &= \int A_{11}\, \bar{x}\, ds \\ S_\omega &= \int A_{11}\, \bar{\omega}\, ds \\ I_{xy} &= \int \left(A_{11}\, \bar{x}\bar{y} - D_{11} \sin\theta \cos\theta \right) ds \\ I_{xx} &= \int \left(A_{11}\, \bar{y}^2 + D_{11} \cos^2\theta \right) ds \\ I_{yy} &= \int \left(A_{11}\, \bar{x}^2 + D_{11} \sin^2\theta \right) ds \\ I_{x\omega} &= I_{\omega x} = \int \left(A_{11}\, \bar{\omega}\bar{y} + D_{11}\, q \cos\theta \right) ds \\ I_{y\omega} &= I_{\omega y} = \int \left(A_{11}\, \bar{\omega}\bar{x} - D_{11}\, q \sin\theta \right) ds \\ I_{\omega\omega} &= \int \left(A_{11}\, \bar{\omega}^2 + D_{11}\, q^2 \right) ds \\ H_s &= 2 \int D_{16} \sin\theta\, ds \\ H_c &= 2 \int D_{16} \cos\theta\, ds \\ H_q &= 2 \int D_{16}\, q\, ds \\ GJ &= 4 \int D_{66}\, ds \end{aligned} \tag{2.26}$$

The elements in the coefficient matrix in Equation (2.25) are determined in terms of the geometry of the cross section and material properties as shown in Equations (2.26). As modulus-weighted section properties they are defined as area, A; first moments of area, S_x and S_y; second moments of area, I_{xx}, I_{yy}, and I_{xy} ; first moment of sectorial area, S_ω; cross-product moments of area, $I_{x\omega}$ and $I_{y\omega}$; second moment of sectorial area, $I_{\omega\omega}$; and torsional stiffness, GJ. The terms H_s, H_c, and H_q reflects twisting and bending coupling due to the anisotropy of laminated composites.

In the beginning of this chapter, the principal coordinate system was mentioned. When in use, the principal coordinate system allows simplification of the governing constitutive equations. The first moments and the product second moments vanish. The only non-zero moduli-weighted terms are area A, second moments of area, I_{xx}, I_{yy}, and $I_{\omega\omega}$, torsional stiffness GJ, and the H-terms.

For bars that are made up of regular cross-ply lay-ups, D_{16} is zero. Thus all H-terms are also zero. In such a special case, the principal coordinate system and the material lay-ups allow complete diagonalization of the constitutive equations. For isotropic materials, the principal coordinate system alone can faciliate the diagonalization. Transformation of an arbitrary coordinate system to the principal coordinate system can simplify the constitutive equations. Transformation laws for the cross-sectional properties are discussed in Gjelsvik [24, pp.46-56], and they allow the cross-sectional properties, computed in one coordinate system, to be expressed in a different coordinate system. In this context, transformation into the principal coordinate system is of utmost inter-

est. In the principal contour system, the origin is referred to the principal origin, and the location of the principal pole is the shear center. The principal Cartesian system has the origin at the centroid with the x- and y- axes aligned with the principal axes. The transformation laws for cross-sectional properties can be found in Appendix A.

For completeness, the remaining bar reactive forces V_x, V_y, and T_ω are recorded below.

$$\begin{bmatrix} V_x \\ V_y \\ T_\omega \end{bmatrix} = - \begin{bmatrix} -S_y & I_{xy} & I_{yy} & I_{\omega y} & -H_s \\ -S_x & I_{xx} & I_{xy} & I_{\omega x} & H_c \\ -S_\omega & I_{\omega x} & I_{\omega y} & I_{\omega\omega} & H_q \end{bmatrix} \begin{bmatrix} W'' \\ V''' \\ U''' \\ \Phi''' \\ \Phi'' \end{bmatrix} - \begin{bmatrix} m_y \\ -m_x \\ m_\omega \end{bmatrix} \qquad (2.27)$$

2.3 LINEAR EQUILIBRIUM EQUATIONS

In Gjelsvik [24] and Bauld and Tzeng [5], the equilibrium equations are derived from principle of virtual work. The derivation is systematic and consistent. On the other hand, it can also be done from a free-body diagram consideration with some intuition. In the free-body diagram consideration, a finite segment of the bar is considered, and bar forces are required to be balanced by external bar loads. Bar forces, external bar forces, and their points of application are shown in Figure 9 on page 37. Six equations can be obtained; three from forces in three orthogonal directions and three from moments about three orthogonal axes. The seventh equation is associated with moment of the moment about the longitudinal axis, and is generally not expected. This higher-order equilibrium equation has no counterpart in Euler-Bernoulli beam theory, yet it is the theme of the extended Vlasov's theory. The seven equilibrium equations for the bar are

$$
\begin{aligned}
&N' + n = 0 \\
&V_x' + v_x = 0 \\
&V_y' + v_y = 0 \\
&M_x' - V_y + m_x = 0 \\
&M_y' + V_x + m_y = 0 \\
&T' + t = 0 \\
&M_\omega' + T - T_s + m_\omega = 0
\end{aligned}
\tag{2.28}
$$

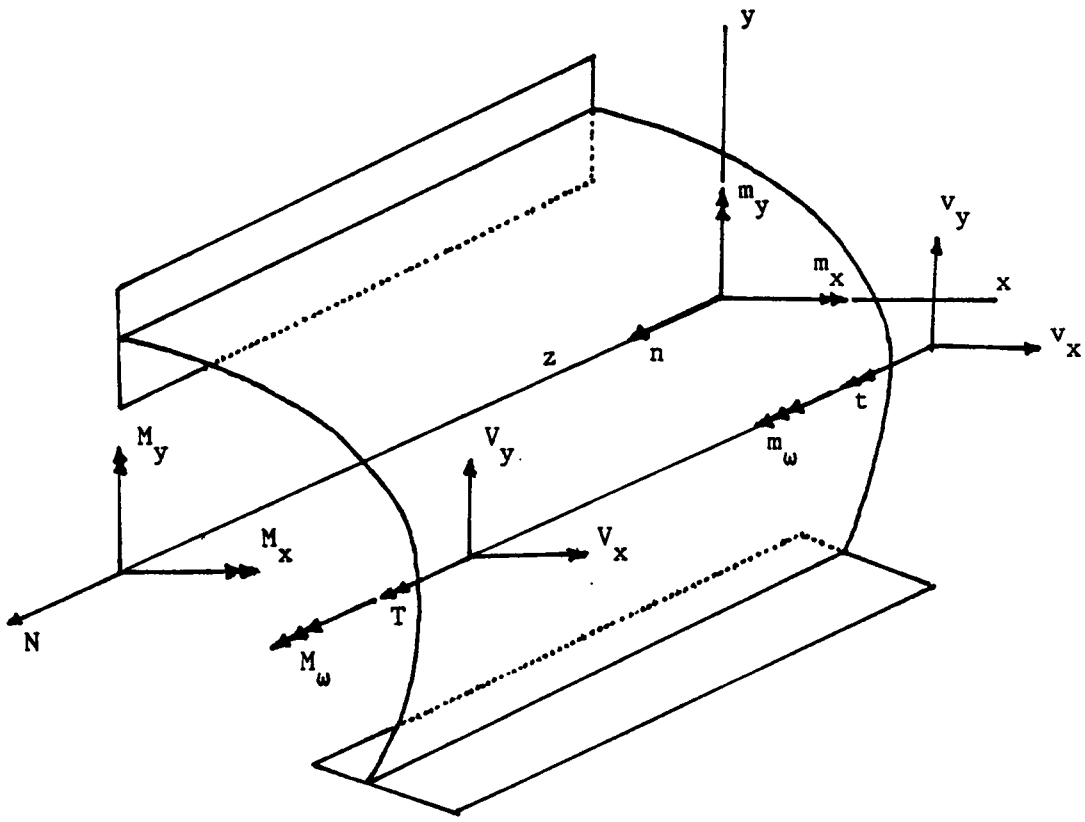

Figure 9. Bar forces and external bar forces

The reactive bar forces can be eliminated from Equation (2.28), giving four equilibrium equations. These four equations correspond to axial deformation, two lateral deformations, and rotational deformation. They are

$$\begin{aligned} N' + n &= 0 \\ M_x'' + v_y + m_x' &= 0 \\ M_y'' - v_x + m_y' &= 0 \\ M_\omega'' - T_s' - t + m_\omega' &= 0 \end{aligned} \tag{2.29}$$

If the governing constitutive Equations (2.25) are substituted in the linear equilibrium Equations (2.29), the order of the system can be clearly seen as fourteen. Therefore, seven boundary conditions are needed at each end of the bar. At each end, one boundary condition corresponds to axial compression, four to flexure about two axes, and two to torsion about the z-axis. The warping effects raise the number of torsional boundary conditions by one. The boundary conditions are listed below as dual pairs, bar forces and displacements (or their derivatives). One quantity in each pair has to be known or prescribed.

Axial force N ; axial displacement W

Bending moment M_x ; rotation about x-axis V'

Shear force V_x ; lateral displacement U

Bending moment M_y ; rotation about y-axis U'

Shear force V_y ; lateral displacement V

Torque T ; rotation about z-axis Φ

Warping moment M_ω ; first derivative of rotation Φ'

2.4 NONLINEAR THEORY

The nonlinearity in the nonlinear theory presented in Gjelsvik [24, pp. 170-184] and Bauld and Tzeng [5] is due to geometric considerations. The bar is assumed to remain linear elastic.

> The difference between the linear theory.... and a nonlinear theory lies in the form of the equilibrium equations used..... In the linear theory it is tacitly assumed that the deformations are too small to seriously affect the results obtained. In the nonlinear theory the equilibrium equations are written for the deformed bar. These equations contain product terms of force and displacements, and consequently result in a nonlinear theory, even if the remainder of the theory is linear... [24, pp. 171].

To assess the effects of force resultants in the deflected state, a new coordinate system is needed. Coordinate systems for the deflected state can be related to coordinate systems for the undeflected state through kinematic considerations. To define a new coordinate system for the deflected state, deflection must be examined. The deflections can be broken down into two components: displacements and rotations of the cross section and warping deformation of the cross section. As mentioned before, warping deformation consists of contour warping and thickness warping. From the kinematic assumption, projection of the cross section onto the flexural plane is required to be the same as the undeformed cross section.

In the first component, the cross section displaces and rotates but remains plane. The section can be considered as a rigid disk, and this plane section will be referred to as the flexural plane. A new Cartesian coordinate system will be referred to this flexural plane. In Figure 10 on page 40 two Cartesian coordinate systems and the bar forces in the flexural plane are shown. This new Cartesian coordinate system (x,y,z)

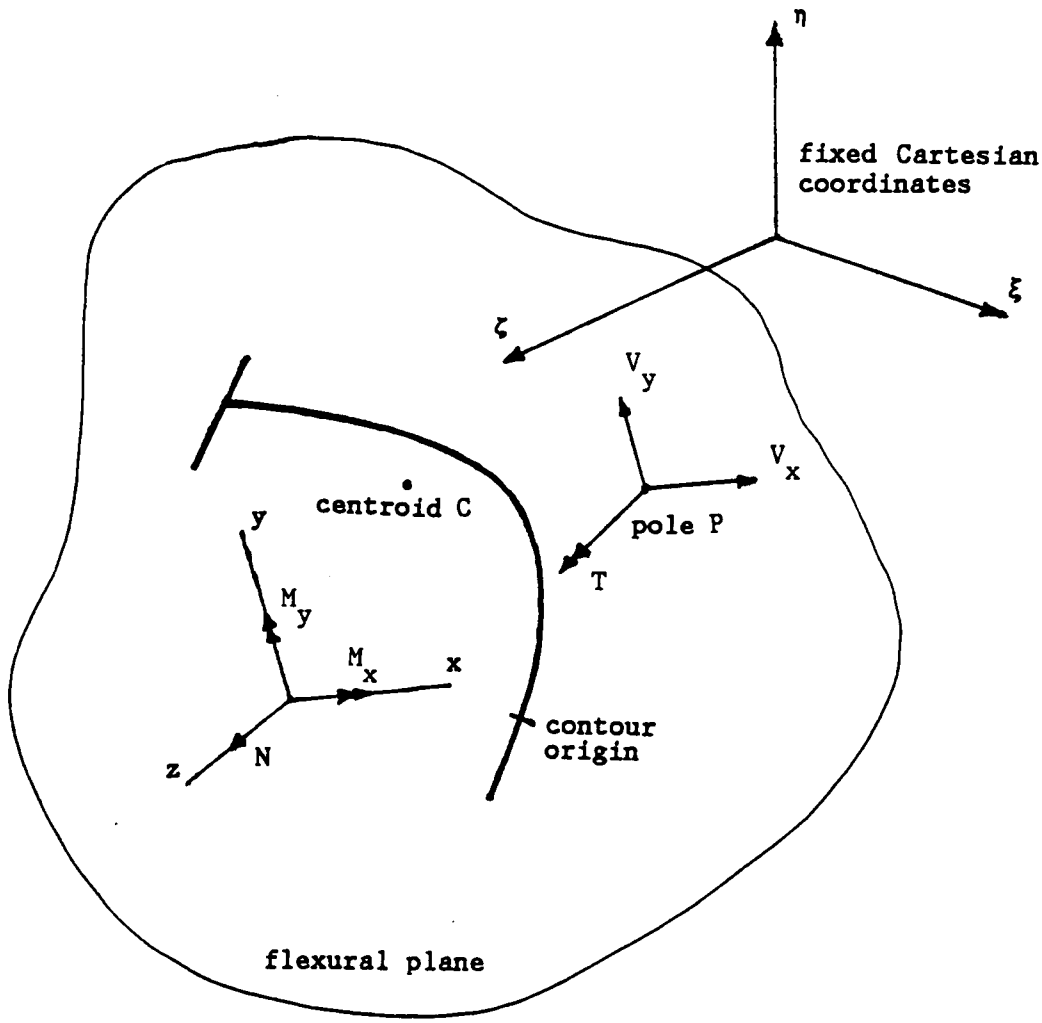

Figure 10. Bar forces in the flexural plane

will have the same origin and orientation as the principal Cartesian coordinate in the undeflected state. The latter is renamed as the fixed Cartesian coordinates (ξ,η,ζ). The bar forces are assumed to follow this new Cartesian coordinates: shear forces V_x, V_y, and torque T follow the pole, and bending moments M_x, M_y, and axial force N follow the new axes.

Similarly, a new contour coordinate system is introduced for the deflected state. This new coordinate (n*,s*,z*) is identified with material points which follow the deflected and warped cross section. While the reference contour coordinate (n,s,z) is located in the flexural plane along the projected contour. In Figure 11 on page 42, the two contour coordinate system are shown. The s*- and z*-axis are not parallel to their conjugate s- and z-axis; the change in directions is a result of combined twisting and warping effects. The kinematic assumptions, Vlasov's and Kirchhoff's, ensure that the new contour coordinate is orthogonal. The shell resultants follow the (n,s,z) coordinate system, and they are called the convected shell resultants.

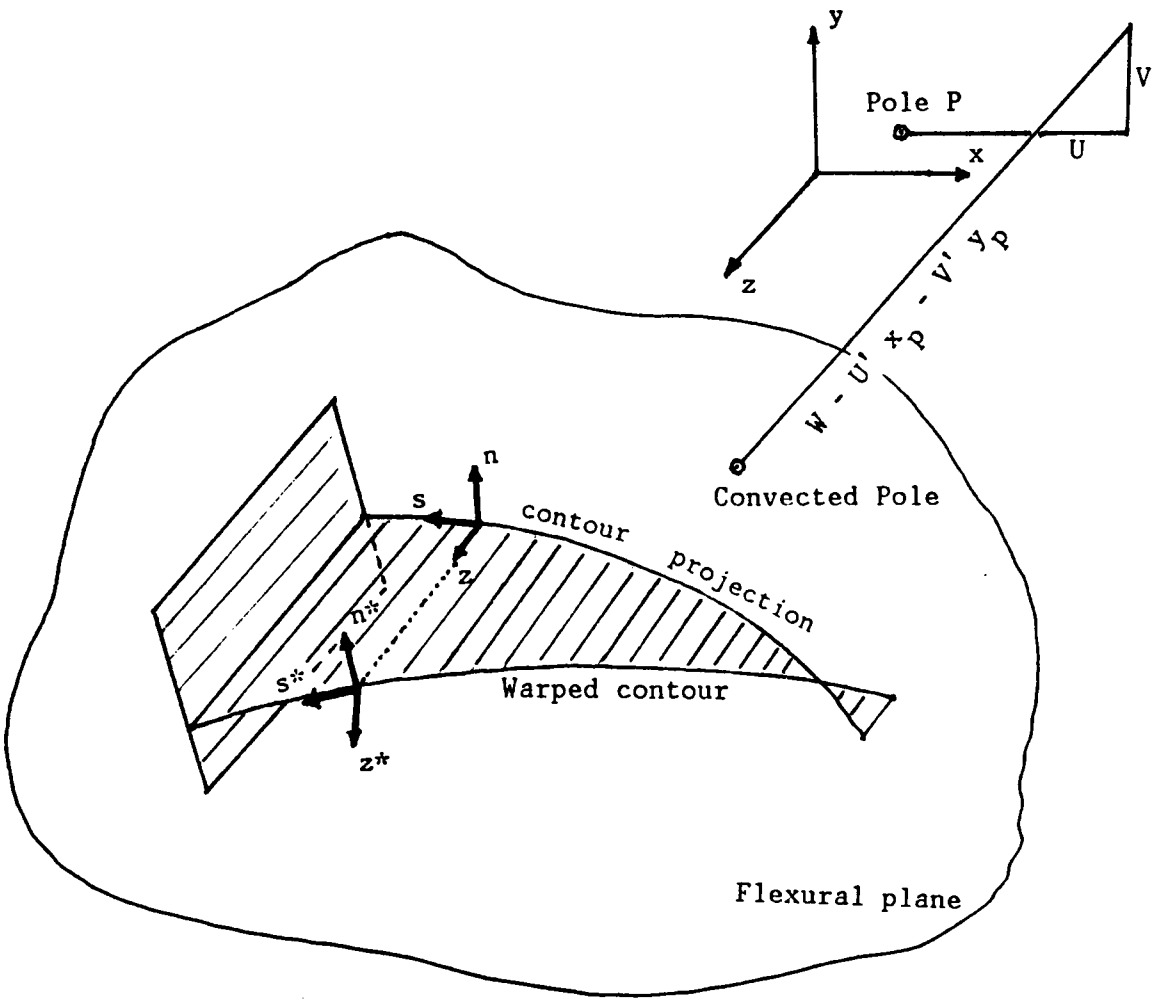

Figure 11. Two contour coordinate systems

Three additional assumptions [24, pp. 174-177] are invoked in the nonlinear theory:

- In the transformation from the (n^*,s^*,z^*) to the (n,s,z) coordinate system, second-order terms, that is, product terms in the stresses and displacements need only be considered for the convected axial stress σ_{zz}^*.

- The active convected shell resultants, N_z, M_z, and M_{zs}, are expressed in terms of the shell displacements by the same equations as in the linear theory.

- The reactive convected bar forces are related to the active convected bar forces by the same equations as in the linear theory.

The first assumption allows a relatively simple analysis by neglecting effects of shear stresses off the middle surface. As a result of the first and second assumptions, only one active convective shell resultant M_{zs} is allowed to have a second-order term. The third assumption is an approximation to simplify the buckling analysis.

The first assumption requires that only σ_{zz}^* be considered. The σ_{zz}^* stress projects onto the flexural plane giving rise to σ_{zz}, σ_{zn}, and σ_{zs}. The relations given by Gjelsvik are

$$\begin{aligned} \sigma_{zn} &= - \Phi' \, q \, \sigma_{zz}^* \\ \sigma_{zs} &= \Phi' \, (r + n) \, \sigma_{zz}^* \\ \sigma_{zz} &= \sigma_{zz}^* \end{aligned} \tag{2.30}$$

From the definition of shell resultants, these additional stresses lead to second-order terms in shell resulants. These additional shell resultants are

$$\begin{aligned} N_{zs} &= \Phi' \, (r \, N_z - M_z) \\ Q_z &= \Phi' \, q \, N_z \\ M_{zs} &= \Phi' \, (r \, M_z - \frac{D_{11}}{A_{11}} \, N_z) \end{aligned} \tag{2.31}$$

These second-order terms are associated with twisting and warping; and they vanish when there is no twisting. These second-order shell terms lead to second-order terms in the bar shear forces and bar torque when they are substituted into the definition of the bar forces in terms of the shell resultants. (See Equations (2.21) and Equations (1.41) in Reference 24 p. 24.) The total convected shear forces and torque consist of reactive parts plus second order terms. On the basis of the third assumption for the nonlinear theory, the reactive parts are related to active convected bar forces by the same equations of the linear theory; that is, by the

fourth , fifth, and seventh equations in Equations (2.28). Hence, the total convected shear forces and torque are

$$
\begin{aligned}
V_x &= - M_y' - m_y + \Phi' (y_p N - M_x) \\
V_y &= M_x' + m_x - \Phi' (x_p N + M_y) \\
T &= T_s - M_\omega' - m_\omega + \Phi' (A R_p^2 W' - K_y I_{yy} U'' - K_x I_{xx} V'' - K_\omega I_{\omega\omega} \Phi'' + H_\phi \Phi')
\end{aligned}
\tag{2.32}
$$

in which the underlined terms are the second order terms, and

$$
\begin{aligned}
R_p^2 &= \frac{1}{A} \int A_{11} \left(r^2 + q^2 + \frac{D_{11}}{A_{11}}\right) ds \\
K_y &= \frac{1}{I_{yy}} \int \left[A_{11} \bar{x} \left(r^2 + q^2 + \frac{D_{11}}{A_{11}}\right) + 2 r D_{11} \sin\theta\right] ds \\
K_x &= \frac{1}{I_{xx}} \int \left[A_{11} \bar{y} \left(r^2 + q^2 + \frac{D_{11}}{A_{11}}\right) - 2 r D_{11} \cos\theta\right] ds \\
K_\omega &= \frac{1}{I_{\omega\omega}} \int \left[A_{11} \bar{\omega} \left(r^2 + q^2 + \frac{D_{11}}{A_{11}}\right) - 2 r D_{11} q\right] ds \\
H_\phi &= \int 4 r D_{16} ds
\end{aligned}
\tag{2.33}
$$

The quantities R_p , K_x ,K_y , and K_ω defined by Equations (2.33) are new modulus weighted cross-sectional properties required in the nonlinear theory with respect to the linear theory. The term R_p is the modulus weighted polar radius of gyration of the cross section about the pole axis. Quantities K_x and K_y have units of length, K_ω is dimensionless.

2.5 NONLINEAR EQUILIBRIUM EQUATIONS

For simplicity, the principal coordinate system is adopted here. Through the principle of virtual work, bar forces in the fixed (ξ,η,ζ)

coordinate system can be related to convected bar forces in the convected Cartesian coordinate system (x,y,z). The relations are [24, pp. 178-179]:

$$\begin{aligned} (N)_\zeta &= N - V_x U' - V_y V' \\ V_\xi &= V_x - V_y \Phi + N U' \\ V_\eta &= V_y - V_x \Phi + N V' \\ (T)_\zeta &= T + N (y_p U' - x_p V') - M_x U' - M_y V' - V_x V + V_y U \end{aligned} \tag{2.34}$$

The last two terms in the first equation are usually small, and hence neglected, for columns in which the axial force is dominate and the shear forces are small [24, p. 179].

The principal of virtual work is used, as described in the linear theory, to obtain the following equilibrium equations for the bar forces in the fixed coordinate system:

$$\begin{aligned} (N)_\zeta' + (n)_\zeta &= 0 \\ V_\xi' + v_\xi &= 0 \\ V_\eta' + v_\eta &= 0 \\ (T)_\zeta' + (t)_\zeta &= 0 \end{aligned} \tag{2.35}$$

In Equations (2.35) the distributed load intensities along the fixed coordinate directions are denoted n_ζ, v_ξ, v_η, and t_ζ. It is assumed that there are no applied distributed moment loads along the ξ-, η-directions and that the applied loads maintain fixed directions but follow the deformed bar. Under moderate rotations of the flexural plane it is assumed $n_\zeta = n$, $v_\xi = v_x$, $v_\eta = v_y$, and $t = -v_x(V + e_x\Phi) + v_y(U - e_y\Phi)$, where e_x e_y are the distances from the pole along the x- and y-directions to the locations of v and v .

Equations (2.34) are substituted into Equations (2.35) to eliminate the bar forces in the fixed coordinate system. Then the convective bar forces are eliminated from the resulting equations via Equations (2.32) to obtain

$$N' + n = 0 \tag{2.36}$$

$$M_y' + (\Phi M_x)'' - [N (U + y_p \Phi)']' - v_x = 0 \tag{2.37}$$

$$M_x' - (\Phi M_y)'' + [N (V - x_p \Phi)']' + v_y = 0 \tag{2.38}$$

$$\begin{aligned} T_s' - M_\omega'' + [N (y_p U - x_p V)']' - M_x U'' - M_y V'' \\ + [\Phi' (A R_p^2 W' - K_y I_{yy} U'' - K_x I_{xx} V'' - K_\omega I_{\omega\omega} \Phi'' + H_\phi \Phi')]' \\ - (v_x e_x + v_y e_y) \Phi = 0 \end{aligned} \tag{2.39}$$

in which third order terms are neglected.

The boundary condition set-up is very similar to the linear theory, except that the bar forces are now referred to the fixed Cartesian coordinate system. To express the boundary conditions in terms of the convected bar forces, Equation (2.32) has to be used.

2.6 EVALUATION OF THE SECTION PROPERTIES

In order to solve the equilibrium equations, coefficients in the matrix of the governing constitutive equations (2.23) should be known. If these cross-sectional properties in the principal coordinate system are known, then the principal form of the governing constitutive equations can be used.

In general, the cross-sectional properties in a set of coordinate systems can be found and transformed into another set of coordinate systems. These transformation laws are purely geometrical, details are

listed in Appendix A. There are two distinct groups of transformation laws: one concerns the change from one Cartesian coordinate system to another, the second group concerns the transformation from one contour coordinate system to another.

Basically, calculations can be carried out in an arbitrarily chosen Cartesian coordinate system, and an arbitrary contour coordinate system. An arbitrary pole and an arbitrary contour origin are defined. The cross section is sub-divided into branches. The cross-sectional properties, in terms of line integrals, are then evaluated for each branch and summed. Details are described in Sub-section 2.6.1 in the context of input data file for Computer Code VLASOV. The principal system, which consists of three unknown parameters, namely location and orientation of the principal Cartesian coordinate system, location of the principal pole, and location of the principal contour origin, can now be defined. Quantities associated with the principal coordinate system are denoted with starred superscripts. The calculation process consists of three steps. The equations which appear in the description of these three steps are obtained from Equations (A1-A9) in Appendix A.

In step one, the location of the centroid, which is the origin of the Cartesian system, is found through the following expressions (cf. Figure A1 in Appendix A):

$$x_c = \frac{S_y}{A} \qquad y_c = \frac{S_x}{A} \tag{2.40}$$

The orientation of the principal Cartesian coordinate is determined by the angle α which is associated with zero product moment of area I_{xy}. The angle α is given by

$$\tan 2\alpha = \frac{2\,(I_{xy} - x_c y_c A)}{(I_{yy} - x_c^2 A) - (I_{xx} - y_c^2 A)} \tag{2.41}$$

Once the principal Cartesian coordinates are known, the cross-sectional properties $I_{x^*x^*}$, $I_{y^*y^*}$, $I_{x^*\omega}$, $I_{y^*\omega}$ and the coordinates of the principal pole $(X_{p^*}^*, Y_{p^*}^*)$ can be obtained as step two. Coordinates of the principal pole are

$$x_{p^*}^* = x_{p^*} + \frac{I_{\omega x^*}}{I_{x^*x^*}} \qquad y_{p^*}^* = y_{p^*} - \frac{I_{\omega y^*}}{I_{y^*y^*}} \tag{2.42}$$

The first moment of the sectorial area S_ω must be transformed, or recomputed, with respect to the principal Cartesian axes, principal pole, and the original contour origin 0. The principal contour origin can then be found from

$$\overline{\omega}_{0^*}^* = -\frac{S_\omega}{A} \tag{2.43}$$

where $\overline{\omega}_{0^*}$ represents the sectorial area defined by points P^*, 0 and 0^*. Although Equation (2.43) determines the sectorial area $\overline{\omega}_{0^*}^*$, it does not locate the principal contour origin 0^* directly. To find point 0^* a trial and error procedure is required. Different trial points for 0^* on the

contour are selected and the sectorial area for each trial point is computed. The correct trial point is the one for which the sectorial area equals $\overline{\omega_{0*}}$. Actually, there may be many points on the contour which yield a sectorial area $\overline{\omega_{0*}}$, and consequently, any of these points may serve as the principal contour origin.

2.6.1 COMPUTER CODE : VLASOV

The transformation method presents two major problems. First, the the trial and error procedure described in Section 2.6 to locate the principal contour origin is cumbersome and difficult to implement, because the sectorial area is in general only a piecewise continous function of the contour coordinate.

Second, the second moment of sectorial area in the principal coordinate systems cannot be found at the outset of the calculation because the principal coordinate systems are not known. The transformation law for the principal second moment of sectorial area was found to be unstable in numerical computations. It is highly sensitive to the original choice of arbitrary pole and arbitrary Cartesian coordinates. The transformation law for $I_{\omega\omega}^{*}$ is as follows,

$$I_{\omega\omega}^{*} = I_{\omega\omega} - I_{xx} * \Delta x_p^{2} - I_{yy} * \Delta y_p^{2} - S_{\omega}^{2} / A \qquad (2.44)$$

All of the four terms on the right-hand side depend on the coordinate system. The term on the left-hand side, the principal second sectorial moment of area, was found to be small compared to any of the four terms

on the right. Subtraction of comparable quantities lead to loss of signifiance. There is no apparent cure for such computational dead-lock.

The computer code VLASOV was written to take advantage of the transformation laws, and at the same time to by-pass the second problem. In the computer codes, the transformation laws are invoked in a number of stages under different restrictive conditions. Each stage is associated with re-computation of selected cross-sectional properties so that crucial information on the coordinate systems is obtained. In the first computation, both the contour and Cartesian coordinate systems are arbitrary. The Cartesian origin, contour origin, and pole are also arbitrary. The computation is carried out on A, S_x, S_y, I_{xy}, I_{xx}, and I_{yy} only. From these section properties, the location of the centroid and the orientation of the principal Cartesian coordinate system can be found. The principal second moments of area are obtained from transformation laws. It is followed by the second computation which involves $I_{\omega x}$ and $I_{\omega y}$. The coordinates of the principal pole can then be determined. The third computation is on S_ω, and a subroutine is called to locate the principal contour origin. In the fourth computation, the coordinate systems are principal systems and the characteristic points are also principal points. The only quantities computed in this step are the second moment of sectorial area $I_{\omega\omega}$ and the H-terms by definition.

In the latest version of VLASOV (VLASOV2), the code continues after the line integrals and the principal systems are found. Geometry of the section is expressed in the computed principal system, and the former is used as input for the successive computation for the required line integrals to ensure consistent yet accurate results. For the second moment

of sectorial area, the last three terms in the transformation law should be identically zero.

Two input files, one on material properties and the other on geometry, are required to run this code. The material input contains elastic moduli in two directions, the principal Poisson's ratio, shear modulus, and thickness, orientation and sequence of each layer. Since the theory for analysis is restricted to mid-plane symmetric laminates, only half of the lay-up is needed. In the geometry input, the contour is represented by straight line elements. Each of these elements are specified by their end points. Curved profiles can be approximated by a series of straight line elements. The order in which the end points are specified dictates the direction of the local contour. The end points are given in an arbitrary Cartesian coordinate system. All this information has to be stored in a connectivity matrix and a coordinate matrix in the input file, from which the code generates a junction connectivity matrix. The latter is used to ensure that the value of the sectorial area is matched at every junction in the cross section. An example can be found in Figure 12 on page 53. The data file is supplied by the user. A cross section is subdivided into branches by the user, and the nodes labelled. As the first part of the data file, the user identifies the branches (first column) with the end nodes, and writes in the connectivity matrix. In the row below the "connectivity" the first number "1" denotes the branch number. The second and third numbers denote the node numbers of the end points. The second part of the input is on the coordinates of these nodes in the arbitrary Cartesian coordinate system, and the location of an arbitrary pole. In the row below the "coordinates" the integer denotes the node

```
CHANNEL SECTION  (ANGLE PLY 19.00)
-----NUMEL= 3     NNODE= 4-----
CONNECTIVITY
    1.              1          2
    2.              2          3
    3.              3          4

COORDINATES
    1.              1.250000000          0.625000000
    2.              0.000000000          0.625000000
    3.              0.000000000         -0.625000000
    4.              1.250000000         -0.625000000

ARBITRARY POLE
    0.000000000     0.000000000
```

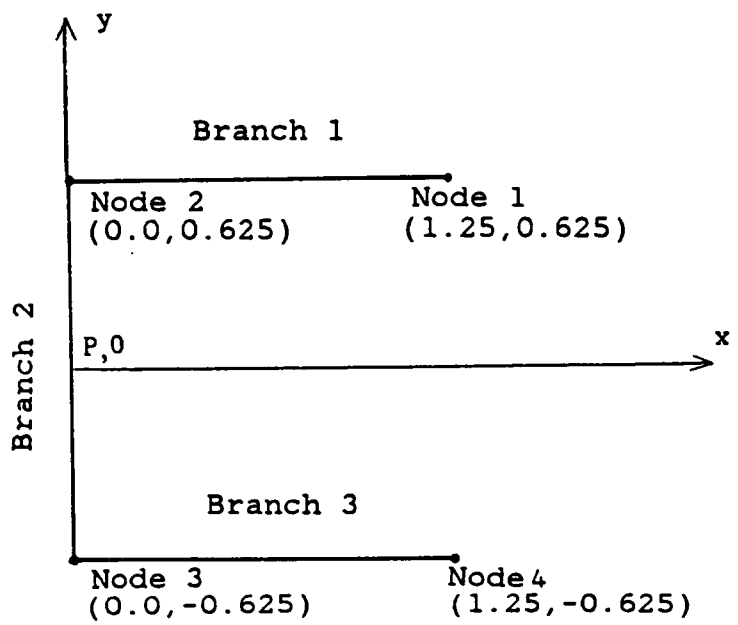

Figure 12. An example of geometric input to Code VLASOV2

number. The second and third numbers are the x- and y-coordinates of the node in the arbitrary Cartesian coordinate system.

The required moduli-weighted line integrals are evaluated in each branch and summed for the cross section. In each branch, the line integrals are evaluated in a local coordinate η. The local coordinates are assigned to have a range from -1.0 to 1.0. Linear transformation from global coordinates to local coordinates allows a standard limits of integrations for all branches.

There are two output files: one on the new coordinates of the cross section in the principal Cartesian coordinate system and one on the cross-sectional properties. The latter contains values of the fourteen cross-sectional properties; location of the centroid in the arbitrary Cartesian coordinate system in the input, rotation of the the principal axes; and location of the principal pole with respect to the centroid in the principal coordinate system.

The code is written to give the users a variety of input choices. In the case of poor input choice, only the efficiency of the code is affected, but not the accuracy of the solution. The flow chart can be found in Figure 13 on page 55. Geometry of the cross section is sub-divided into branches and described in the input data file by the user. The main program calls the subroutine KONST. The latter calculates cross-sectional properties with respected to the specified coordinate systems. The coordinates of the cross section in the principal coordinate sytems are also computed. The subroutine is called again after coordinate transformations, and the entire process is repeated. The above procedure is stopped when the the change the quantity $I_{\omega\omega}$ between successive calcu-

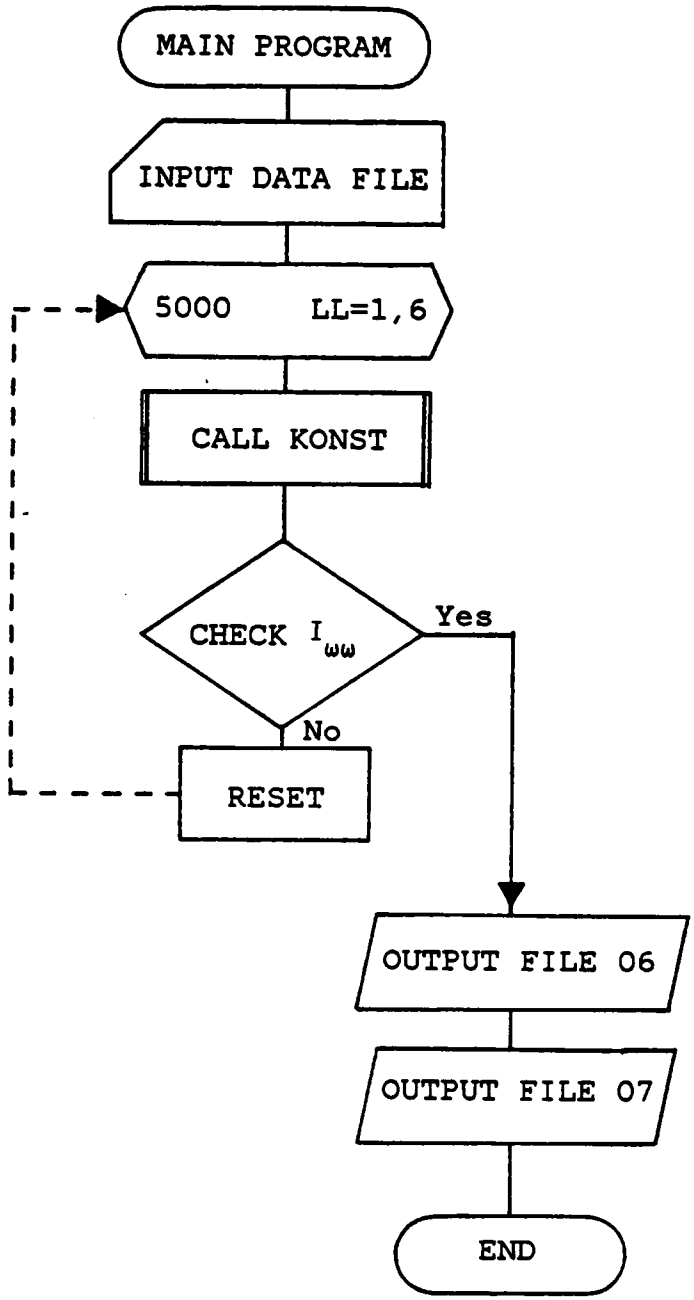

Figure 13. Flow chart of code VLASOV2

lations is smaller than a prescribed tolerance. Alternatively, the computation is aborted when the tolerance is not observed after six successive calculations.

2.6.2 COMPUTER CODE : ISOKON

Code ISOKON is the counterpart of VLASOV, but for the isotropic cross sections. It has a program structure similar to that of code VLASOV, but ISOKON was developed prior to VLASOV. In ISOKON, the input material properties are considerably simpler, and the section properties are not moduli-weighed. For consistent evaluation of the section properties, ISOKON2 should be used, as in the case of VLASOV2 for laminated composite sections.

3.0 LINEAR BIFURCATION ANALYSIS

3.1 STABILITY EQUATIONS

The nonlinear equilibrium Equations (2.36-2.39) contain products of derivatives of the bar displacements and bar resultants. These equations can be written in terms of the displacements and their derivatives by using the governing constitutive equations to eliminate the bar resultants. In this chapter and the next, the bar is referred to as a beam column. The four equations are as follows:

$$A\,W'' = 0 \tag{3.1}$$

$$I_{yy}\,U'''' - H_s\,\Phi''' - I_{xx}\,(\Phi''\,V'' + 2\,\Phi'\,V''' + \Phi\,V'''') - H_c\,(3\,\Phi'\,\Phi'' + \Phi\,\Phi''') - [\,A\,W'\,(U' + y_p\,\Phi')\,]' = 0 \tag{3.2}$$

$$I_{xx}\,V'''' + H_c\,\Phi''' + I_{yy}\,(\Phi''\,U'' + 2\,\Phi'\,U''' + \Phi\,U'''') - H_s\,(3\,\Phi'\,\Phi'' + \Phi\,\Phi''') - [\,A\,W'\,(V' - x_p\Phi')\,]' = 0 \tag{3.3}$$

$$I_{\omega\omega}\,\Phi'''' - H_c\,V''' + H_s\,U''' - JG\,\Phi'' - [\,A\,W'\,(y_pU' - x_pV')\,]' - (I_{xx} - I_{yy})\,U''\,V'' - H_c\,\Phi'\,U'' - H_s\,\Phi'\,V'' - [\Phi'\,(A\,R_p^{\,2}W' - I_{yy}K_y\,U'' - I_{xx}K_x\,V'' - I_{\omega\omega}K_\omega\,\Phi'' + H_\phi\,\Phi')]' = 0 \tag{3.4}$$

The criterion for linear bifurcation is that there exists a deflected configuration infinitestimally close to the straight undeflected equilibrium form. The equilibrium Equations (3.1-3.4) can be separated into prebuckling equations and buckling equations by means of perturbation method, in which the displacements are perturbed about some equilibrium state. When terms of the same order are collected, a set of

prebuckling equilibrium equations and a set of buckling equations are obtained. The same technique is applied to the associated boundary conditions. The expansion on displacement is

$$\begin{bmatrix} U \\ V \\ W \\ \Phi \end{bmatrix} = \begin{bmatrix} U_o \\ V_o \\ W_o \\ \Phi_o \end{bmatrix} + \begin{bmatrix} U_1 \\ V_1 \\ W_1 \\ \Phi_1 \end{bmatrix} \tag{3.5}$$

The first column on the right-hand side in the above equation, written in the vector form as $\underset{\sim}{U}_o$, satisfies the original nonlinear equilibrium equations; the second column $\underset{\sim}{U}_1$ contains small perturbations about $\underset{\sim}{U}_o$.

To faciliate bifurcation analysis, physical assumptions have to be made to allow the occurrence of bifurcation. The prebuckling equations obtained from asymptotic expansion are nonlinear. The column is assumed to be loaded by a concentric end load only, acting through the centroid. The lateral displacements and rotation remain zero until the applied end load reaches the bifurcation level. Thus, the prebuckling state is actually a problem in linear analysis and can be summarized as

$$\begin{bmatrix} U_o \\ V_o \\ W_o \\ \Phi_o \end{bmatrix} = \begin{bmatrix} 0 \\ 0 \\ -Pz/A \\ 0 \end{bmatrix} \tag{3.6}$$

where P is the compressive end load.

An additional assumption invoked in the Bauld and Tzeng paper allows decoupling of material response. The lay-ups of composite beam columns are restricted to orthotropic regular cross-ply. The D_{16} term in the

constitutive equation vanishes. Therefore, H_s, H_c, and H_q terms are identically zero. It is, however, felt that such an assumption has no theoretical basis. It is merely made for mathematical convenience. In the bifurcation analysis, the prebuckling state is undeflected and the end load induces no bending nor twisting resultants. The existence of coupling between bending and twisting at this point is irrelevant. At the bifurcation point, the column can follow the secondary path in the load-deflection space; the lateral displacements and rotation are no longer zero on the secondary path. The material coupling causes the deformations to interact; but under pure compression in the prebuckling state, it has no influence on the response. The above assumption will be addressed at the end of the chapter.

3.2 SOLUTION OF THE STABILITY EQUATIONS

For the equilibrium state of pure axial compression, the stability equations are

$$
\begin{aligned}
&A\,W_1'' = 0 \\
&I_{yy}\,U_1'''' - H_s\,\Phi_1''' + P\,(U_1'' + y_p\,\Phi_1'') = 0 \\
&I_{xx}\,V_1'''' + H_c\,\Phi_1''' + P\,(V_1'' - x_p\,\Phi_1'') = 0 \\
&I_{\omega\omega}\,\Phi_1'''' + H_s\,U_1''' - H_c\,V_1''' + (P\,R_p^2 - JG)\,\Phi_1'' + P\,(y_p U_1'' - x_p V_1'') = 0
\end{aligned}
\tag{3.7}
$$

and the associated homogeneous boundary conditions at each end of the bar are

$$
\begin{aligned}
&A\,W_1' = 0 \quad \text{or} \quad W_1 = 0 \\
&-I_{xx}V_1'' - H_c\Phi_1' - P\,(V_1 - x_p\Phi_1) = 0 \quad \text{or} \quad V_1' = 0 \\
&-I_{xx}V_1''' - H_c\Phi_1'' - P\,V_1' = 0 \quad \text{or} \quad V_1 = 0 \\
&I_{yy}U_1'' - H_s\Phi_1' + P\,(U_1 + y_p\Phi_1) = 0 \quad \text{or} \quad U_1' = 0 \\
&I_{yy}U_1''' - H_s\Phi_1'' + P\,V_1' = 0 \quad \text{or} \quad U_1 = 0 \\
&I_{\omega\omega}\Phi_1'' + H_q\Phi_1' = 0 \quad \text{or} \quad \Phi_1' = 0 \\
&-I_{\omega\omega}\Phi_1''' + H_cV_1'' - H_sU_1'' + GJ\,\Phi_1' - \\
&\qquad P^2(R_p\,\Phi_1' - x_pV_1' + y_pU_1') = 0 \quad \text{or} \quad \Phi_1 = 0
\end{aligned}
$$

In the eigenvalue problem only the trivial solution exists for the axial displacement due to buckling ($W_1 = 0$). Thus the buckling mode consists of U_1, V_1, and Φ_1. Assuming a solution of the form

$$
\begin{aligned}
U &= C_u \exp(\lambda z i) \\
V &= C_v \exp(\lambda z i) \\
\Phi &= C_\phi \exp(\lambda z i)
\end{aligned}
\tag{3.8}
$$

where $i = \sqrt{-1}$, results in the following homogeneous set of equations for constants C_u, C_v, and C_ϕ.

$$\lambda^2 \begin{bmatrix} I_{yy}\lambda^2 - P & 0 & H_s\lambda i - P\, y_p \\ 0 & I_{xx}\lambda^2 - P & -H_c\lambda i + P\, x_p \\ H_s\lambda i - P\, y_p & -H_c\lambda i + P\, x_p & I_{\omega\omega}^2\lambda^2 + JG - P^2 R_p \end{bmatrix} \begin{bmatrix} C_u \\ C_v \\ C_\phi \end{bmatrix} = 0 \tag{3.9}$$

Nontrivial solutions for the coefficients C_u, C_v, and C_ϕ in Equations (3.9) require the determinate of coefficients to vanish, which leads to a twelfth degree polynomial in λ. The twelve roots for λ from the characteristic polynomial are used in the usual mnner to construct a general solution for U_1, V_1, and Φ_1 in terms of twelve arbitrary constants. Then, prescribing the appropriate six homogeneous boundary conditions at each end of the beam column leads to an eigenvalue problem for the axial compressive load P. The lowest eigenvalue for P is the critical (buckling) load. This customary analytic method to compute the critical load was not used because of the lengthy algebraic manipulations involved. Instead a simplified, but restrictive, analytic method was programmed in code BUCKEQ. In addition, the general eigenvalue problem given by Equations (3.7) with the associated homogeneous boundary conditions was solved by the finite element method. The matrix eigenvalue problem for the buckling loads obtained from the finite element method was programmed in code LBIFUR. The codes BUCKEQ and LBIFUR are discussed in Section 3.3. The remainder of this section is devoted to a discussion of the simplified analytic method used for code BUCKEQ.

A simplified analytic solution of the stability Equations (3.7) and the associated boundary conditions is based on the boundary conditions in flexure and torsion are correlated. For example, correlated clamped end conditions are $U_1 = U_1' = V_1 = V_1' = \Phi_1 = \Phi_1' = 0$. Under these assumptions, however, the stability equations are still coupled since the centroid and shear center do not in general coincide ($x_p \neq 0$, $y_p \neq 0$).

In the completely uncoupled problem x_p and y_p are zero (double symmetric section) in addition to the H-terms being zero. Let P_x, P_y, and P_t denote the buckling loads for flexural buckling about the x-axis, flexural buckling about the y-axis, and torsional buckling about the z-axis, respectively, for the completely uncoupled problem. These uncoupled buckling loads are

$$\begin{aligned} P_x &= \frac{\pi^2 \, I_{xx}}{(Kx \, L)^2} \\ P_y &= \frac{\pi^2 \, I_{yy}}{(Ky \, L)^2} \\ P_t &= \frac{1}{R_p^2}\left[\frac{\pi^2 \, I_{\omega\omega}}{(Kt \, L)^2} + GJ\right] \end{aligned} \tag{3.10}$$

in which K_xL, K_yL, and K_tL are effective column lengths for flexural buckling about the x- and y-axes, and for torsional buckling about the z-axis, respectively. See Figure 14 on page 63 for values of K_x, K_y, and K_t for some classical end conditions. The non-zero values of λ^2 in Equations (3.9) for the completely uncoupled problem are

$$\begin{aligned} \lambda^2 &= P_x \, / \, I_{xx} \\ \lambda^2 &= P_y \, / \, I_{yy} \\ \lambda^2 &= (P_t \, R_p^2 - GJ) \, / \, I_{\omega\omega} \end{aligned} \tag{3.11}$$

Correlated End Conditions	Effective Length Factor
1. Both ends fixed Uj = 0 Uj' = 0 Uk = 0 Uk' = 0	Ki = 0.50
2. One end fixed, the other simply supported Uj = 0 Uj' = 0 Uk = 0 Mk = 0	Ki = 0.70
3. One end fixed, the other on roller which is normal to the deflection Uj = 0 Uj' = 0 Vk = 0 Uk' = 0	Ki = 1.00
4. Both ends simply supported Uj = 0 Mj = 0 Uk = 0 Mk = 0	Ki = 1.00
5. One end fixed, the other free Uj = 0 Uj' = 0 Vk = 0 Mk = 0	Ki = 2.00

Ki are the boundary coefficients, i=x, y, and t

Uj : general displacement at support j

Vj : general transverse force at support j

Mj : general moment at support j

Figure 14. The boundary coefficients

which, after eliminating P_x, P_y, and P_t via Equations (3.10), become

$$\begin{aligned} \lambda^2 &= \pi^2 / (K_x L)^2 \\ \lambda^2 &= \pi^2 / (K_y L)^2 \\ \lambda^2 &= \pi^2 / (K_t L)^2 \end{aligned} \tag{3.12}$$

For correlated end conditions the numerical values of K_x, K_y, and K_t are the same. Thus λ is the same value for flexure and torsion for correlated end conditions.

With x_p and y_p non-zero and the H-terms equal to zero, a solution of the form of Equation (3.8) is possible with the non-zero values of λ given by

$$\lambda = \pi / (K L) \tag{3.13}$$

where

$$K = K_x = K_y = K_t \tag{3.14}$$

for correlated end conditions. With the value of λ known, the vanishing of the determinate of coefficients in Equations (3.9) leads to

$$R_p^2 (P_y - P)(P_x - P)(P_t - P) - P^2 x_p^2 (P_y - P) - P^2 y_p^2 (P_x - P) = 0 \tag{3.15}$$

In which P_x, P_y, and P_t are given by Equations (3.10). Equation (3.15) is the characteristic equation for the buckling loads in the simplified analysis. The buckling modes are

$$\begin{bmatrix} U_1 \\ V_1 \\ \Phi_1 \end{bmatrix} = \begin{bmatrix} \xi_1 \\ \xi_2 \\ 1 \end{bmatrix} \left[A + B\, z + C \cos\left(\frac{\pi\, z}{K\, L}\right) + D \sin\left(\frac{\pi\, z}{K\, L}\right)\right] \tag{3.16}$$

where A, B, C, and D are arbitrary constants and

$$\xi_1 = \frac{P_y}{P_y - P_P}$$
$$\xi_2 = -\frac{P_x}{P_x - P_P} \tag{3.17}$$

If Equations (3.16) are substituted in the boundary conditions, then three identical sets of four homogeneous equations are obtained for constants A, B, C, and D [24, p. 192].

3.3 BUCKLING CODES : BUCKEQ, LBIFUR

In each computer code, the section properties are required. Efforts have been made to format the output of code VLASOV in such a way that it can be directly read as input to codes BUCKEQ and LBIFUR. For flexibility, boundary conditions, and length of the beam can either be read interactively or from a separate data file. Three sets of boundary conditions are needed; one for flexural supports in the X-direction, one for the flexural supports in the Y-direction, and one for the torsional supports. It is assumed that each of the boundary condition sets are independent for LBIFUR, but flexural and torsional boundary conditions must be correlated for BUCKEQ.

The buckling loads in BUCKEQ are computed as roots to the characteristic polynomial given by Equation (3.15). In the general case where there is no axis of symmetry, the polynomial is of third degree. For each axis of symmetry, the degree of the polynomial reduces by one. For two axes of symmetry, the solution corresponds to lowest value of the uncou-

pled loads. For the asymmetric section the roots to the cubic polynomial were obtained by the Newton-Raphson method rather than by using the exact formula. The initial guess is taken as the lowest of the uncoupled buckling loads, and this was found to be efficient. The existence of the solution corresponds to buckling in a combined flexural-torsional mode. In the case where the polynomial diverges, the lowest of the uncoupled buckling loads is taken as the load for bifurcation.

In LBIFUR, the section is discretized into a number of short-beam elements. The degree of discretization is specified by the user in the input; for simplicity, all the short-beam elements have the same length. The global elastic and geometric stiffness matrices are assembled. The boundary conditions, in form of restrained degrees of freedom at the ends, are imposed; the two global stiffness matrices are reduced accordingly. The analysis is followed by calling a packaged routine EIGZF on the International Mathematics Subroutine Library (IMSL). In addition to the buckling load, the eigenvectors can also be obtained.

The two computer codes give results very close to each other. For LBIFUR, the higher computational cost is offset by a more detailed solution which contains the eigenvectors. The flow chart of BUCKEQ can be found in Figure 15 on page 67. The parameter NSYM, the number of axes of symmetry present in the cross section, is specified by the user. In the case where there are two axes of symmetry, the uncoupled loads are calculated. The lowest value of the uncoupled loads is determined, and the analysis is completed. In other cases, it is followed by iterations to find the flexural-torsional coupled load.

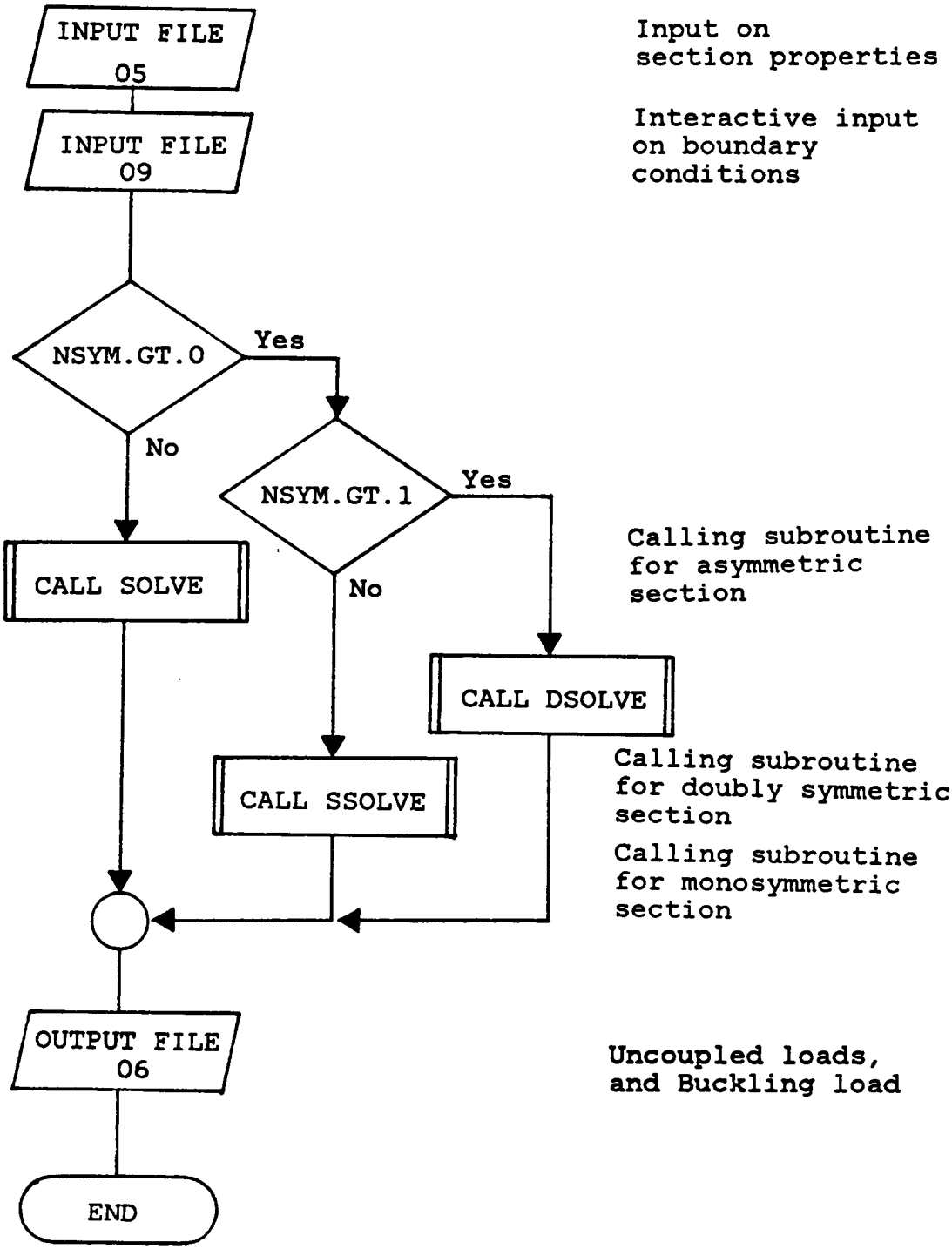

Figure 15. Flow chart for computer code BUCKEQ

To verify the assumption that the H-terms can be neglected, a finite element code (LBIFUR) has been written to compare the results with H-terms and the results without H-terms. The eigenvalue solution is much more difficult in the presence of these H-terms. The characteristic polynomial is complex, and so are the eigenvalues. It was found that the two results for laminated composite cross section of general lay-ups are very close, the approximation is good. In the case of lay-ups with strong angle-ply characteristics, where the H-terms take up sizable values, the approximation is still very good. Thus discarding the H-terms allows a simplistic eigenvalue analysis which involves an algebraic polynomial of order three. Analytic results can be found in Chapter 5, with quantitative results on five example sections.

4.0 NONLINEAR ANALYSIS

4.1 NONLINEAR ANALYSIS

In the buckling analysis the column is assumed to remain straight and untwisted in prebuckling. At a certain load level, the column exhibits non-zero lateral displacements and twist. For a concentric axial load, a perfectly straight column, and no bending - extension coupling, an equilibrium state of pure compression is theoretically possible. However, the reality of even carefully conducted tests and high-quality manufacturing cannot guarantee absolute perfection. Hence, unavoidable imperfections initiate bending and/or twist of the column to occur even at low a axial load level. The purpose of this chapter is to present solutions to the nonlinear equilibrium equations with small imperfections initiating lateral deflection and twist.

Two standard nonlinear two-point boundary value solvers, DVCPR in IMSL and PASVART [55] by Computer Sciences Corporation, have been used to try to solve the nonlinear equilibrium Equations (3.1-3.4). Both routines use the finite difference method with variable step size, and very similiar input formulation. In each case, the nonlinear equations are replaced by nonlinear algebraic difference equations and solved by Newton's method. The nonlinear equations are put into the following form

$$\begin{aligned} \underset{\sim}{U}' &= F\ (\ z\ ,\ \underset{\sim}{U}(z)\ ) \qquad\qquad A < z < B \\ G &= G\ (\ \underset{\sim}{U}(A)\ ,\ \underset{\sim}{U}(B)\ ) = 0 \end{aligned} \tag{4.1}$$

where vector $\underset{\sim}{U}$ is the N-dimensional generalised displacement vector, and the end points of the one-dimensional domain are denoted A and B. The boundary conditions at A and B are formatted in the boundary condition matrix G. The original higher order system of differential equations is replaced by a number of first-order differential equations by defining new dependent variables. The order of the system remains the same but the number of differential equations increases. Codes DVCPR and PASVART require the matrix

$$[J] = \left[\frac{\partial F_i}{\partial U_j}(\underset{\sim}{U}) \right] \qquad i,j = 1,2,.....N \qquad (4.2)$$

to be computed for Newton's method. The determinant of matrix [J] is the Jacobian of the functions $F_i(\underset{\sim}{U})$. Unfortunately, the absence of the lower order derivatives of W, U, V, and Φ in Equations (3.1-3.4) means the vanishing of some columns in matrix [J]. Thus, the Jacobian is zero and Newton's method breaks down. Theoretically, if the equations are integrable, terms such as W", U", V", and Φ" can be treated as basic variables. However, the mechanics of the present problem do not give consistent boundary conditions to the equations in the newly defined variables. Therefore, the nonlinear equations have to be solved by other methods. In the following section the finite element formulation and its implementation will be described and discussed as a means to solve the nonlinear Equations (3.1-3.4).

4.2 SOLUTION BY THE FINITE ELEMENT METHOD

In the finite element method the nonlinear ordinary differential equations (3.1-3.4) are reduced to a set of nonlinear algebraic equations of the form

$$[\ K_L + K_{NL}\ (\underset{\sim}{U})\ ]\ \underset{\sim}{U} = \underset{\sim}{F} \tag{4.3}$$

in which $\underset{\sim}{U}$ denotes the vector of nodal displacements, $[K_L]$ is the linear portion of the global stiffness matrix, $[K_{NL}]$ is the nonlinear portion of the global stiffness matrix, and $\underset{\sim}{F}$ is the nodal force vector. For prescribed values of the applied loads, Equation (4.3) is solved for the displacements by the Picard iteration. The iterative scheme is based on

$$[\ K_L + K_{NL}\ (\underset{\sim}{U}^k)\ ]\ \underset{\sim}{U}^{k+1} = \underset{\sim}{F} \qquad k = 1,2,.....N \tag{4.4}$$

in which $\underset{\sim}{U}^k$ is the kth iterate of a sequence that, hopefully, converges to the solution $\underset{\sim}{U}$. Equations (4.4) are a linear set for $\underset{\sim}{U}^{k+1}$ if $\underset{\sim}{U}^k$ is known. The initial iterate $\underset{\sim}{U}^1$ is assumed: either it is assumed to be the solution obtained at the last load step, or it is assumed to be zero. Convergence is defined in the numerical computations if the magnitudes of each corresponding element in two successive iterates $\underset{\sim}{U}^{N-1}$ and $\underset{\sim}{U}^N$ differ by less than a prescribed error tolerance.

4.2.1 ELEMENT DESCRIPTION

In Figure 16 on page 72, a two-noded beam-column element is shown. There are seven degrees of freedom per node. The large number of degrees of freedom per node imposes indirect restrictions on the interpolation: the order of the interpolation functions is related to the number of de-

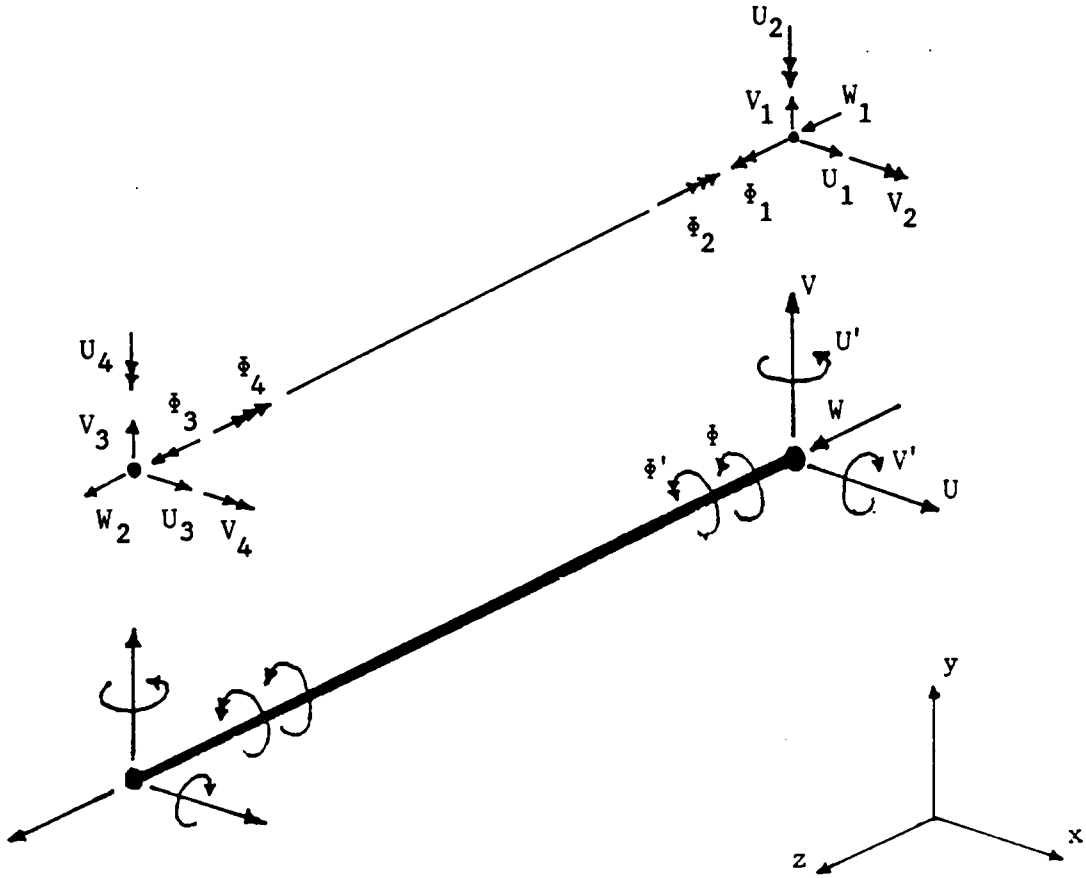

Figure 16. Schematic representation of the beam-column element

grees of freedom in an element. Thus, elements of large number of nodes are not desirable. For three-noded elements, for example, the interpolation polynomials have order twenty one. It is felt that comparable details can also be achieved by refining the mesh with large number of two-noded elements.

The fourteen degrees of freedom in the two-noded element can be identified as four distinct groups. Displacement W at each node associates with the axial deformation. The quantities U and U' (at each node) associate with flexural displacements in the x-direction and V and V' flexural displacements in the y-direction. The fourth group containing Φ and Φ' is related to the torsional deformations. For the axial displacements, the interpolation is linear,

$$W(z) = \sum_{N=1}^{2} {}^{w}\psi_i \; W_i \qquad (4.5)$$

$${}^{w}\psi_1 = 1 - \frac{z}{h} \qquad {}^{w}\psi_2 = \frac{z}{h}$$

where h is element length and z is a local coordinate. For each of the three remaining groups, the U's, V's and Φ's take on the same interpolation form of Hermitian cubics; i.e.,

$$\underset{\sim}{U}(z) = \sum_{N=1}^{4} {}^{u}\psi_i \; \underset{\sim}{U}_i$$

$${}^{u}\psi_1 = 1 - 3\left(\frac{z}{h}\right)^2 + 2\left(\frac{z}{h}\right)^3 \qquad {}^{u}\psi_2 = -z\left(1 - \frac{z}{h}\right)^2 \qquad (4.6)$$

$${}^{u}\psi_3 = 3\left(\frac{z}{h}\right)^2 - 2\left(\frac{z}{h}\right)^3 \qquad {}^{u}\psi_4 = -z\left[\left(\frac{z}{h}\right)^2 - \frac{z}{h}\right]$$

where the displacement vectors $\underset{\sim}{U}$ and $\underset{\sim}{U}_i$ are

$$\underset{\sim}{U} = \begin{bmatrix} U(z) \\ V(z) \\ \Phi(z) \end{bmatrix}$$

$$\underset{\sim}{U}_i = \begin{bmatrix} U_i \\ V_i \\ \Phi_i \end{bmatrix} \tag{4.7}$$

The derivation of the element stiffness matrix begins with the variational form of the nonlinear equilibrium equations. Each of the four equations is multiplied by a separate test function and integrated over the domain of a typical element ($z_e < z < z_{e+1}$). Then integration by parts is performed such that the highest derivative on W that appears is the first derivative, and the highest derivatives on U, V, and Φ that appear are second derivatives. At this point the variational equations and associated boundary conditions are complete. However, it is necessary to obtain the iterative form of the stiffness matrix per Equation (4.4) and not the actual stiffness matrix per Equation (4.3). Thus, the iterative form of the variational equations are obtained by a quasi-linearization process.

As an example of this quasi-linearization process, consider the nonlinear term

$$I_1 = \int_{z_e}^{z_{e+1}} (\widetilde{U}\, V'\, \Phi''')\, dz$$

in which $\widetilde{U}(z)$ denotes the test function. This term is integrated by parts to get

$$I_1 = -\int_{z_e}^{z_{e+1}} (V'\, \Phi''\, \widetilde{U}' + V''\, \Phi''\, \widetilde{U})\, dz + V'\, \Phi''\, \widetilde{U}\Big|_{z_e}^{z_{e+1}}$$

The nonlinear terms in V and Φ are replaced by the iterative form

$$I_1 = -\frac{1}{2}\int_{z_e}^{z_{e+1}} [(V^k)'(\Phi^{k+1})''\tilde{U}' + (\Phi^k)''(V^{k+1})'\tilde{U}' + (V^k)''(\Phi^{k+1})''\tilde{U}$$

$$+ (\Phi^k)''(V^{k+1})''\tilde{U}]\, dz + \frac{1}{2}[(V^k)'(\Phi^{k+1})'' + (\Phi^k)''(V^{k+1})']\,\tilde{U}\Big|_{z_e}^{z_{e+1}}$$

in which the superscript k denotes the kth iterate and superscript k+1 denotes the k+1st iterate. The kth iterate is assumed to be known. When the kth and k+1st iterate of a dependent variable are equal the exact value of that variable, then an integral such as I_1 is equal to its exact value. The iterative form of the variational equations obtained from the nonlinear equilibrium equations by the process just described are shown in Figure 17 on page 76. To save on writing, the kth iterates are written with an overbar, and the k+1st iterates are not superscripted in the figure. Also the boundary terms are not explicitly shown, but are indicated by the letters B.C. in brackets.

The finite element representations of the displacement field, Equation (4.5) and (4.6), are substituted into the iterative form of the variational equations and explicit integrations over the element's length are performed. The linear portion of the element stiffness matrix is written in the partitioned form

$$[K]_L = \begin{bmatrix} [K_{11}]_L & [K_{12}]_L \\ [K_{21}]_L & [K_{22}]_L \end{bmatrix}$$

in which each of the partitioned matrices are 7x7 and $[K_{21}]_L^T = [K_{12}]_L$.

$$\int_{z_e}^{z_{e+1}} A\, W'\, \hat{W}'\, dz = [B.C.]$$

$$\int_{z_e}^{z_{e+1}} I_{yy}\, U''\, \hat{U}'' + H_s\, \Phi''\, \hat{U}' - \tfrac{1}{2} I_{xx} (\bar{\Phi}\, V''\, \hat{U}'' + \bar{V}''\, \Phi\, \hat{U}'')$$
$$+ \tfrac{1}{2} H_c (6\, \bar{\Phi}'\, \Phi'\, \hat{U}' + 4\, \bar{\Phi}''\, \Phi'\, \hat{U} + 4\, \bar{\Phi}'\, \Phi''\, \hat{U}$$
$$+ \bar{\Phi}\, \Phi''\, \hat{U}' + \bar{\Phi}''\, \Phi\, \hat{U}')$$
$$+ \tfrac{1}{2} A\, \bar{W}' (U' + y_p \Phi')\, \hat{U}' + \tfrac{1}{2} A\, (\bar{U}' + y_p\, \bar{\Phi}')\, W'\, \hat{U}'\, dz = [B.C.]$$

$$\int_{z_e}^{z_{e+1}} I_{xx} V''\, \hat{V}'' - H_c\, \Phi''\, \hat{V}' + \tfrac{1}{2} I_{yy} (\bar{\Phi}\, U''\, \hat{V}'' + \bar{U}''\, \Phi\, \hat{V}'')$$
$$+ \tfrac{1}{2} H_s (6\, \bar{\Phi}'\, \Phi'\, \hat{V}' + 4\, \bar{\Phi}''\, \Phi'\, \hat{V} + 4\, \bar{\Phi}'\, \Phi''\, \hat{V}$$
$$+ \bar{\Phi}\, \Phi''\, \hat{V}' + \bar{\Phi}''\, \Phi\, \hat{V}')$$
$$+ \tfrac{1}{2} A\, \bar{W}' (V' - x_p\, \Phi')\, \hat{V}' + \tfrac{1}{2} A\, (\bar{V}' - x_p\, \bar{\Phi}')\, W'\, \hat{V}'\, dz = [B.C.]$$

$$\int_{z_e}^{z_{e+1}} I_{\omega\omega}\, \Phi''\, \tilde{\Phi}'' + H_c\, V''\, \tilde{\Phi}' - H_s\, U''\, \tilde{\Phi}' + JG\, \Phi'\, \tilde{\Phi}'$$
$$+ \tfrac{1}{2} A\, \bar{W}' (y_p\, U' - x_p\, V')\, \tilde{\Phi}' + \tfrac{1}{2} A\, (y_p\, \bar{U}' - x_p\, \bar{V}')\, W'\, \tilde{\Phi}'$$
$$- \tfrac{1}{2} (I_{xx} - I_{yy}) (\bar{U}''\, V''\, \tilde{\Phi} + \bar{V}''\, U''\, \tilde{\Phi})$$
$$+ \tfrac{1}{2} H_c (\bar{\Phi}'\, U'\, \tilde{\Phi}' + \bar{U}'\, \Phi'\, \tilde{\Phi}' + \bar{\Phi}''\, U'\, \tilde{\Phi} + \bar{U}'\, \Phi''\, \tilde{\Phi})$$
$$+ \tfrac{1}{2} H_s (\bar{\Phi}'\, V'\, \tilde{\Phi}' + \bar{V}'\, \Phi'\, \tilde{\Phi}' + \bar{\Phi}''\, V'\, \tilde{\Phi} + \bar{V}'\, \Phi''\, \tilde{\Phi})$$
$$+ \tfrac{1}{2} A\, R_p^2\, (\bar{\Phi}'\, W'\, \tilde{\Phi}' + \bar{W}'\, \Phi'\, \tilde{\Phi}')$$
$$- \tfrac{1}{2} K_y\, I_{yy} (\bar{U}''\, \Phi'\, \tilde{\Phi}' + \bar{\Phi}'\, U''\, \tilde{\Phi}') - \tfrac{1}{2} K_x\, I_{xx} (\bar{V}''\, \Phi'\, \tilde{\Phi}' + \bar{\Phi}'\, V''\, \tilde{\Phi}')$$
$$- \tfrac{1}{2} K_\omega\, I_{\omega\omega} (\bar{\Phi}''\, \Phi'\, \tilde{\Phi}' + \bar{\Phi}'\, \Phi''\, \tilde{\Phi}') + H_s (\bar{\Phi}'\, \Phi'\, \tilde{\Phi}')\, dz = [B.C.]$$

Figure 17. The variational equations

The 7x7 partitioned matrices are shown in Figure 18 on page 78. The remaining stiffness elements, which originate from the nonlinear terms are given in Appendix B.

4.3 COMPUTER CODE: FEMNL

A computer code FEMNL was written to implement the iterative finite element solution described in Section 4.2 . The flow chart of FEMNL can be found in Figure 19 on page 81. The input data is read in through three different units, and will be discussed in Section 4.3.1. The main program can be divided into two parts. The first part consists of establishing connectivity in the domain and computation of shape functions and their derivatives. To establish connectivity in the one-dimensional domain, two connectivity matrices are generated. The latter are used internally in the computer code. Subroutine SHAPE computes shape functions and their derivatives numerically at various Gaussian points. The second part consists of an iterative scheme, and a subroutine INCORE is called repeatedly from the main program. Within INCORE two subroutines, COEFF and STIFF, and two IMSL subroutines, LINV2F and VMULFF, are called. COEFF is used to calculate the stiffness terms that depend on the last iterate, and assemble the element stiffness matrix. The stiffness terms that depend on the last iterate are called nonlinear coefficients. STIFF is used to assemble the global stiffness matrix and impose the boundary conditions. LINV2F is for inversion and VMULFF for multiplication. Together they are used to implement the iterative scheme. At each load level, the iteration procedure is repeated until the number of iterations reaches a predeter-

$$[K_{11}]_L =$$

$$\begin{bmatrix}
A(1/h) & 0 & 0 & 0 & 0 & 0 & 0 \\
0 & I_{yy}(12/h^3) & 0 & H_s(0) & I_{yy}(-6/h^2) & 0 & H_s(-1/h) \\
0 & 0 & I_{xx}(12/h^3) & -H_c(0) & 0 & I_{xx}(-6/h^2) & -H_c(-1/h) \\
0 & -H_s(0) & H_c(0) & I_{\omega\omega}(12/h^3) + JG(6/5h) & -H_s(-1/h) & H_c(-1/h) & I_{\omega\omega}(-6/h^2) + JG(-1/10) \\
0 & I_{yy}(-6/h^2) & 0 & H_s(1/h) & I_{yy}(4/h) & 0 & H_s(-1/2) \\
0 & 0 & I_{xx}(-6/h^2) & -H_c(1/h) & 0 & I_{xx}(4/h) & -H_c(-1/2) \\
0 & -H_s(1/h) & H_c(1/h) & I_{\omega\omega}(-6/h^2) + JG(-1/h) & -H_s(-1/2) & H_c(-1/2) & I_{\omega\omega}(2/h) + JG(2h/15)
\end{bmatrix}$$

Figure 18. The linear portion of element stiffness matrix $[\ K\ ]_L$

$$[K_{12}]_L =$$

$$\begin{bmatrix}
A(-1/h) & 0 & 0 & 0 & 0 & 0 & 0 \\
0 & I_{yy}(-12/h^3) & 0 & H_s(0) & I_{yy}(-6/h^2) & 0 & H_s(1/h) \\
0 & 0 & I_{xx}(-12/h^3) & -H_c(0) & 0 & I_{xx}(-6/h^2) & -H_c(1/h) \\
0 & -H_s(0) & H_c(0) & I_{\omega\omega}(-12/h^3) + JG(-6/5h) & -H_s(1/h) & H_c(0) & I_{\omega\omega}(-6/h^2) + JG(-1/10) \\
0 & I_{xx}(6/h^2) & 0 & H_s(-1/h) & I_{yy}(2/h) & 0 & H_s(-1/2) \\
0 & 0 & I_{xx}(6/h^2) & -H_c(1/h) & 0 & I_{xx}(2/h) & -H_c(-1/2) \\
0 & -H_s(-1/h) & H_c(-1/h) & I_{\omega\omega}(6/h^2) + JG(1/10) & -H_s(-1/2) & H_c(-1/2) & I_{\omega\omega}(2/h) + JG(-1/30)
\end{bmatrix}$$

$$[K_{22}]_L =$$

$$\begin{bmatrix}
A(1/h) & 0 & 0 & 0 & 0 & 0 & 0 \\
0 & I_{yy}(12/h^3) & 0 & H_s(0) & I_{yy}(6/h^2) & 0 & H_s(-1/h) \\
0 & 0 & I_{xx}(12/h^3) & -H_c(0) & 0 & I_{xx}(6/h^2) & -H_c(-1/h) \\
0 & -H_s(0) & H_c(0) & I_{\omega\omega}(12/h^3) + JG_1(6/5h) & -H_s(-1/h) & H_c(-1/h) & I_{\omega\omega}(6/h^2) + JG_1(1/10) \\
0 & I_{yy}(6/h^2) & 0 & H_s(1/h) & I_{yy}(4/h) & 0 & H_s(1/2) \\
0 & 0 & I_{xx}(6/h^2) & -H_c(1/h) & 0 & I_{xx}(4/h) & -H_c(1/2) \\
0 & -H_s(1/h) & H_c(1/h) & I_{\omega\omega}(6/h^2) + JG_1(1/10) & -H_s(1/2) & H_c(1/2) & I_{\omega\omega}(4/h) + JG_1(2h/15)
\end{bmatrix}$$

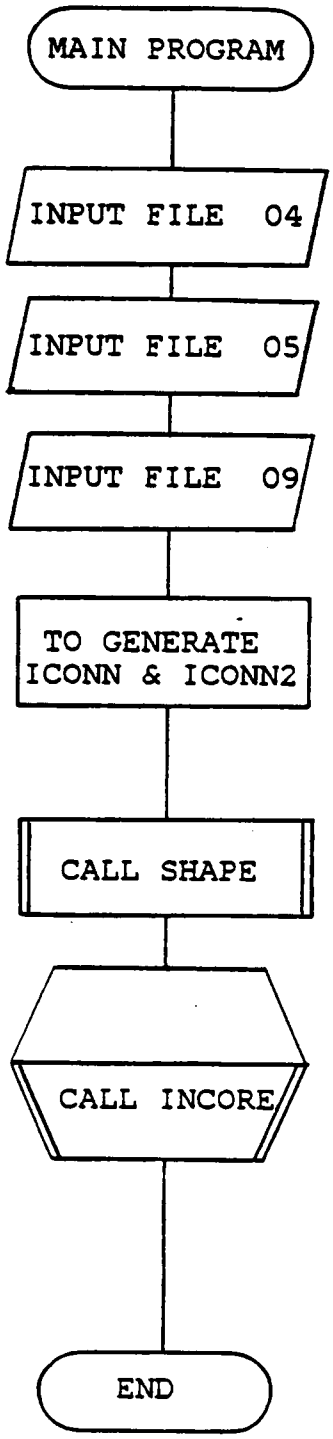

Figure 19. Flow chart of code FEMNL

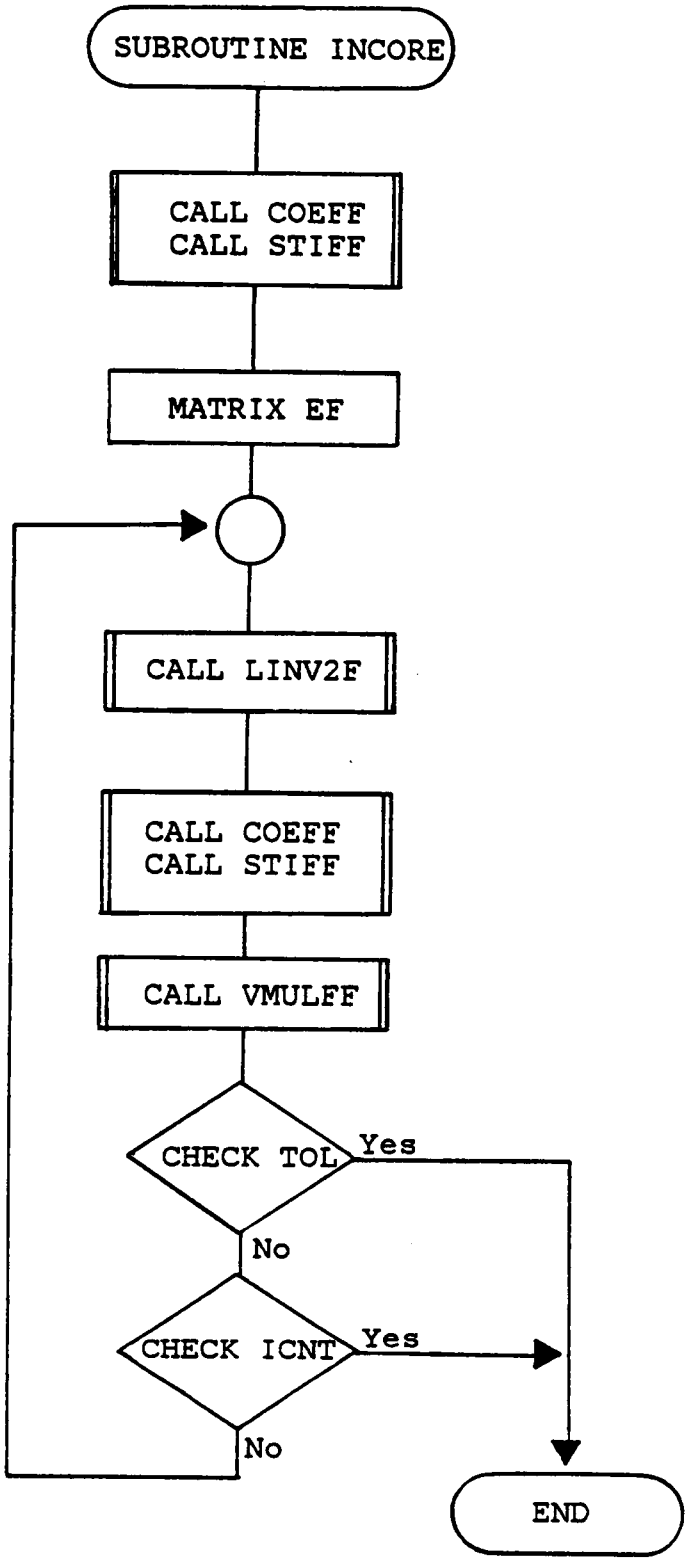

Figure 19 ..concluded

mined limit, or when the tolerance on displacements is observed. In all but the first iteration, the nonlinear coefficients are computed prior to the assembly process. In the first iteration, nonlinear coefficients are assigned zero values.

4.3.1 INPUT

The computer code requires three different sources of input for the analysis. The cross-sectional properties, which are essential in Vlasov's theory, are required. As before, the output from VLASOV2 can be used directly; data are read in through input unit 04. The second source of input contains finite element data and is read in through unit 05. A typical data file can be found in Figure 20 on page 84. The data file contains three control parameters: length of the domain (mesh), the restrained degrees of freedom, and the tolerance of displacements in the solution. The control parameters are NPRNT, NEM, and NBDY which indicate the amount of details to be included in the output, the number of elements to be used in the domain, and the number of restrained degrees of freedom, respectively. Control parameter NPRNT will be discussed in Section 4.3.4. The third source is on loading: the initial load, the increment size, the number of increments, and the type of load imperfection. The first three load parameters can control the analysis to be carried out at a single load level as well as in a scaled range. The fourth load parameter will be discussed in the forthcoming section on Loading and Boundary Condi-

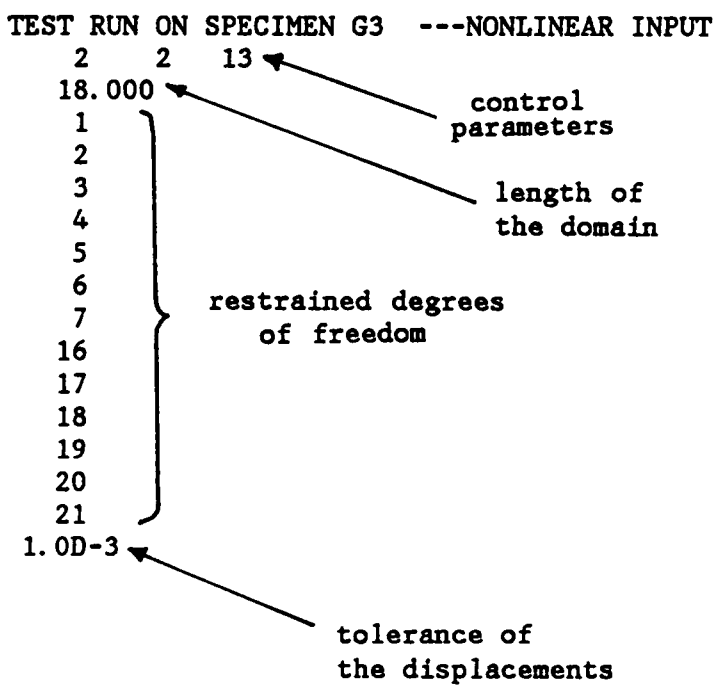

Figure 20. Nonlinear finite element data file input

tions. This data file is read interactively so as to allow a quick turn-around.

4.3.2 ASSEMBLY PROCESS

In the assembly process, the nonlinear coefficients have to be evaluated to allow the computation of the element stiffness matrix, then the global stiffness matrix. The nonlinear coefficients are obtained from the previous iterates and are evaluated at four Guassian points in every element. The element stiffness matrix is then obtained by four-point Guassian integration. It is followed by an assembly routine to give the global stiffness matrix. The values of nonlinear coefficients are generally different in each element and they change after each iteration, the assembly process has to be repeated in each iteration to update the element stiffness matrix.

4.3.3 LOADING AND BOUNDARY CONDITIONS

The concentric axial compressive load acting alone cannot drive the nonlinear solution process. An imperfection must be present to cause lateral deflections. To faciliate the nonlinear solution, there are three options available. One is to introduce eccentricity into the end load, which will cause non-zero moment resultants. The moments give rise to the displacements associated with flexure. The second is to introduce small distributed load along the length of the specimen. The distributed load will cause bending and/or torsion of the bar which will interact with the

axial load through the nonlinear terms. The third option is to prescribe an initial imperfection in the shape of the column. For this approach, the imperfection is usually taken geometrically in form of a buckling mode shape along the length. Of the three methods available, the second method was the easiest method to implement. The geometric imperfection is complex since the formulation will have to be changed to describe the new geometry. The introduction of the distributed load does not involve new interpolation functions or any other kind of major re-structuring. The result will be discussed in the following chapter.

The distributed load is given a small value compared to the axial compressive load. Both loads are included in the element force vectors, which are assembled into the global force vector. The distributed load magnitude and axial load are increased proportionally. The nonlinearity portion of the load vector (last term in Equation (2.39)) is neglected in the iterative scheme.

Once the assembly process is accomplished, boundary conditions are applied. The rows and columns in the global stiffness matrix that are associated with the specified degrees of freedom are eliminated. The corresponding force terms in the global force vector are removed as well; these terms can be calculated directly after the assembled equations are solved. The order of both the global stiffness matrix and the global force vector are reduced as a result.

Seven boundary conditions are needed at each end of the beam column. In the case of clamped conditions at both ends, seven essential boundary conditions are prescribed at one end. At the other end, the natural boundary condition, or the axial compressive force, that associates with

Seven boundary conditions are needed at each end of the beam column. In the case of clamped conditions at both ends, seven essential boundary conditions are prescribed at one end. At the other end, the natural boundary condition, or the axial compressive force, that associates with the axial displacement is prescribed in additional to six other essential boundary conditions.

4.3.4 OUTPUT

The size of the output from FEMNL can be controlled in the input file. The amount of details is governed by the integral input value of NPRNT (1-3): a higher value of NPRNT leads to more lengthy output.

The output basically consists of a title, cross-sectional properties of the beam-column, details of discretization, and iteration results. The results of iteration at each load level consist of the current displacement vector, and the difference of the same vector between two iterations. Based on the current values of the displacements, a force vector is computed and compared to the actual force vector. The comparison provides a cross-check to the solution.

4.4 DISCUSSION

The solution method in the nonlinear analysis is complex. While the iterative procedure at specified load level is automatic, the choice of load level and load increments has to be made by the user. From experience, a nonlinear analysis should be conducted, after linear bifurcation

analysis, in two separate runs. In the first run, the buckling load from linear bifurcation is used as a first estimate to the range of load level for iteration. The buckling mode should be noted from the linear bifurcation analysis so that the distributed load can be selected to trigger displacements that are associated with the buckling mode. Large and regular load increments are used starting from a small value up to the bifurcation load. The results at these regular intervals form an overall picture of the loading history. The buckling load, in this analysis, is defined as the lowest load at which one or more displacements become large. Near the buckling load, the global stiffness matrix is singular or near-singular therefore the displacement vector takes on large or unpredictable values. Beyond the buckling load, results are unstable and significant changes in displacements are observed in successive iterations. To acquire a better estimate of the buckling load, the nonlinear analysis should be conducted with small load increments starting from some load level lower than the buckling load (estimated in the first run).

At the present time, estimation of the buckling load is not automatic; the results of a nonlinear analysis have to be plotted manually. Close to the buckling load, the displacements become excessive. This is usually accompanied by large changes in the displacement vector in successive iterations. Furthermore, at load level higher that the buckling load, the calculated force vector shows sizable discrepancies from the assembled force vector. This suggest instability of the system beyond the buckling load. The results of the nonlinear analysis will be presented in the next chapter.

5.0 RESULTS AND DATA

5.1 EXPERIMENTAL DATA

To determine the credibility of the linear bifurcation analysis and the nonlinear analysis, the results of the two analyses are compared to available experimental data.

Two sources of experimental data on global buckling of thin-walled laminated composite beams with open cross section were used. The first source is from published data in the literature. It is found that very few experimental data are available in the area of torsional-flexural buckling of laminated composite columns. Of the existing data, experimental investigations tended to be conservative and restrictive. The second source is from the work of Tyahla [52].

A paper by Chailleux et al [53] includes eight specimens of flat rectangular laminates. All specimens are symmetric and there are angle-ply lay-ups, cross-ply lay-ups and unidirectional lay-ups. Two fiber systems, glass and boron, and two matrix systems, resin epoxy and aluminium, are used in combination. The geometry of these specimens are the simplest possible for beam columns. However, analyses of these specimens is not possible, because there is insufficient data on the engineering properties of the fibers and matrices. As a point of interest, the authors discussed in some length on the use of Southwell plots to determine the buckling loads of composite beam columns and plates.

Lee and Hewson [54] conducted tests on unidirectional channel sections for global and local buckling. The local buckling test data and results will not be discussed in this text. The matrix system used was Araldite MY753/HY956 from Ciba-Giegy. Glass and carbon fibers were used to make up two groups of specimens. These channel sections have various lengths and flange-to-web ratios (the width of the web is kept constant). A typical section is shown in Figure 21 on page 91. Lee and Hewson attempted to correlate these two parameters based on the test results. Also included in the paper are the analytical results from the linear bifurcation analysis. The approach used in the paper [54] is apparently similar to that of Vlasov [4, p. 330; 24, pp. 185-189]. The distinction lies in the way the section properties are being calculated. It will be shown later in the chapter that these two methods yield significant discrepancies. There are six glass fiber-reinforced specimens and twelve carbon fiber-reinforced specimens. They are listed in Table 1 and 2, respectively. In the tables, each specimen is assigned a specimen number for identification (this identification may not be the same as one assigned in the original research papers). The flange-to-web ratio, the length and the experimental buckling loads are also displayed.

In Tyahla's research [52], thin-walled open sections of general lay-ups were tested. The specimens were clamped at both ends, and subjected to axial compression. Four specimens buckled in global modes and were labelled as group two specimens. They consist of three channels and one zee section. The lay-ups are either quasi-isotropic, $[\pm 45/0/90]_{2s}$, or $[\pm 45/\mp 45/90/0_3]_s$. Details are listed in Table 3 in the same form as described for Table 1 and Table 2. Experimental data available from the

Channel Section

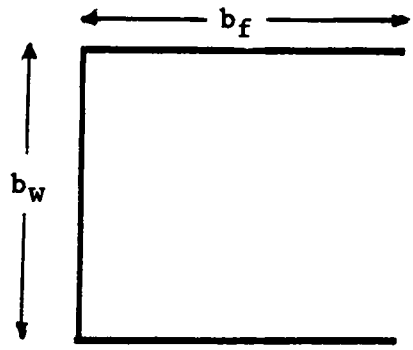

Flange-to-web ratio = b_f / b_w

Zee Section

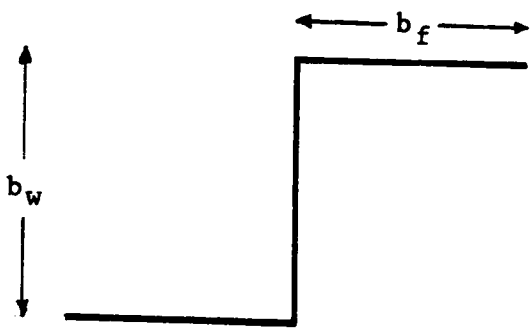

Figure 21. Cross sections of test specimens

Table 1. Unidirectional Glass Fiber-Reinforced Channel Specimens [54].

SPECIMEN NUMBER	FLANGE/WEB RATIO	LENGTH IN INCHES	BUCKLING LOAD IN POUNDS (MODE)*
G1	0.36	18.504	1169.1 (F)
G2	0.46	18.504	2045.9 (F)
G3	0.52	18.110	2877.7 (F)
G4	0.60	15.354	4451.4 (T/F)
G5	0.85	15.945	3821.9 (T/F)
G6	1.03	17.913	3282.9 (T/F)

* F= FLEXURE F/T = FLEXURE AND TORSION

Table 2. Unidirectional Carbon Fiber-Reinforced Channel Specimens [54].

SPECIMEN NUMBER	FLANGE/WEB RATIO	LENGTH IN INCHES	BUCKLING LOAD IN POUNDS (MODE)*
C1	0.17	9.843	2383.1 (F)
C2	0.17	13.780	1641.2 (F)
C3	0.17	17.717	966.7 (F)
C4	0.50	13.780	6812.1 (T/F)
C5	0.61	13.780	9644.8 (T/F)
C6	0.61	17.717	7104.3 (T/F)
C7	0.61	21.654	5283.2 (T/F)
C8	0.39	9.843	11488.3 (F)
C9	0.39	13.780	9015.3 (F)
C10	0.39	13.780	5530.6 (F)
C11	0.83	13.780	10004.5 (T/F)
C12	0.83	17.717	9240.1 (T/F)

* F= FLEXURE F/T = FLEXURE AND TORSION

Table 3. Graphite Fiber-Reinforced Specimens [52].

SPECIMEN NUMBER	LAY-UP	FLANGE/WEB RATIO	LENGTH IN INCHES	EXPERIMENTAL LOAD IN POUNDS (MODE)*
2-1 Channel	$[\pm 45/0/90]_{2s}$	1.0	19.00	7000.0 (T/F)
2-2 Channel	$[\pm 45/\mp 45/90/0_3]_s$	1.0	19.00	6830.0 (T/F)
2-3 Channel	$[\pm 45/0/90]_{2s}$	0.6	12.00	9670.0 (T/F)
2-4 Zee	$[\pm 45/0/90]_{2s}$	0.6	15.00	6540.0 (F)

* F=FLEXURE T/F=FLEXURE AND TORSION

tests include strain guage measurements at various stations along the specimens; readings from displacement transducers at mid-span and quarter-span; and readings from the crosshead monitor. These readings were taken with instantaneous records in time and load level. The loading history and gauge readings can be found in Appendix B.

5.2 LINEAR BIFURCATION

The linear bifurcation analysis described in Chapter 3 was implemented for the test specimens given in Table 1 to 3. Two computer codes are used, BUCKEQ and LBIFUR. The Computer Code BUCKEQ computes the bifurcation load as the lowest positive root to the characteristic polynomial (Equation (3.15)), and in due course the buckling mode is identified. In all cases, the predicted buckling modes agreed with the experimental observation. In code BUCKEQ the H-terms are neglected and the boundary conditions in torsion and flexure must be correlated (see Section 3.2). The computer code LBIFUR is based on a matrix eigenvalue analysis of a finite element representation of the stability boundary value problem. In the code LBIFUR the boundary conditions do not have to be correlated, and the H-terms are also neglected. However, a modified version of the code LBIFUR was written which incorporates the H-terms. The influence of the H-terms will be discussed later in this section. In Tables 4 and 5 bifurcation results are listed alongside with the analytical results provided by Lee and Hewson, against the experimental results. It can be seen that the results by Lee and Hewson are in the same range as the linear bifurcation results. The differences between the two

Table 4. Buckling Loads for the Unidirectional Glass Fiber-Reinforced Channel Specimens [54].

SPECIMEN NUMBER	EXPERIMENTAL LOAD IN POUNDS (MODE)*	ANALYTICAL RESULTS (LEE-HEWSON)	ANALYTICAL RESULTS (LBIFUR)
G1	1169.1 (F)	2967.6 (+159%)•	1458.0 (+24.7%)
G2	2045.9 (F)	3777.0 (+84.6%)	2765.9 (+35.2%)
G3	2877.7 (F)	4271.6 (+48.4%)	4015.3 (+39.5%)
G4	4451.4 (T/F)	6969.4 (+56.6%)	6366.3 (+43.0%)
G5	3821.9 (T/F)	6295.0 (+64.7%)	6690.6 (+75.1%)
G6	3282.9 (T/F)	6857.0 (+109%)	5971.4 (+81.9%)

* F=FLEXURE T/F=FLEXURE AND TORSION

• % discrepancy with respect to experimental buckling load

Table 5. Buckling Loads for the Unidirectional Carbon Fiber-Reinforced Channel Specimens [54].

SPECIMEN NUMBER	EXPERIMENTAL LOAD IN POUNDS (MODE)*	ANALYTICAL RESULTS (LEE-HEWSON)	ANALYTICAL RESULTS (LBIFUR)
C1	2383.1 (F)	2248.2 (-5.7%)	3159.0 (+32.6%)
C2	1641.2 (F)	1124.1 (-31.5%)	1611.8 (-1.8%)
C3	966.7 (F)	674.5 (-30.2%)	975.0 (-0.9%)
C4	6812.1 (T/F)	13264.4 (+94.7%)	15123.0 (+122%)
C5	9644.8 (T/F)	13938.9 (+44.5%)	18661.0 (+93.4%)
C6	7104.3 (T/F)	8992.8 (+26.6%)	11825.0 (+66.4%)
C7	5283.2 (T/F)	7643.9 (+44.7%)	8362.3 (+58.3%)
C8	11488.3 (F)	14613.3 (+27.2%)	20061.0 (+74.6%)
C9	9015.3 (F)	9217.6 (+2.2%)	11216.0 (+24.4%)
C10	5530.6 (F)	6295.0 (+13.8%)	7239.8 (+30.9%)
C11	10004.5 (T/F)	18884.9 (+88.8%)	24688.0 (+147%)
C12	9240.1 (T/F)	12814.8 (+38.7%)	15311.0 (+65.7%)

* F=FLEXURE T/F=FLEXURE AND TORSION

predictions are due to the different ways that are adopted in the calculation of cross-sectional properties. In Lee and Hewson, the method is based on Timoshenko's analysis [47, p.233]. The general discrepancies between bifurcation loads and experimental loads are from -1.8% to +74.9%, with an average of +30.7% for specimens that buckled in flexure; for specimens that buckled in coupled flexural-torsional mode, the range of discrepancies are from +41.0% to 146.8% with an average of 78%. The numerical results from LBIFUR are given in Tables 4 and 5 and not from BUCKEQ because the buckling loads computed from both codes are nearly the same.

In Table 6 the buckling loads from code LBIFUR are compared to the experimental data from Reference [52]. The discrepancies range from 41 to 56 percent with respect to the experimental buckling loads.

The results of the linear bifurcation are thought to be very unconservative as first approximations to the buckling loads. The linearization process in the bifurcation analysis allows a relatively simple analysis on one hand, but the mechanics of the problem is compromised. A better approximation can be expected if the nonlinear nature of the physical probelm is fully treated.

To complete the linear bifurcation analysis, the effects of the H-terms are investigated. In the modified version of LBIFUR, the H-terms are included. Specimens with off-axis lay-ups are chosen since the coupling between the bending and twisting modes, thus the H-terms, is expected to be predominant. They are all channel sections with flange to web ratio of unity and length of 19.0 inches. The comparision of analytical results from LBIFUR and the modified LBIFUR are presented in Table

Table 6. Buckling Loads for the Graphite Fiber-Reinforced Channel Specimens [52].

SPECIMEN NUMBER	LAY-UP	EXPERIMENTAL LOAD IN POUNDS (MODE)*	ANALYTICAL RESULTS (LBIFUR)
2-1 Channel	$[\pm 45/0/90]_{2s}$	7000.0 (T/F)	9872 (+41.0%)
2-2 Channel	$[+45/\mp 45/90/0_3]_s$	6830.0 (T/F)	12540 (+83.6%)
2-3 Channel	$[\pm 45/0/90]_{2s}$	9670.0 (T/F)	15830 (+63.7%)
2-4 Zee	$[\pm 45/0/90]_{2s}$	6540.0 (F)	10230 (+56.4%)

Table 7. Comparison of Buckling Loads computed by neglecting the H-terms (LBIFUR) and retaining the H-terms.

SPECIMEN NUMBER	LAY-UP	ANALYTICAL RESULTS (LBIFUR)	ANALYTICAL RESULTS (LBIFUR*)
2-1	$[\pm 45/0/90]_{2s}$	9872	9920
2-2	$[\pm 45/\mp 45/90/0_3]_s$	12540	12691
A1	$[\pm 45]_{2s}$	8101	8186
A2	$[\pm 30]_{2s}$	13101	13255
A3	$[\pm 15]_{2s}$	17550	17732

* modified verision of LBIFUR to include the H-terms

7. The first set of results are generated by the computer code BUCKEQ which solves the characteristic polynomial (Equation 3.11) with the H-terms being neglected. The second set of results are given by the modified version of LBIBUR. It is found that the difference in the bifurcation load is small, even for off-axis lay-ups. Thus, the procedure of neglecting the H-terms in linear bifurcation is a good approximation as originally given in Reference [5].

In Chapters One and Two, the Euler-Bernoulli beam theory on thin-walled open sections has been critized. A diversion at this point aims to confirm that Euler-Bernoulli beam theory is inadequate for thin-walled open sections. To generate the relevant data, BUCKEQ is modified to accommodate the plane sections remain plane assumption. The second sectorial moment of area is reduced to zero. This quantity is the resistance of the thin-walled section to warping, which contributes to the overall torsional rigidity. Some results are obtained for the glass-reinforced specimens for the purpose of illustration. In Table 8 results from the modified BUCKEQ are presented in the E.B. Beam Theory column, and are compared to results from linear bifurcation analysis (LBIFUR) and experimental data. It can be seen that the predictions of the flexurally buckled specimens are compatible to the results from LBIFUR, but are not compatible for the torsionally buckled specimens. The rigidity to resist warping in these thin-walled sections can be an order of magnitude higher than the torsional stiffness, GJ. Thus, the total torsional rigidity as a whole is underestimated. The prediction on flexural buckling is the same as Vlasov's linear bifurcation load; while prediction on flexural torsional buckling are vastly different. If Euler-Bernoulli theory is

Table 8. Buckling Loads for the Lee-Hewson Glass Fiber-Reinforced Channel Specimens [54].

SPECIMEN NUMBER	EXPERIMENTAL BUCKLING LOAD IN POUNDS (MODE)*	ANALYTICAL RESULT (LBIFUR)	E.B. BEAM THEORY•
G1	1169.1 (F)	1458.0	1458.0
G2	2045.9 (F)	2765.8	2765.9
G3	2877.7 (F)	4015.2	3283.4
G4	4451.4 (T/F)	6366.3	2971.4
G5	3821.9 (T/F)	6690.6	2086.5
G6	3282.9 (T/F)	5971.4	1660.5

* F=FLEXURE T/F=FLEXURE AND TORSION

• EULER-BERNOULLI BEAM THEORY

used for thin-walled open section, over-design can be expected for sections which buckle in the flexural torsional mode.

5.3 NONLINEAR ANALYSIS

Output from the nonlinear finite element code can contain variable amount of information. The basic, the least detailed, output contains the numerical values of the cross-sectional properties, the length of the domain, the degree of discretization, the tolerance specified on the displacements, the restrained degrees of freedom, and the connectivity in the domain. Second part of the output is given at each load level, after each iteration. It contains the assembled force vector, the computed force vector, computed displacement vector, and the change in displacement vector due to each iteration. The computed force vector provides a cross-check at each iteration point. In addition, information on the element stiffness matrix, and the global stiffness matrix at each iteration point can also be printed.

The nonlinear analysis results are given in terms of the axial displacement, lateral displacements, and the rotation. At the buckling load, the displacements (or rotation) become excessive. For practical purposes, the critical load is taken as the lowest load at which one or more of the displacements (or rotation) change in order of magnitude. At the present time, the buckling load has to be determined graphically. The displacement solution is plotted against the compressive load, and the buckling load is identified using the criterion above.

Results of the nonlinear analysis can be found in Tables 9, 10 and 11. In these tables the nonlinear results are compared to the linear bifurcation results, the experimental results, and other analytical results, if possible. The general discrepancies range from -9.1% to +99.9%. The average is about 36%. The above figures are for specimens that buckled in the coupled mode. The nonlinear analysis is unable to deliver solutions for specimens that buckled in pure flexure or torsion. Compared to the discrepancies between the experimental results and the linear bifurcation results, which range from +4.1% to +146%, the discrepancies between the experimental results and the nonlinear solution analysis, represent an improvement of 15% to 60% with respect to the experimental buckling loads.

The nonlinear analysis has been conducted on six glass specimens and twelve carbon specimens from Lee and Hewson, and four graphite specimens from Tyhala. The patterns of result are very similiar: a typical displacement curve would have a short linear portion, followed by a region of decreasing slope; finally the slope becomes very small, and change of displacement with respect to change of load becomes excessive. It is, therefore, felt that presentations of all the nonlinear data are unnecessary. For illustration purposes, analytical solutions for three specimens, G5 , C12 and 2-2 are presented (see Figure 22 on page 108, Figure 23 on page 109, and Figure 24 on page 110, respectively). In these three plots, displacements are plotted against concentric end load, up to the buckling value. The plotted points are solution points from FEMNL, they are joined by cubic splines. Results beyond this load, by definition, are unstable and meaningless. It can be seen, in these three cases, that

Table 9. Glass Fiber-Reinforced Channel Specimens [54].

SPECIMEN NUMBER	EXPERIMENTAL LOAD IN POUNDS (MODE)	ANALYTICAL RESULTS (LEE-HEWSON)	ANALYTICAL RESULTS (LBIFUR)	NONLINEAR RESULTS (FEMNL)
G1	1169.1 (F)	2967.6	1458.0	---
G2	2045.9 (F)	3777.0	2765.9	---
G3	2877.7 (F)	4271.6	4015.3	---
G4	4451.4 (T/F)	6969.4 (+56.6%)	6366.3 (+43%)	5770.0 (+29.6%)
G5	3821.9 (T/F)	6295.0 (+64.7%)	6690.6 (+75%)	6100.0 (+59.6%)
G6	3282.9 (T/F)	6857.0 (109%)	5971.4 (+81.9%)	5400.0 (+64.5%)

Table 10. Carbon Fiber-Reinforced Channel Specimens [54].

SPECIMEN NUMBER	EXPERIMENTAL LOAD IN POUNDS (MODE)	ANALYTICAL RESULTS (LEE-HEWSON)	ANALYTICAL RESULTS (LBIFUR)	NONLINEAR RESULTS (FEMNL)
C1	2383.1 (F)	2248.2	3159.0	---
C2	1641.2 (F)	1124.1	1611.8	---
C3	966.7 (F)	674.5	975.0	---
C4	6812.1 (T/F)	13264.4 (+94.7%)	15123.0 (+122%)	8400.0 (+23.3%)
C5	9644.8 (T/F)	13938.9 (+44.5%)	18661.0 (+93.5%)	11500.0 (+19.2%)
C6	7104.3 (T/F)	8992.8 (+26.6%)	11825.0 (+66.4%)	7800.0 (-1.5%)
C7	5283.2 (T/F)	7643.9 (+44.7%)	8362.3 (+58.3%)	4800.0 (-9.1%)
C8	11488.3 (F)	14613.3	20061.0	---
C9	9015.3 (F)	9217.6	11216.0	---
C10	5530.6 (F)	6295.0	7239.8	---
C11	10004.5 (T/F)	18884.9 (+88.8%)	24688.0 (+146.8%)	20000.0 (+99.9%)
C12	9240.1 (T/F)	12814.8 (+38.7%)	15311.0 (+65.7%)	9600.0 (+3.9%)

Table 11. Graphite Fiber-reinforced Specimens [52].

SPECIMEN NUMBER	LAY-UP	EXPERIMENTAL LOAD IN POUNDS (MODE)	ANALYTICAL RESULTS (LBIFUR)	NONLINEAR RESULTS (FEMNL)
2-1 Channel	$[\pm 45/0/90]_{2s}$	7000.0 (T/F)	9872 (41%)	6500.0 (-7.1%)
2-2 Channel	$[\pm 45/\mp 45/90/0_3]_s$	6830.0 (T/F)	12540 (83.6%)	8600.0 (+25.9%)
2-3 Channel	$[\pm 45/0/90]_{2s}$	9670.0 (T/F)	15830 (63.7%)	11400.0 (+17.9%)
2-4 Zee	$[\pm 45/0/90]_{2s}$	6540.0 (F)	10230	---

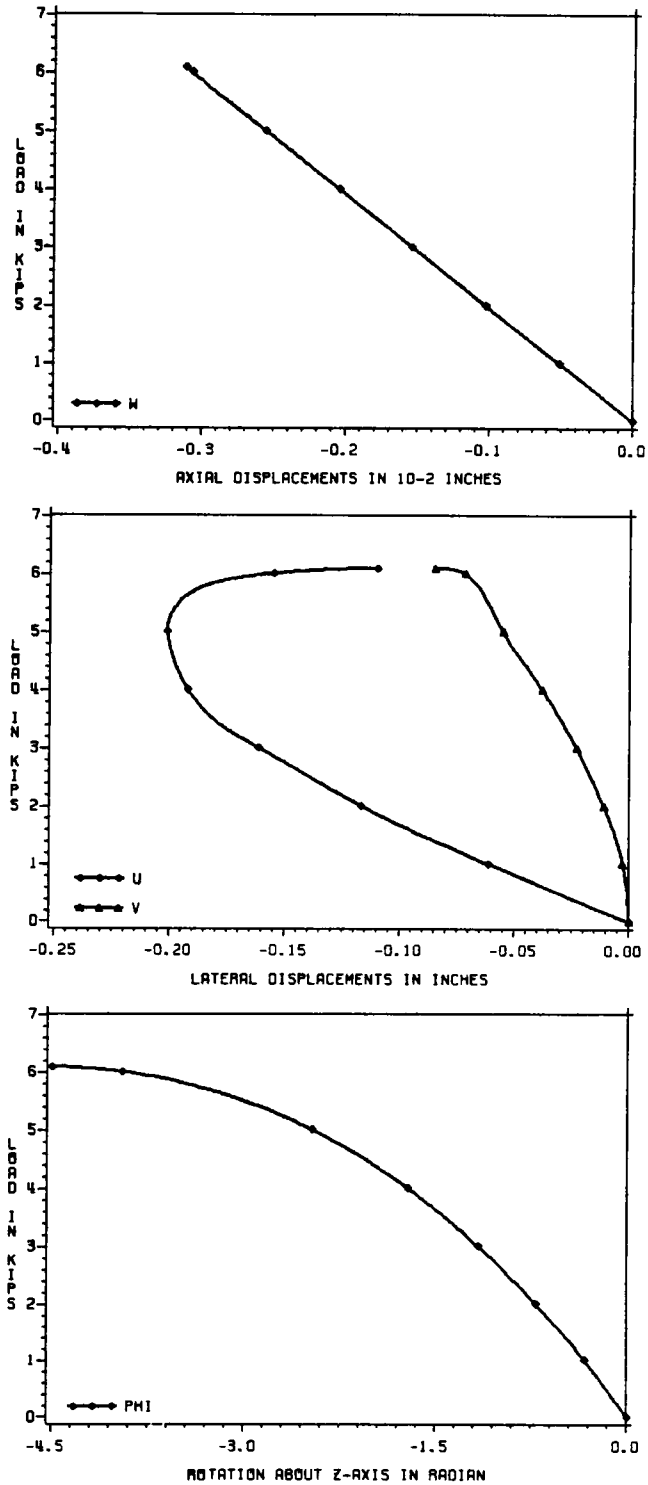

Figure 22. The nonlinear solution to specimen G5

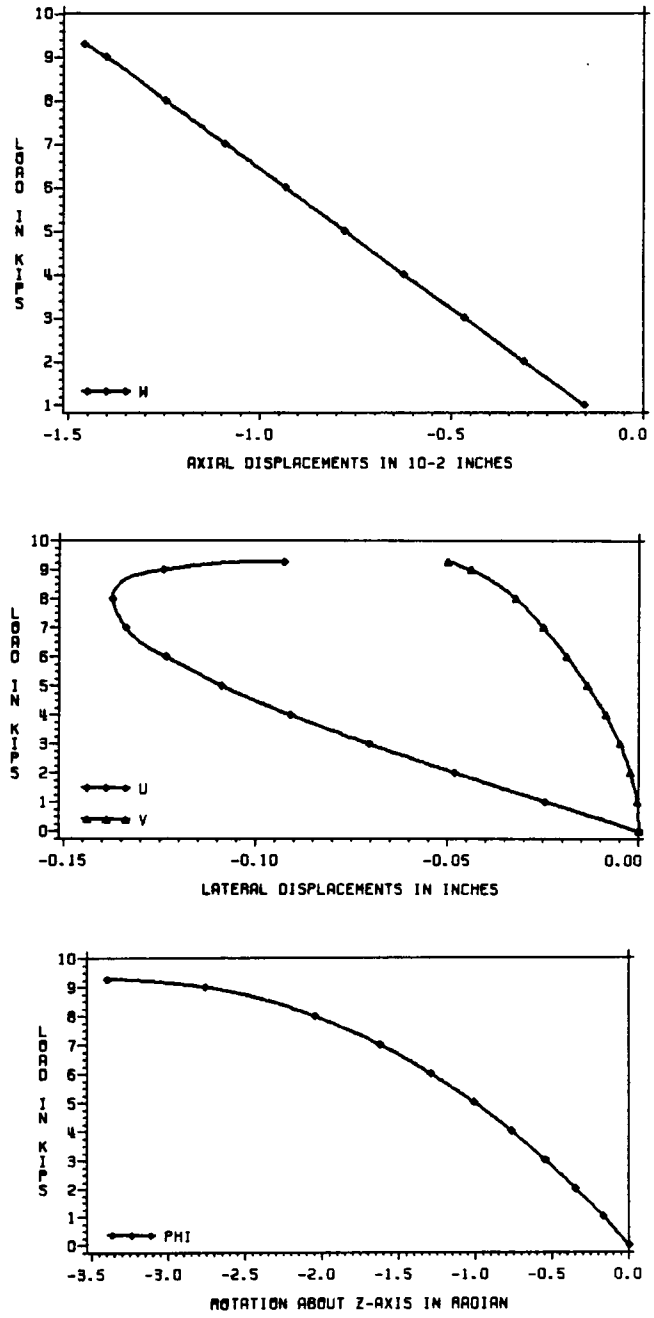

Figure 23. The nonlinear solution to specimen C12

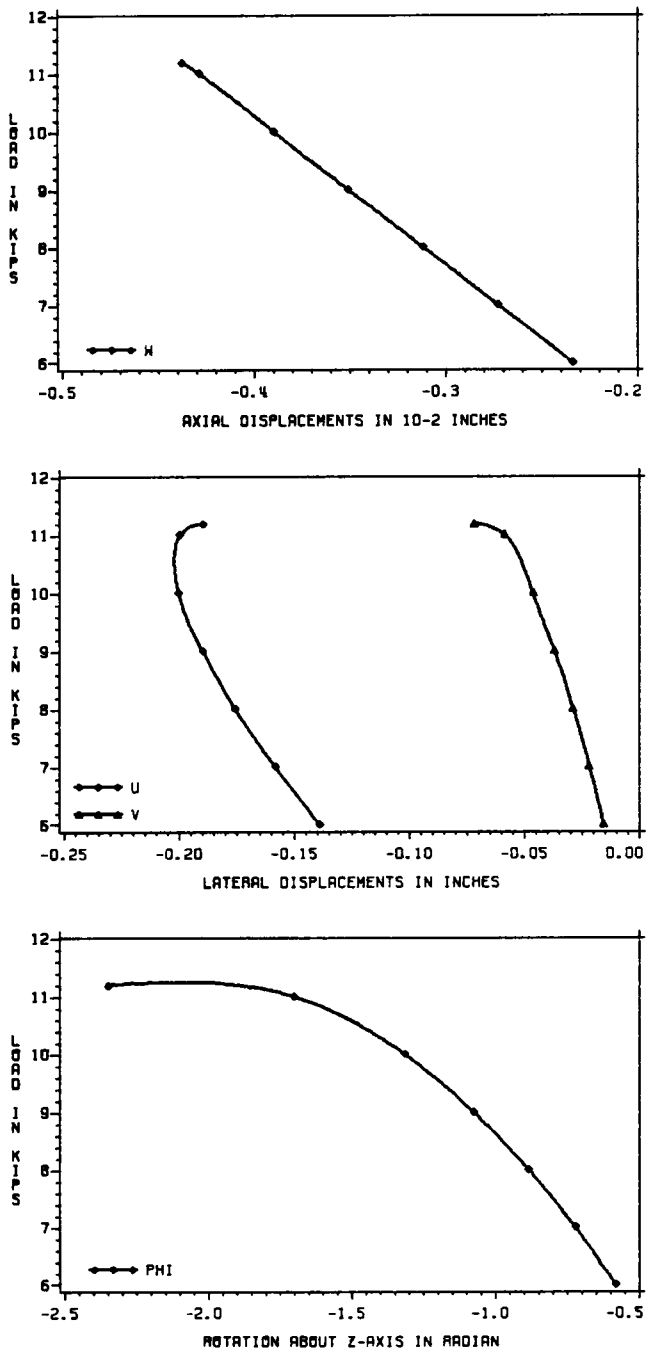

Figure 24. The nonlinear solution to specimen 2-2

the flexural torsional buckling phenomenon is driven by torsion: the onset of buckling is dominated by torsion. This should be distinguished from the case of pure torsional buckling which produces no lateral displacements.

The linear response of W is distracting in the context of nonlinear analysis. Such inconsistency can be traced back to the nature of the nonlinearity in Vlasov's theory. The latter does not cover all aspects of the geometric nonlinearity. Thus the interactions, or geometric coupling, of these displacements do not appear in the equilibrium equations.

6.0 CONCLUSIONS AND RECOMMENDATIONS

6.1 CONCLUSIONS

In extending Vlasov's thin-walled open section bar theory to include wall constructions of mid-plane symmetric laminated composite materials, Bauld and Tzeng [5] have shown additional coupling terms exist in the bar constitutive equations. These coupling terms are denoted by H_s, H_c, and H_q, and depend directly on the normal moment-twist curvature term D_{16} of classical lamination theory. The terms H_s, H_c, and H_q in the bar constitutive equations materially couple the bending and torsion of the bar. Thus, in the linear theory for mid-plane symmetric laminated bars it is possible to uncouple the bending and torsional equilibrium equations as is the case in Vlasov's theory for isotropic bars.

The essential geometric nonlinearity included in Vlasov's nonliner theory is the coupling between twist and lateral deflections. Bauld and Tzeng also include this geometric nonlinearity in the extended theory. The nonlinear equations are the basis for deriving the linear bifurcational buckling equations. For the test specimens analyzed in this thesis, the computed buckling loads were relatively unaffected by the H-terms in the bifurcation buckling analysis with respect to including them in the analysis. The linear bifurcation analysis is found to give unconservative predictions of buckling loads. In the cases where buckling loads from linear bifurcation analysis are compared to experimental

buckling loads, the discrepancies range from -1.8% to +146%, and the average is about 60%.

It has been shown that Euler-Bernoulli beam theory predicts buckling load poorly when the buckling mode is flexural-torsional coupled. The assumption of plane sections remain plane does not include the effects of warping thus the resistance to warping is not accounted for. The resistance of the bar to warping provides additional torsional rigidity, and is often of larger magnitude than the torsional stiffness GJ of the bar. Failure to include this additional rigidity under-estimates the buckling load where torsion plays a part in the buckling mode.

It should be pointed out that the extended theory also employs the Vlasov assumption that the mid-plane shear strain is zero. Thus, the extended theory a priori neglects shear-extension coupling. Strictly speaking a mid-plane symmetric laminate can have a nonzero value of A_{16} in classical lamination theory. The term A_{16} couples the normal axial force resultant to the mid-plane shear strain. The term A_{16} is zero for a balanced laminate (a laminate which has a $-\theta$ ply for every $+\theta$ ply). Thus, the Vlasov assumption is credible for a balanced and symmetric laminate, but is perhaps a little less credible if the laminate is symmetric but unbalanced. All laminate lay-ups considered for study in this thesis are of the balanced and symmetric type.

In the nonlinear analysis, initial imperfections are needed to faciliate the nonlinear solutions. The nonlinear analysis gives solutions on axial displacement, lateral displacements, and rotation at given load level. The buckling load is taken as the lowest load value at which one or more of the displacements (and/or rotation) become excessive. Results

of the nonlinear analysis when compared to the experimental results give discrepancies from -9.1% to +99.9%, with an average of 36%. At present, the load vector is approximated in a linear fashion. In a fully nonlinear solution the load vector as well as the stiffness matrix are functions of the displacement vector. The performance of the nonlinear solution should be improved by including the nonlinear portion of the load vector in the iterative scheme.

6.2 RECOMMENDATIONS FOR FUTURE RESEARCH

The nonlinear analysis gives good estimates of the buckling load. It is, however, thought that a fully nonlinear theory would have wider scope of application. A fully nonlinear theory should include all aspects of geometric nonlinearity. In the present nonlinear theory, the axial displacement response is always linear even when the beam column is displaced laterally. This response is very much in contradiction with general intutition. The fully nonlinear theory should reflect lateral displacements in the response of axial displacement. In the fully nonlinear solution method, the nonlinearity in the load vector should also be included in the iterative scheme to be consistent with Equations (2.36-2.39).

The variational method can be used to develop the fully nonlinear theory. Such derivation can be started from kinematic assumptions on shell strains. The derived equations would be consistent, and consistent boundary conditions would also be obtained. In such a theory, pure flexure buckling and pure torsional buckling should be recovered as special cases.

To fully exploit the extended Vlasov's theory and the extended theory, the stress and deflection analyses should be developed for composite bars. Comparison between experimental data, the extended Vlasov theory, and Euler-Bernoulli beam theory for deflections and strains of utmost interest. Potentially, experimental data could be used to establish creditability of the law of sectorial area over the assumption of plane section remains plane for thin-walled open section bars. These two analyses together with some failure criterion can be used to determine the static ultimate strength of laminated composite mid-plane symmetric bars. Furthermore, the investigation can be expanded to a larger scale and applied to structures that are made up of bar members.

Finally, it would be desirable to develop a one-dimensional laminated composite bar theory for closed sections which includes warping. Structures such as wing boxes could be analysed in a one-dimensional manner for preliminary design. The simplicity of one-dimensional analysis of complicated built-up structures makes it attractive for structural optimization codes.

APPENDIX A. TRANSFORMATION LAWS

Cross-sectional properties depend on the choice of Cartesian and contour coordinate systems. Kinematic considerations allow for transformation of these cross-sectional properties when one or both of the coordinate systems are changed without re-computation. Some of these transformation laws are implemented in codes ISOKON2 and VLASOV2 for efficient evaluations while the others are not used because they pose serious numerical problems.

Some of the cross-sectional properties are affected by change of Cartesian coordinate system only. These include S_x, S_y, I_{xx}, I_{yy}, and I_{xy}. The others are affected by change of the contour coordinate system only; that is, a shift of the pole and/or the contour origin. Thus, the transformation laws can be distinguished into two different groups by the types of cross-sectional properties on which they apply. The initial Cartesian coordinates in the cross section are x and y, and the initial contour coordinate system is given by arc length s, contour origin O, and pole P. The cross-sectional properties are assumed to be known in the initial coordinate systems. The new coordinate systems are denoted by star superscripts on the variables; that is, x^*, y^*, s^*, O^*, and P^* (See Figure A1). The transformation laws relate the cross-sectional properties in the new coordinate systems to the initial coordinate system.

In the first group of transformation laws the change is entirely with respect to the Cartesian coordinate system; it is shown in the upper diagram in Figure A1. The origin of the new Cartesian system has coor-

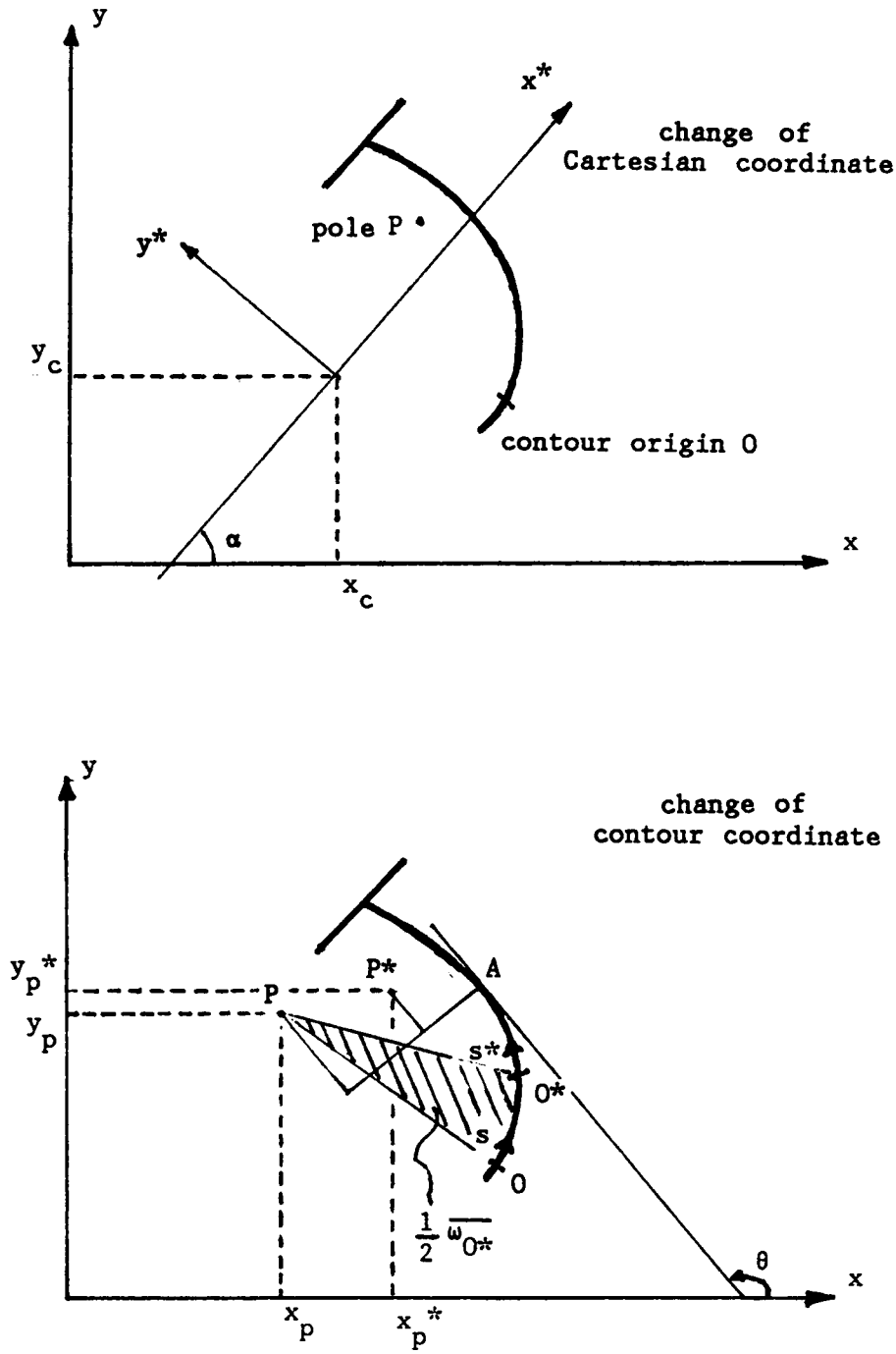

Figure A1. Coordinate Transformation

dinates (x_c, y_c) in the unstarred system. And the angle of inclination of the new Cartesian coordinate system relative to the unstarred Cartesian coordinate system is α. The locations of the contour origin and the pole remain the same. The first set of transformation equations are

$$S_{x^*} = (S_x - y_c A)\cos\alpha - (S_y - x_c A)\sin\alpha \tag{A1}$$

$$S_{y^*} = (S_x - y_c A)\sin\alpha + (S_y - x_c A)\cos\alpha \tag{A2}$$

$$I_{x^*x^*} = (I_{xx} - 2 y_c S_x + y_c^2 A)\cos^2\alpha + (I_{yy} - 2 x_c S_y + x_c^2 A)\sin^2\alpha - 2 (I_{xy} - y_c S_y - x_c S_x + x_c y_c A)\sin\alpha\cos\alpha \tag{A3}$$

$$I_{y^*y^*} = (I_{xx} - 2 y_c S_x + y_c^2 A)\sin^2\alpha + (I_{yy} - 2 x_c S_y + x_c^2 A)\cos^2\alpha + 2 (I_{xy} - y_c S_y - x_c S_x + x_c y_c A)\sin\alpha\cos\alpha \tag{A4}$$

$$I_{x^*y^*} = (I_{xx} - I_{yy} - 2 y_c S_x + 2 x_c S_y + y_c^2 A - x_c^2 A)\sin\alpha\cos\alpha + (I_{xy} - x_c S_x - y_c S_y + x_c y_c A)(\cos^2\alpha - \sin^2\alpha) \tag{A5}$$

The second set of transformation equations is based on the change of the locations of the pole and/or the contour origin, as shown in the lower diagram in Figure A1. $\overline{\omega_{0^*}}$ denotes the sectorial area at 0*, with respect to 0 and P. The second set of transformation equations are

$$S_{\omega^*} = S_\omega - \overline{\omega_{0^*}} A - (x_{p^*} - x_p)(S_x - y_{0^*} A) + (\overline{y_{p^*}} - y_p)(S_y - \overline{x_{0^*}} A) \tag{A6}$$

$$I_{\omega^* y} = I_{\omega y} - \overline{\omega_{0^*}} S_y - (x_{p^*} - x_p)(I_{xy} - \overline{y_{0^*}} S_y) + (y_{p^*} - y_p)(I_{yy} - \overline{x_{0^*}} S_y) \quad \text{(A7)}$$

$$I_{\omega^* x} = I_{\omega x} - \overline{\omega_{0^*}} S_x - (x_{p^*} - x_p)(I_{xx} - \overline{y_{0^*}} S_x) + (y_{p^*} - y_p)(I_{xy} - \overline{x_{0^*}} S_x) \quad \text{(A8)}$$

$$\begin{aligned} I_{\omega^* \omega^*} = {} & I_{\omega\omega} - 2\overline{\omega_{0^*}} S_\omega + \omega_{0^*}^2 A \\ & + (x_{p^*} - x_p)^2 [I_{xx} - 2\overline{y_{0^*}} S_x + \overline{y_{0^*}^2} A] \\ & + (y_{p^*} - y_p)^2 [I_{yy} - 2\overline{x_{0^*}} S_y + \overline{x_{0^*}^2} A] \\ & - 2(x_{p^*} - x_p)[I_{\omega x} - \overline{\omega_{0^*}} S_x - \overline{y_{0^*}} S_\omega + \overline{\omega_{0^*}}\,\overline{y_{0^*}} A] \\ & + 2(y_{p^*} - y_p)[I_{\omega y} - \overline{\omega_{0^*}} S_y - \overline{x_{0^*}} S_\omega + \overline{\omega_{0^*}}\,\overline{x_{0^*}} A] \\ & - 2(x_{p^*} - x_p)(y_{p^*} - y_p)[I_{xy} - \overline{x_{0^*}} S_x - \overline{y_{0^*}} S_y + \overline{x_{0^*}}\,\overline{y_{0^*}} A] \end{aligned} \quad \text{(A9)}$$

APPENDIX B. EXPERIMENTAL DATA

In this appendix, experimental data on specimen 2-1, 2-2, and 2-4 are presented. The purpose of this appendix is to show how the experimental data are utilized to determine buckling loads. The data points are discrete points recorded in the experimental research; the lines joining these data points are drawn for visualisation purpose only.

Two types of instrumentation were used in the testing: displacement transducers and strain gauges. The positions of the monitors are shown in Figure B1. Four available transducer readings and only three axial strain gauge pairs (all at mid-span) will be presented here. The set up of the displacement transducers (DCDT) were as follows,

- DCDT1 : at mid-span, at the free edge of a flange.
- DCDT2 : at mid-span, at the mid web.
- DCDT3 : at quarter-span, at the free edge of a flange.
- DCDT4 : crosshead, the end shortening monitor.

The strain gauges were set up as back-to-back pairs. For the channel sections (2-1 and 2-2),

- Gauge Pair 1, 2 : close to the free edge of a flange.
- Gauge Pair 11, 12 : close to the free edge of the second flange.
- Gauge Pair 21, 24 : at the mid web.

The strain gauges set up for for the zee section,

- Gauge Pair 1, 2 : close to the free edge of a flange.
- Gauge Pair 9, 10 : close to the free edge of the second flange.
- Gauge Pair 13, 16 : at the mid web.

B.1 DETERMINATION OF BUCKLING LOADS

The plots of load against displacement transducer readings, essentially displacements, give similiar patterns. In each case, the loading curve climbs with increasing load level; beyond certain load level, the slope of the curve decreases with the load increment; at a higher load, the slope diminishes and the displacement becomes large. Since flexural deformations and twisting deformation are generally coupled, the overall deformation of the beam column is difficult to visualized from the plots

(Figure B2, B4, B6). Theoretically, the buckling load can be determined from these loading curves; close examination reviews that such a method is inconclusive and impractical.

The strain gauge readings are much more useful. No matter how the specimen deforms, the buckling phenonemon is marked by excessive lateral displacements and/or rotation. The buckling load is defined as the load at which excessive curvature effects are recorded in the back-to-back gauges. This method is found to be quite reliable, and was used to determine the experimental buckling loads in Tyhala's research.

B.2 NOTE ON SPECIMEN 2-1

The loading history of this specimen shown that there was an abrupt disturbance during the experiment. The back-to-back gauges also recorded such unexpected deformation, which rules out the possibility of faulty DCDT monitors.

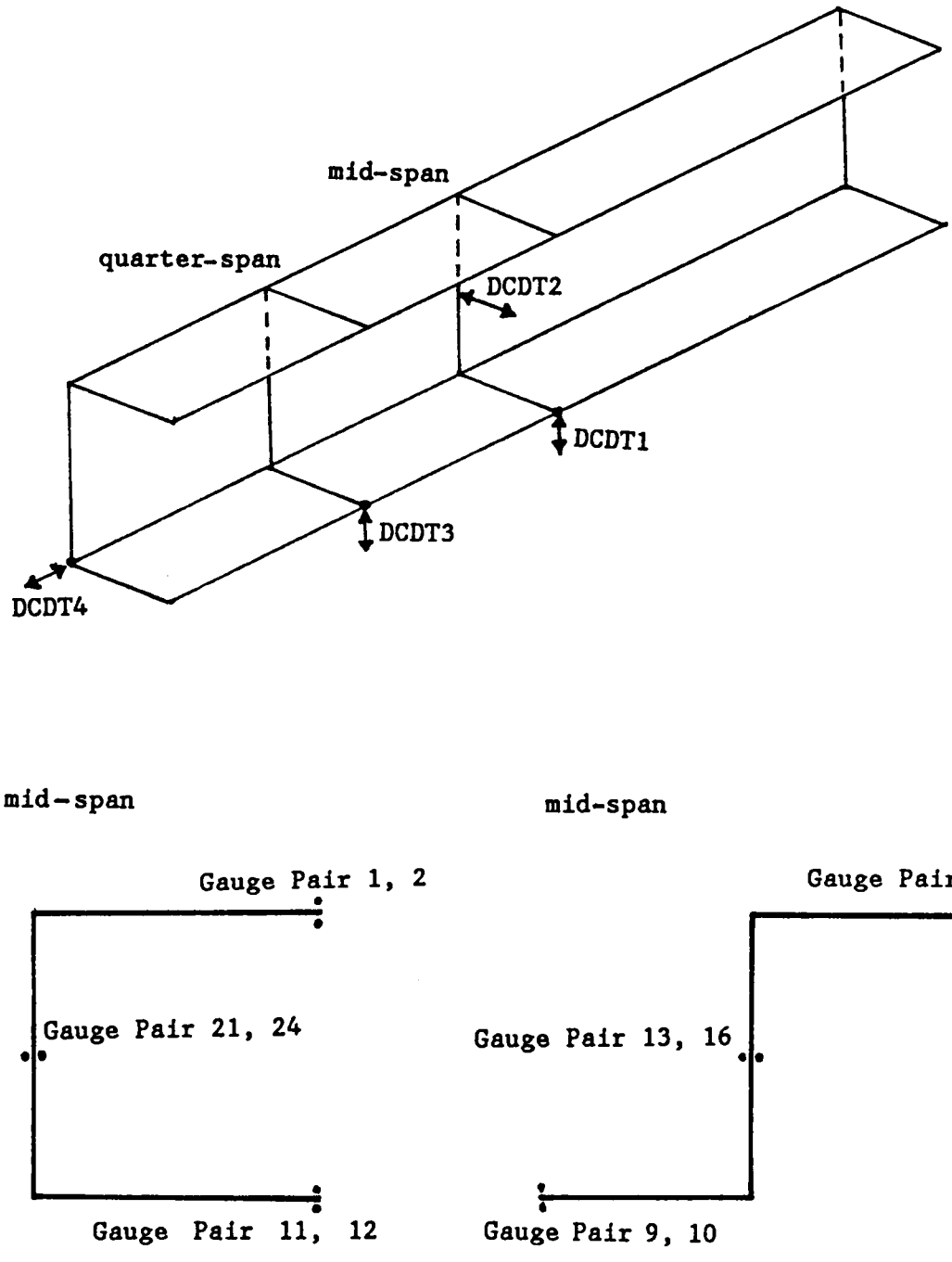

Figure B1. Schematic description of the experimental instrumentation

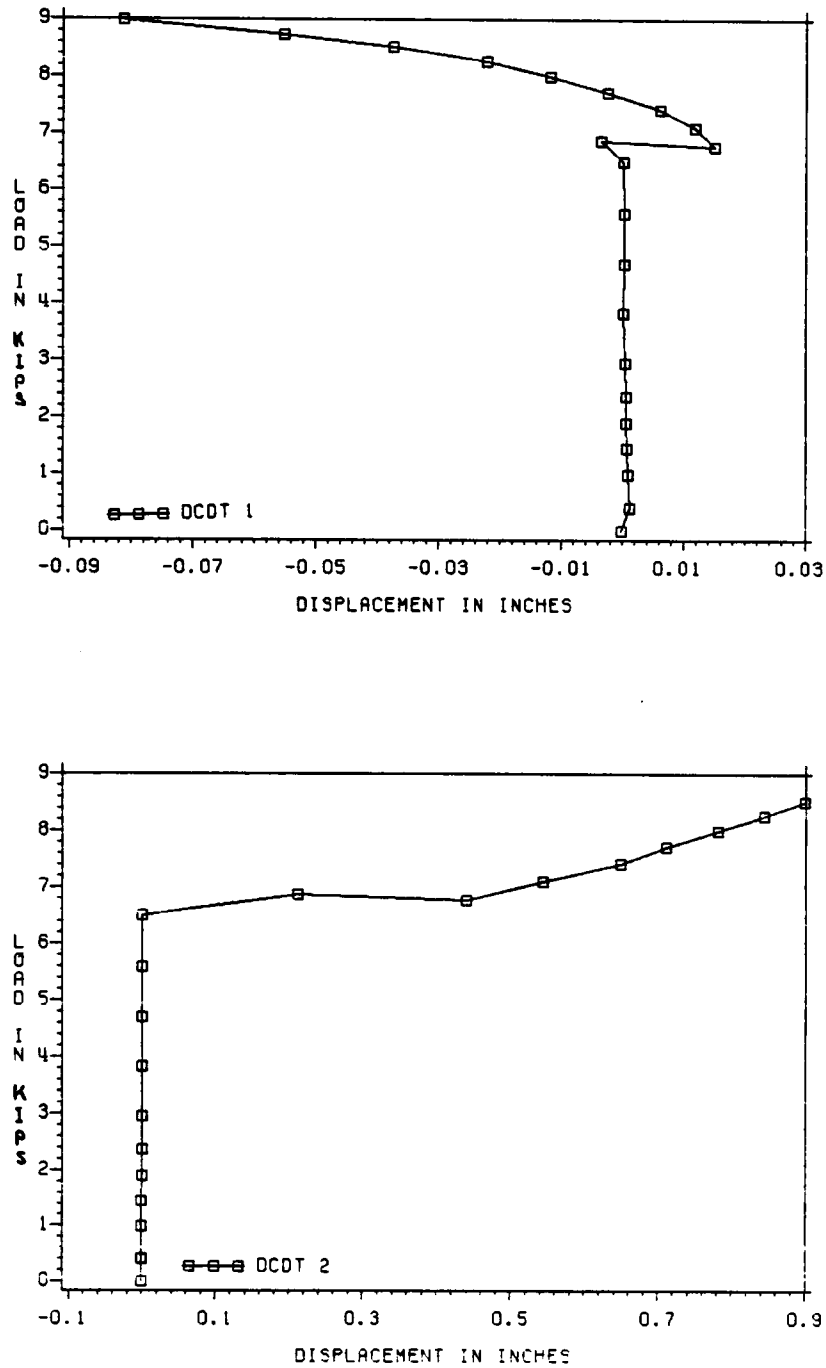

Figure B2. DCDT readings on Specimen 2-1

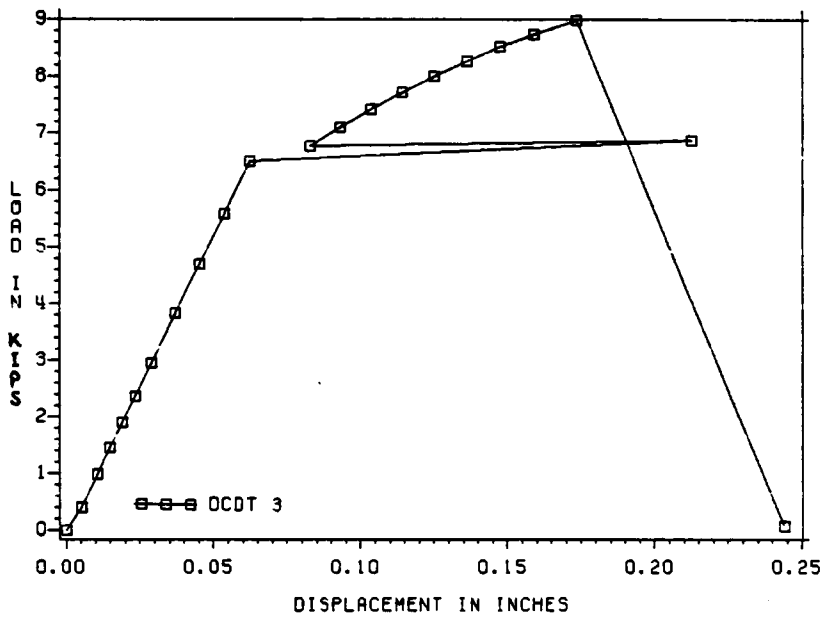

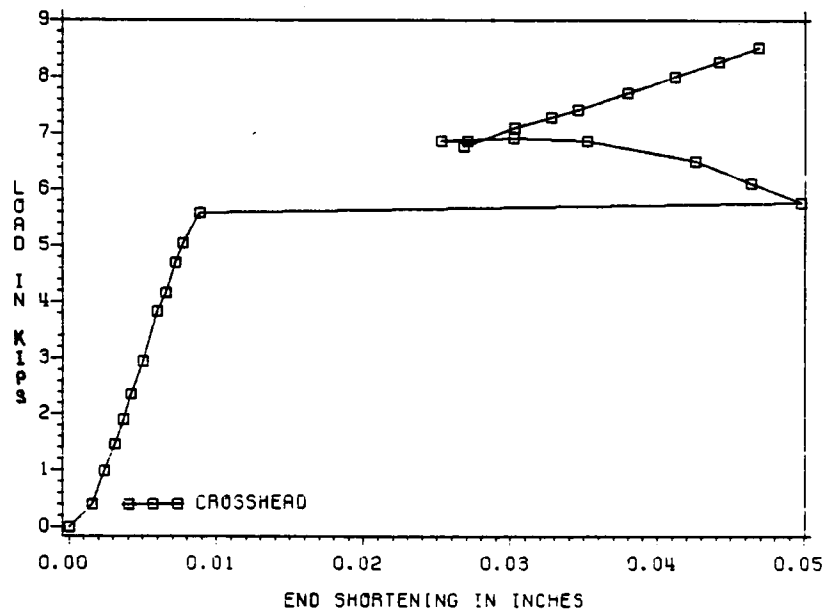

Figure B3. DCDT readings on Specimen 2-1

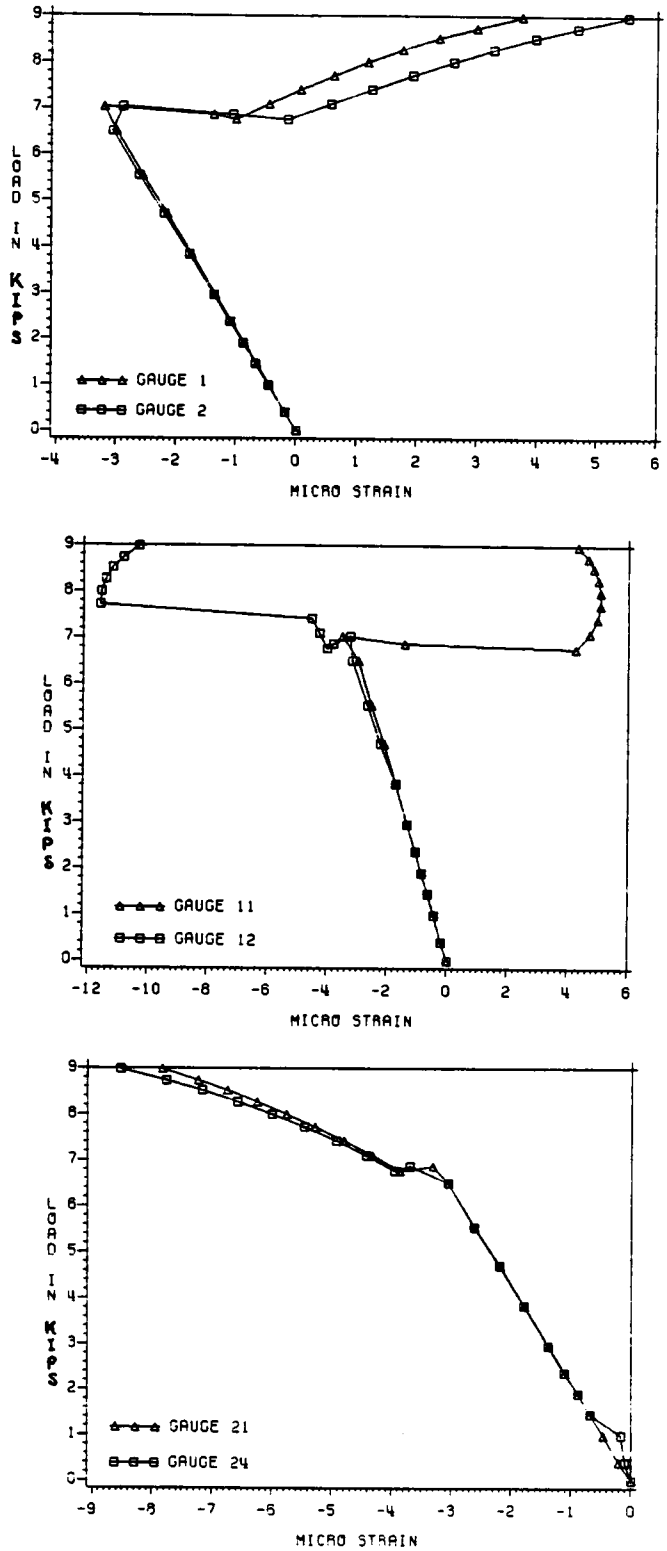

Figure B4. Strain gauge readings on Specimen 2-1

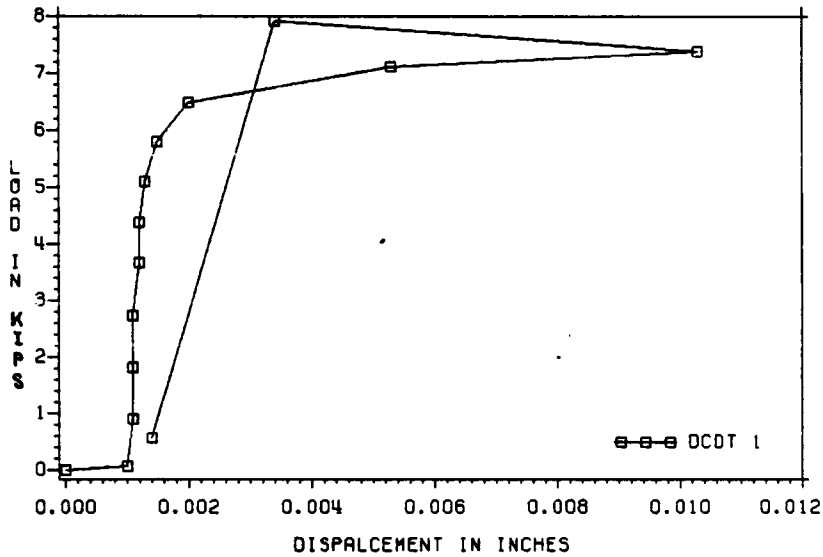

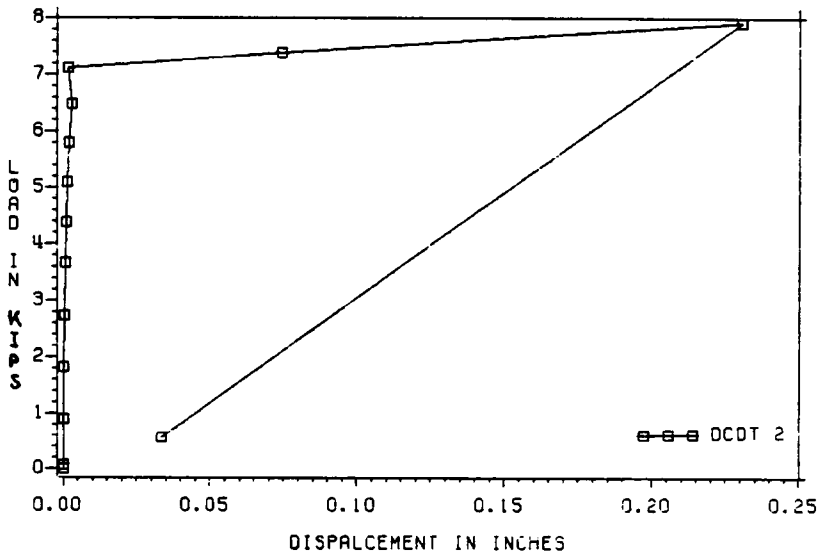

Figure B5. DCDT readings on Specimen 2-2

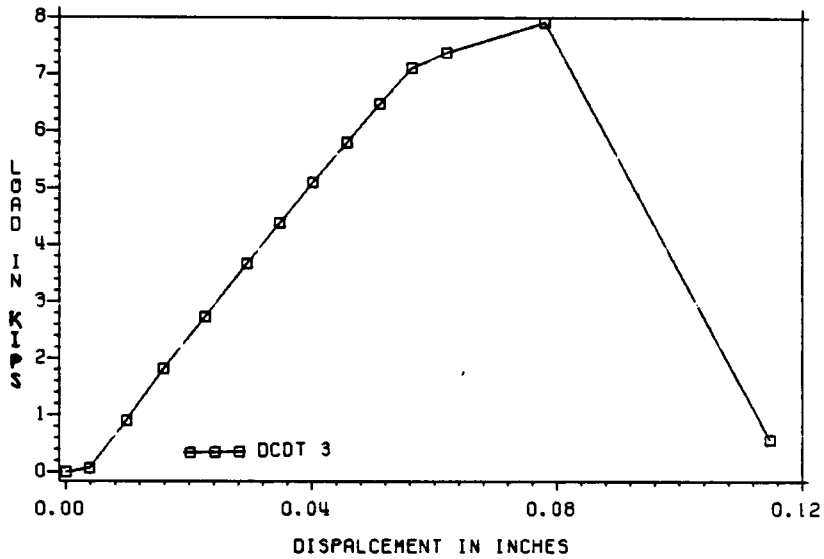

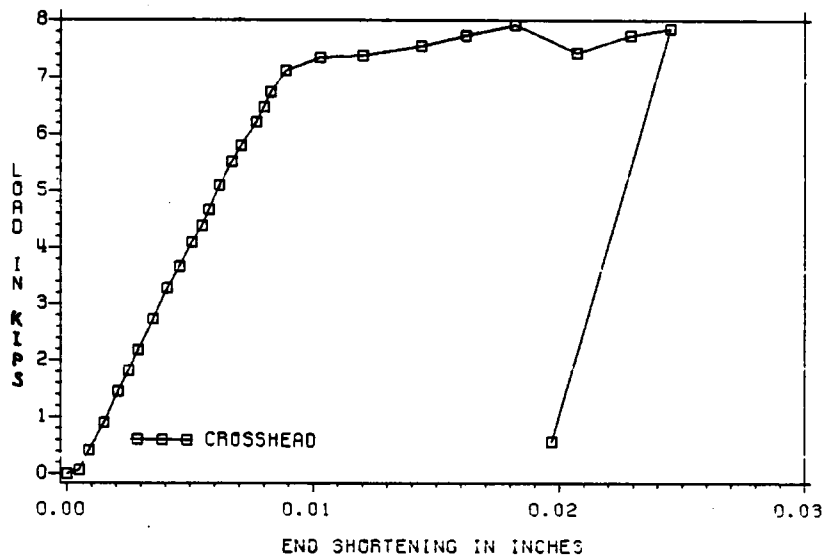

Figure B6. DCDT readings on Specimen 2-2

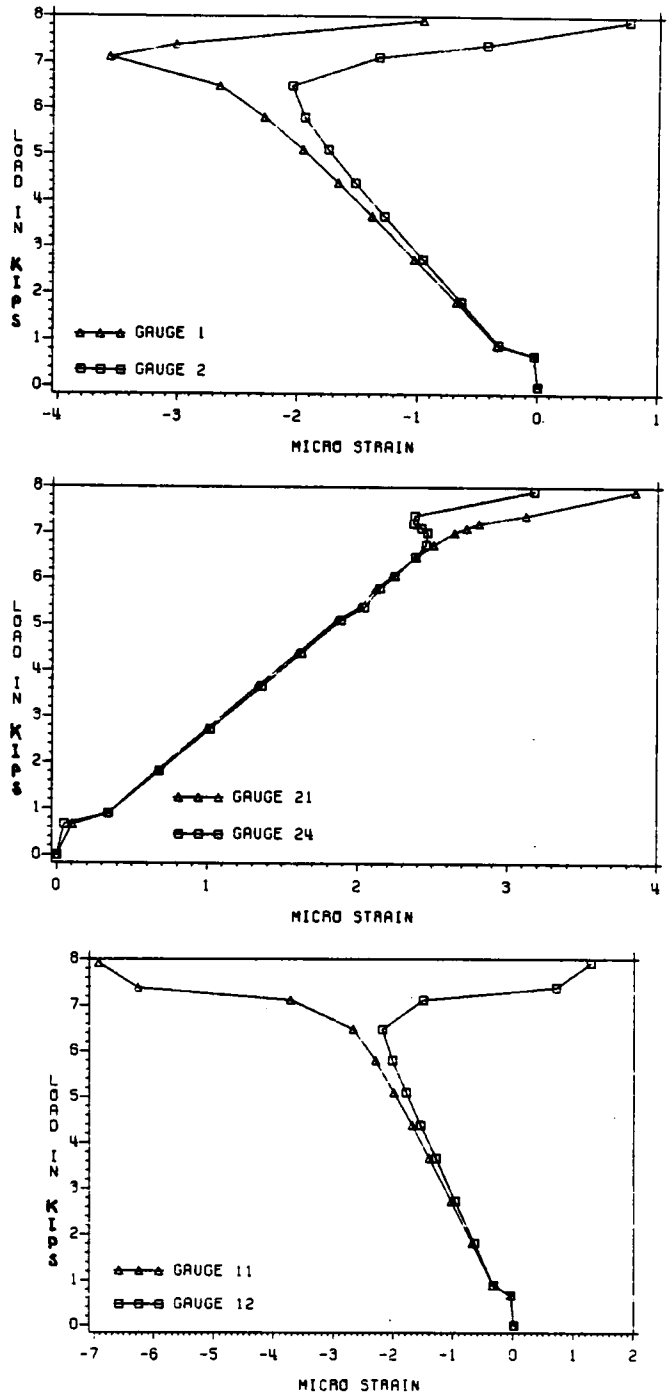

Figure B7. Strain gauge readings on Specimen 2-2

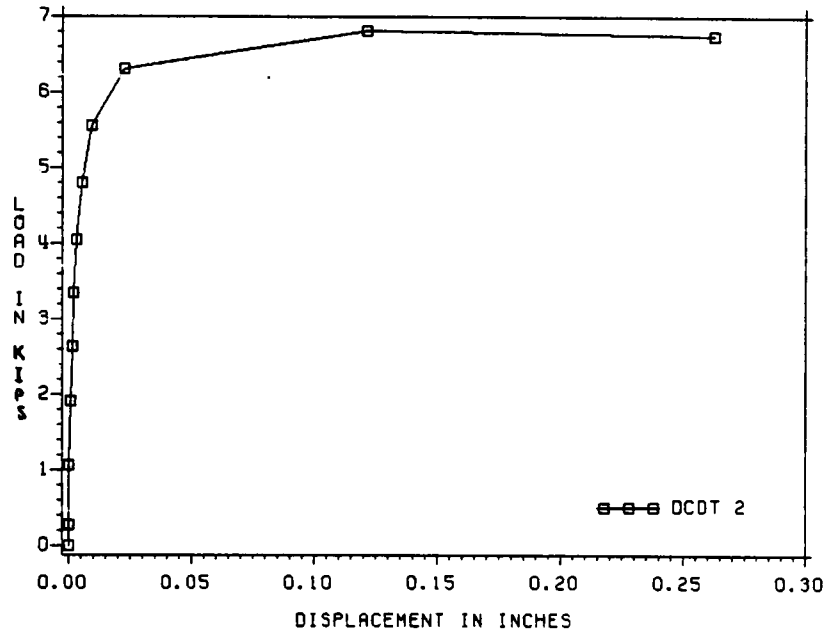

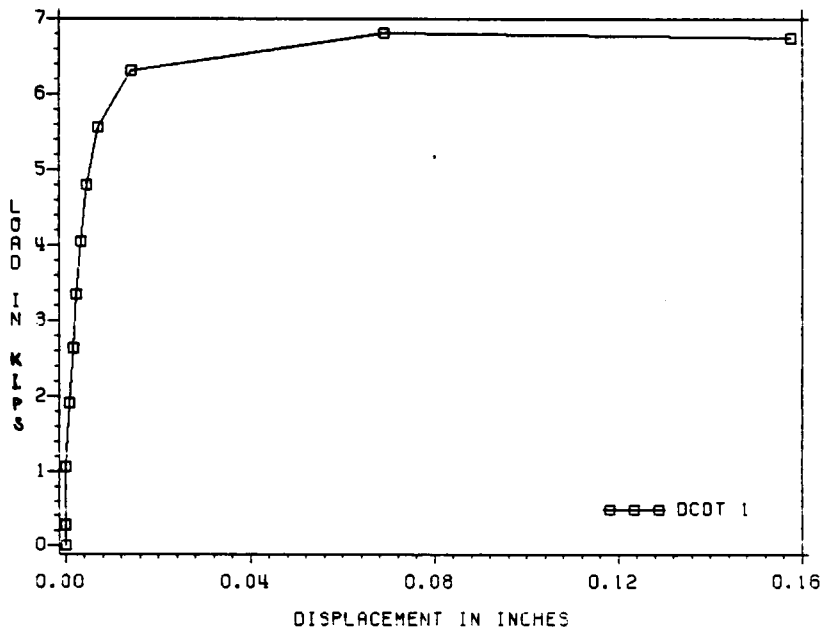

Figure B8. DCDT readings on Specimen 2-4

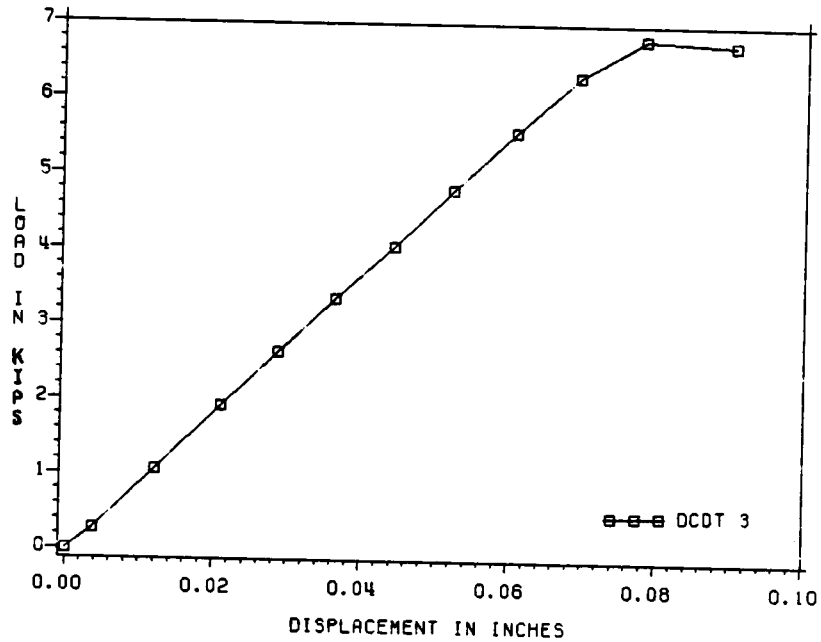

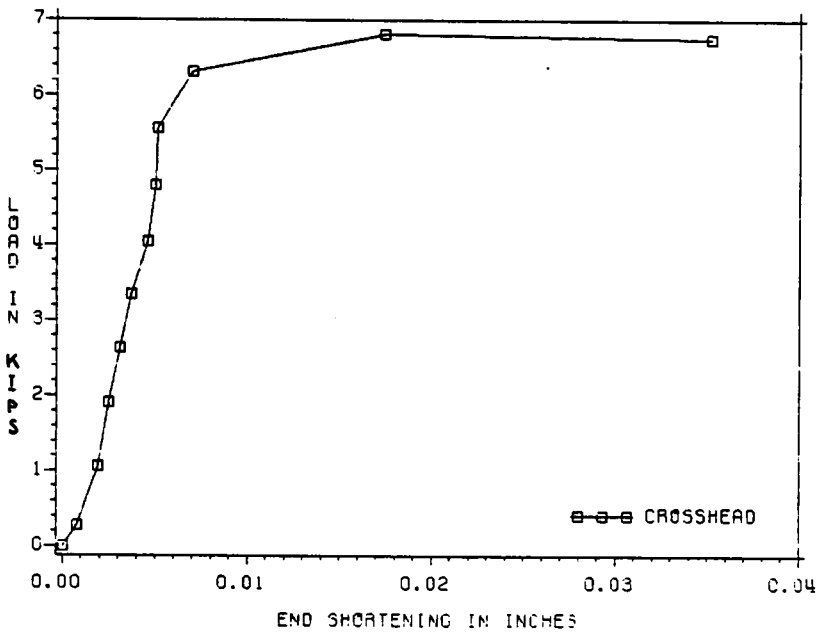

Figure B9. DCDT readings on Specimen 2-4

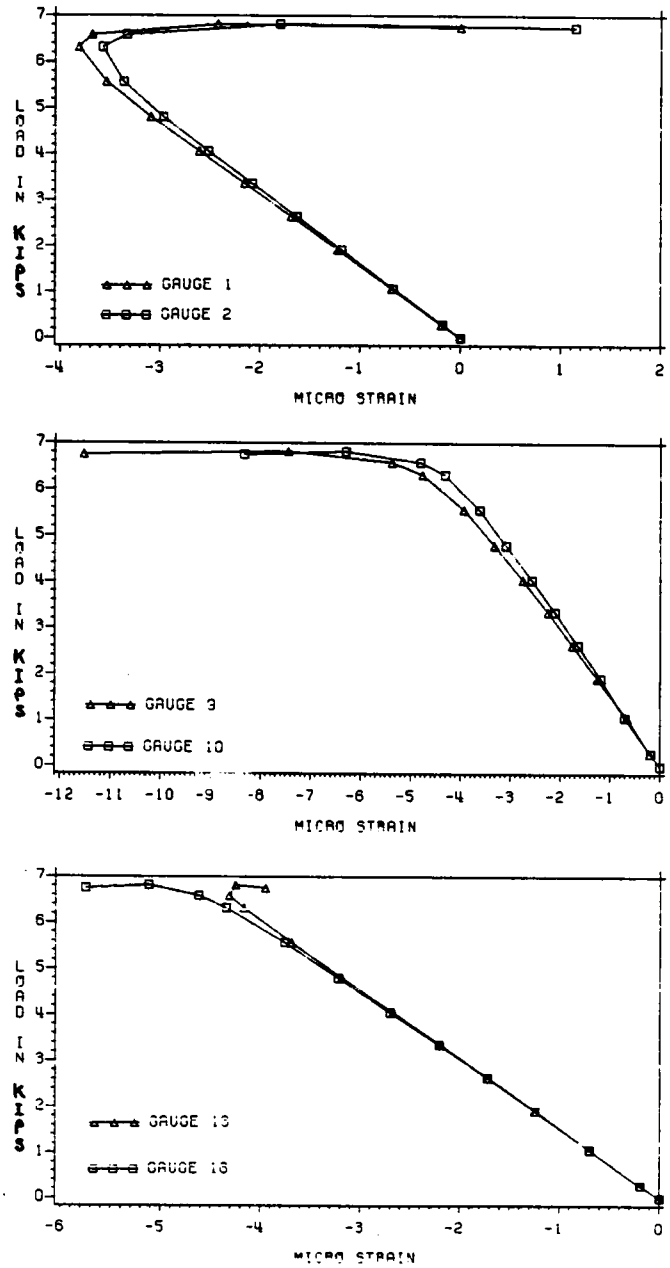

Figure B10. Strain gauge readings on Specimen 2-4

APPENDIX C. ELEMENT STIFFNESS MATRIX

In this appendix, the complete element stiffness is listed. The linear terms in the element stiffness has been introduced in Chapter 4 and are written in short form as $[K_{ij}]_L$; some linear terms are written explicitly and are underlined for clarification.

$$\left[k_{11} \quad k_{12} \quad k_{13} \quad k_{14} \quad k_{15} \quad k_{16} \quad k_{17}\right] =$$

$$\left[\underline{k_{11}}^L \quad \underline{k_{12}}^L \quad \underline{k_{13}}^L \quad \underline{k_{14}}^L \quad \underline{k_{15}}^L \quad \underline{k_{16}}^L \quad \underline{k_{17}}^L\right]$$

$$\left[k_{18} \quad k_{19} \quad k_{1\,10} \quad k_{1\,11} \quad k_{1\,12} \quad k_{1\,13} \quad k_{1\,14}\right] =$$

$$\left[\underline{k_{1\,8}}^L \quad \underline{k_{1\,9}}^L \quad \underline{k_{1\,10}}^L \quad \underline{k_{1\,11}}^L \quad \underline{k_{1\,12}}^L \quad \underline{k_{1\,13}}^L \quad \underline{k_{1\,14}}^L\right]$$

$$\left[K_{21}\right] = \left[A\int(\bar{u}' + y_p\bar{\theta}')\,{}^{w}\psi_1'\psi_1'\,dz\right]$$

$$\left[k_{22}\quad k_{23}\right] = \left[k_{22}^{L} + A\int\bar{w}'\psi_1'\psi_1'dz \qquad -I_{xx}\int\bar{\theta}\,\psi_1''\psi_1''\,dz\right]$$

$$\begin{aligned}\left[K_{24}\right] = \Big[k_{24}^{L} &- I_{xx}\int\bar{v}''\psi_1\psi_1''dz + 6H_c\int\bar{\theta}'\psi_1'\psi_1''\,dz\\ &+ 4H_c\int\bar{\theta}''\psi_1'\psi_1\,dz + 4H_c\int\bar{\theta}'\psi_1''\psi_1\,dz\\ &+ H_c\int\bar{\theta}\,\psi_1''\psi_1'dz + H_c\int\bar{\theta}''\psi_1\psi_1'dz + A\,y_p\int\bar{w}'\psi_1'\psi_1'dz\Big]\end{aligned}$$

$$\left[K_{25}\quad K_{26}\right] = \left[K_{25}^{L} + A\int\bar{w}'\psi_1'\psi_2'dz \qquad -I_{xx}\int\bar{\theta}\,\psi_1''\psi_2''\,dz\right]$$

$$\begin{aligned}\left[K_{27}\right] = \Big[K_{27}^{L} &- I_{xx}\int\bar{v}''\psi_1\psi_2''\,dz + 6H_c\int\bar{\theta}'\psi_1'\psi_2'\,dz\\ &+ 4H_c\int\bar{\theta}''\psi_1'\psi_2\,dz + 4H_c\int\bar{\theta}'\psi_1''\psi_2\,dz\\ &+ H_c\int\bar{\theta}\,\psi_1''\psi_2'dz + H_c\int\bar{\theta}''\psi_1\psi_2'dz + A\,y_p\int\bar{w}'\psi_1'\psi_2'dz\Big]\end{aligned}$$

$$\left[K_{28}\right] = \left[A\int(\bar{u}' + y_p\bar{\theta}')\,{}^{w}\psi_2'\psi_1'\,dz\right]$$

$$\left[K_{29}\quad K_{2\,10}\right] = \left[k_{29}^{L} + A\int\bar{w}'\psi_1'\psi_3'dz \qquad -I_{xx}\int\bar{\theta}\,\psi_1''\psi_3''dz\right]$$

$$\begin{aligned}\left[K_{2\,11}\right] = \Big[K_{2\,11}^{L} &- I_{xx}\int\bar{v}''\psi_1\psi_3''\,dz + 6H_c\int\bar{\theta}'\psi_1'\psi_3'\,dz\\ &+ 4H_c\int\bar{\theta}''\psi_1'\psi_3\,dz + 4H_c\int\bar{\theta}'\psi_1''\psi_3\,dz\\ &+ H_c\int\bar{\theta}\,\psi_1''\psi_3'dz + H_c\int\bar{\theta}''\psi_1\psi_3''dz + A\,y_p\int\bar{w}'\psi_1'\psi_3'dz\Big]\end{aligned}$$

$$\left[K_{2\,12}\quad K_{2\,13}\right] = \left[K_{2\,12}^{L} + A\int\bar{w}'\psi_1'\psi_4'dz \qquad -I_{xx}\int\bar{\theta}\,\psi_1''\psi_4''\,dz\right]$$

$$\begin{aligned}\left[K_{2\,14}\right] = \Big[K_{2\,14}^{L} &- I_{xx}\int\bar{v}''\psi_1\psi_4''\,dz + 6H_c\int\bar{\theta}'\psi_1'\psi_4'\,dz\\ &+ 4H_c\int\bar{\theta}''\psi_1'\psi_4\,dz + 4H_c\int\bar{\theta}'\psi_1''\psi_4\,dz\\ &+ H_c\int\bar{\theta}\,\psi_1''\psi_4'dz + H_c\int\bar{\theta}''\psi_1\psi_4'dz + A\,y_p\int\bar{w}'\psi_1'\psi_4'dz\Big]\end{aligned}$$

$$\left[K_{31}\right] = \left[A\int(\bar{v}'+x_p\bar{\phi}')^{w}\psi_1'\psi_1'\,dz\right]$$

$$\left[K_{32}\quad K_{33}\right] = \left[I_{yy}\int\bar{\phi}\,\psi_1''\psi_1''dz \qquad k_{33}^{L} + A\int\bar{w}'\psi_1'\psi_1'dz\right]$$

$$\left[K_{34}\right] = \left[-\underline{H_c\int\psi_1''\psi_1'\,dz} + I_{yy}\int\bar{u}''\psi_1'\psi_1''dz + 6H_s\int\bar{\phi}'\psi_1'\psi_1'dz\right.$$
$$+ 4H_s\int\bar{\phi}''\psi_1'\psi_1\,dz + 4H_s\int\bar{\phi}'\psi_1''\psi_1\,dz$$
$$\left.+ H_s\int\bar{\phi}\,\psi_1''\psi_1'dz + H_s\int\bar{\phi}''\psi_1'\psi_1'dz - A\int\bar{w}'\psi_1'\psi_1'dz\right]$$

$$\left[K_{35}\quad K_{36}\right] = \left[I_{yy}\int\bar{\phi}\,\psi_1''\psi_2''dz \qquad k_{36}^{L} + A\int\bar{w}'\psi_1'\psi_2'dz\right]$$

$$\left[K_{37}\right] = \left[-\underline{H_c\int\psi_1''\psi_2'\,dz} + I_{yy}\int\bar{u}''\psi_1'\psi_2''dz + 6H_s\int\bar{\phi}'\psi_1'\psi_2'dz\right.$$
$$+ 4H_s\int\bar{\phi}''\psi_1'\psi_2\,dz + 4H_s\int\bar{\phi}'\psi_1''\psi_2\,dz$$
$$\left.+ H_s\int\bar{\phi}\,\psi_1''\psi_2'dz + H_s\int\bar{\phi}''\psi_1'\psi_2'dz - A\int\bar{w}'\psi_1'\psi_2'dz\right]$$

$$\left[K_{38}\right] = \left[A\int(\bar{v}'+x_p\bar{\phi}')^{w}\psi_2'\psi_1'dz\right]$$

$$\left[K_{39}\quad K_{3\,10}\right] = \left[I_{yy}\int\bar{\phi}\,\psi_1''\psi_3''dz \qquad k_{3\,10}^{L} + A\int\bar{w}'\psi_1'\psi_3'dz\right]$$

$$\left[K_{3\,11}\right] = \left[-\underline{H_c\int\psi_1''\psi_3'\,dz} + I_{yy}\int\bar{u}''\psi_1'\psi_3''dz + 6H_s\int\bar{\phi}'\psi_1'\psi_3'dz\right.$$
$$+ 4H_s\int\bar{\phi}''\psi_1'\psi_3\,dz + 4H_s\int\bar{\phi}'\psi_1''\psi_3\,dz$$
$$\left.+ H_s\int\bar{\phi}\,\psi_1''\psi_3'dz + H_s\int\bar{\phi}''\psi_1'\psi_3'dz - A\int\bar{w}'\psi_1'\psi_3'dz\right]$$

$$\left[K_{3\,12}\quad K_{3\,13}\right] = \left[I_{yy}\int\bar{\phi}\,\psi_1''\psi_4''dz \qquad k_{3\,13}^{L} + A\int\bar{w}'\psi_1'\psi_4'dz\right]$$

$$\left[K_{3\,14}\right] = \left[-\underline{H_c\int\psi_1''\psi_4'\,dz} + I_{yy}\int\bar{u}''\psi_1'\psi_4''dz + 6H_s\int\bar{\phi}'\psi_1'\psi_4'dz\right.$$
$$+ 4H_s\int\bar{\phi}''\psi_1'\psi_4\,dz + 4H_s\int\bar{\phi}'\psi_1''\psi_4\,dz$$
$$\left.+ H_s\int\bar{\phi}\,\psi_1''\psi_4'dz + H_s\int\bar{\phi}''\psi_1'\psi_4'dz - A\int\bar{w}'\psi_1'\psi_4'dz\right]$$

$$[k_{41}] = \left[A\int (y_p \bar{u}' - x_p \bar{v}')''' \psi_1' \psi_1' \, dz + A R_p^2 \int \bar{\theta}' \, ''' \psi_1' \psi_1' \, dz \right]$$

$$[k_{42}] = \left[-H_s \int \psi_1'' \psi_1' \, dz + A y_p \int \bar{w}' \psi_1' \psi_1' \, dz - (I_{xx} - I_{yy}) \int \bar{v}'' \psi_1'' \psi_1 \, dz \right.$$
$$\left. + H_c \int (\bar{\theta}' \psi_1' \psi_1' + \bar{\theta}'' \psi_1' \psi_1) \, dz - K_y I_{yy} \int \bar{\theta}' \psi_1'' \psi_1' \, dz \right]$$

$$[k_{43}] = \left[H_c \int \psi_1'' \psi_1' \, dz - A x_p \int \bar{w}' \psi_1' \psi_1' \, dz - (I_{xx} - I_{yy}) \int \bar{u}'' \psi_1'' \psi_1 \, dz \right.$$
$$\left. + H_s \int (\bar{\theta}' \psi_1' \psi_1' + \bar{\theta}'' \psi_1' \psi_1) \, dz - K_x I_{xx} \int \bar{\theta}' \psi_1'' \psi_1' \, dz \right]$$

$$[k_{44}] = \left[I_{\omega\omega} \int \psi_1'' \psi_1'' \, dz + JG \int \psi_1' \psi_1' \, dz + A R_p^2 \int \bar{w}' \psi_1' \psi_1' \, dz \right.$$
$$+ H_c \int (\bar{u}' \psi_1' \psi_1' + \bar{u}' \psi_1'' \psi_1) \, dz - K_y I_{yy} \int \bar{u}'' \psi_1' \psi_1' \, dz$$
$$+ H_s \int (\bar{v}' \psi_1' \psi_1' + \bar{v}' \psi_1'' \psi_1) \, dz - K_x I_{xx} \int \bar{v}'' \psi_1' \psi_1' \, dz$$
$$\left. - K_\omega I_{\omega\omega} \int (\bar{\theta}'' \psi_1' \psi_1' + \bar{\theta}' \psi_1'' \psi_1') \, dz + 2 H_\phi \int \bar{\theta}' \psi_1' \psi_1' \, dz \right]$$

$$[k_{45}] = \left[-H_s \int \psi_1'' \psi_2' \, dz + A y_p \int \bar{w}' \psi_1' \psi_2' \, dz - (I_{xx} - I_{yy}) \int \bar{v}'' \psi_1'' \psi_2 \, dz \right.$$
$$\left. + H_c \int (\bar{\theta}' \psi_1' \psi_2' + \bar{\theta}'' \psi_1' \psi_2) \, dz - K_y I_{yy} \int \bar{\theta}' \psi_1'' \psi_2' \, dz \right]$$

$$[k_{46}] = \left[H_c \int \psi_1'' \psi_2' \, dz - A x_p \int \bar{w}' \psi_1' \psi_2' \, dz - (I_{xx} - I_{yy}) \int \bar{u}'' \psi_1'' \psi_2 \, dz \right.$$
$$\left. + H_s \int (\bar{\theta}' \psi_1' \psi_2 + \bar{\theta}'' \psi_1' \psi_2) \, dz - K_x I_{xx} \int \bar{\theta}' \psi_1'' \psi_2' \, dz \right]$$

$$[k_{47}] = \left[I_{\omega\omega} \int \psi_1'' \psi_2'' \, dz + JG \int \psi_1' \psi_2' \, dz + A R_p^2 \int \bar{w}' \psi_1' \psi_2' \, dz \right.$$
$$+ H_c \int (\bar{u}' \psi_1' \psi_2' + \bar{u}' \psi_1'' \psi_2) \, dz - K_y I_{yy} \int \bar{u}'' \psi_1' \psi_2' \, dz$$
$$+ H_s \int (\bar{v}' \psi_1' \psi_2' + \bar{v}' \psi_1'' \psi_2) \, dz - K_x I_{xx} \int \bar{v}'' \psi_1' \psi_2' \, dz$$
$$\left. - K_\omega I_{\omega\omega} \int (\bar{\theta}'' \psi_1' \psi_1' + \bar{\theta}' \psi_1'' \psi_1') \, dz + 2 H_\phi \int \bar{\theta}' \psi_1' \psi_2' \, dz \right]$$

$$[K_{4\,8}] = \left[A \int (y_p \bar{u}' - x_p \bar{v}') \, {}^{w}\psi_2' \, \psi_1' \, dz + A R_p^2 \int \bar{\theta}' \, {}^{w}\psi_2' \psi_1' \, dz \right]$$

$$[K_{4\,9}] = \left[-H_s \int \psi_1'' \psi_3' \, dz + A y_p \int \bar{w}' \psi_1' \psi_3' \, dz - (I_{xx} - I_{yy}) \int \bar{v}'' \psi_1'' \psi_3 \, dz \right.$$
$$\left. + H_c \int (\bar{\theta}' \psi_1' \psi_3' + \bar{\theta}'' \psi_1' \psi_3) \, dz - K_y I_{yy} \int \bar{\theta}' \psi_1'' \psi_3' \, dz \right]$$

$$[K_{4\,10}] = \left[H_c \int \psi_1'' \psi_3' \, dz - A x_p \int \bar{w}' \psi_1' \psi_3' \, dz - (I_{xx} - I_{yy}) \int \bar{u}'' \psi_1'' \psi_3 \, dz \right.$$
$$\left. + H_s \int (\bar{\theta}' \psi_1' \psi_3' + \bar{\theta}'' \psi_1' \psi_3) \, dz - K_x I_{xx} \int \bar{\theta}' \psi_1'' \psi_3' \, dz \right]$$

$$[K_{4\,11}] = \left[I_{ww} \int \psi_1'' \psi_3'' \, dz + JG \int \psi_1' \psi_3' \, dz + A R_p^2 \int \bar{w}' \psi_1' \psi_3' \, dz \right.$$
$$+ H_c \int (\bar{u}' \psi_1' \psi_3' + \bar{u}' \psi_1'' \psi_3) \, dz - K_y I_{yy} \int \bar{u}'' \psi_1' \psi_3' \, dz$$
$$+ H_s \int (\bar{v}' \psi_1' \psi_3' + \bar{v}' \psi_1'' \psi_3) \, dz - K_x I_{xx} \int \bar{v}'' \psi_1' \psi_3' \, dz$$
$$\left. - K_\omega I_{ww} \int (\bar{\theta}'' \psi_1' \psi_3' + \bar{\theta}' \psi_1'' \psi_3') \, dz + 2 H_\phi \int \bar{\theta}' \psi_1' \psi_3' \, dz \right]$$

$$[K_{4\,12}] = \left[-H_s \int \psi_1'' \psi_4' \, dz + A y_p \int \bar{w}' \psi_1' \psi_4' \, dz - (I_{xx} - I_{yy}) \int \bar{v}'' \psi_1'' \psi_4 \, dz \right.$$
$$\left. + H_c \int (\bar{\theta}' \psi_1' \psi_4' + \bar{\theta}'' \psi_1' \psi_4) \, dz - K_y I_{yy} \int \bar{\theta}' \psi_1'' \psi_4' \, dz \right]$$

$$[K_{4\,13}] = \left[H_c \int \psi_1'' \psi_4' \, dz - A x_p \int \bar{w}' \psi_1' \psi_4' \, dz - (I_{xx} - I_{yy}) \int \bar{u}'' \psi_1'' \psi_4 \, dz \right.$$
$$\left. + H_s \int (\bar{\theta}' \psi_1' \psi_3' + \bar{\theta}'' \psi_1' \psi_3) \, dz - K_x I_{xx} \int \bar{\theta}' \psi_1'' \psi_3' \, dz \right]$$

$$[K_{4\,14}] = \left[I_{ww} \int \psi_1'' \psi_4'' \, dz + JG \int \psi_1' \psi_4' \, dz + A R_p^2 \int \bar{w}' \psi_1' \psi_4' \, dz \right.$$
$$+ H_c \int (\bar{u}' \psi_1' \psi_4' + \bar{u}' \psi_1'' \psi_4) \, dz - K_y I_{yy} \int \bar{u}'' \psi_1' \psi_4' \, dz$$
$$+ H_s \int (\bar{v}' \psi_1' \psi_3' + \bar{v}' \psi_1'' \psi_3) \, dz - K_x I_{xx} \int \bar{v}'' \psi_1' \psi_4' \, dz$$
$$\left. - K_\omega I_{ww} \int (\bar{\theta}'' \psi_1' \psi_3' + \bar{\theta}' \psi_1'' \psi_3') \, dz + 2 H_\phi \int \bar{\theta}' \psi_1' \psi_4' \, dz \right]$$

$$\left[k_{51}\right] = \left[A \int (\bar{u}' + y_p \bar{\theta}')\, \psi_1' \psi_2' \, dz\right]$$

$$\left[k_{52} \quad k_{53}\right] = \left[k_{52}^{L} + A \int \bar{w}' \psi_2' \psi_1' \, dz \qquad -I_{yy} \int \bar{\theta} \psi_2'' \psi_1'' \, dz\right]$$

$$\left[k_{54}\right] = \left[k_{54}^{L} - I_{xx} \int \bar{v}'' \psi_2 \psi_1'' \, dz + 6 H_c \int \bar{\theta}' \psi_2' \psi_1' \, dz \right.$$
$$+ 4 H_c \int \bar{\theta}'' \psi_2' \psi_1 \, dz + 4 H_c \int \bar{\theta}' \psi_2'' \psi_1 \, dz$$
$$\left. + H_c \int \bar{\theta} \psi_2'' \psi_1' \, dz + H_c \int \bar{\theta}'' \psi_2 \psi_1' \, dz + A y_p \int \bar{w}' \psi_2' \psi_1' \, dz\right]$$

$$\left[K_{55} \quad K_{56}\right] = \left[k_{55}^{L} + A \int \bar{w}' \psi_2' \psi_2' \, dz \qquad -I_{xx} \int \bar{\theta} \psi_2'' \psi_2'' \, dz\right]$$

$$\left[k_{57}\right] = \left[k_{57}^{L} - I_{xx} \int \bar{v}'' \psi_2 \psi_2'' \, dz + 6 H_c \int \bar{\theta}' \psi_2' \psi_2' \, dz \right.$$
$$+ 4 H_c \int \bar{\theta}'' \psi_2' \psi_2 \, dz + 4 H_c \int \bar{\theta}' \psi_2'' \psi_2 \, dz$$
$$\left. + H_c \int \bar{\theta} \psi_2'' \psi_2' \, dz + H_c \int \bar{\theta}'' \psi_2 \psi_2' \, dz + A y_p \int \bar{w}' \psi_2' \psi_2' \, dz\right]$$

$$\left[k_{58}\right] = \left[A \int (\bar{u}' + y_p \bar{\theta}')\, \psi_2' \psi_2' \, dz\right]$$

$$\left[k_{59} \quad k_{5\,10}\right] = \left[k_{59}^{L} + A \int \bar{w}' \psi_2' \psi_3' \, dz \qquad -I_{xx} \int \bar{\theta} \psi_2'' \psi_3'' \, dz\right]$$

$$\left[k_{5\,11}\right] = \left[k_{5\,11}^{L} - I_{xx} \int \bar{v}'' \psi_2 \psi_3'' \, dz + 6 H_c \int \bar{\theta}' \psi_2' \psi_3' \, dz \right.$$
$$+ 4 H_c \int \bar{\theta}'' \psi_2' \psi_3 \, dz + 4 H_c \int \bar{\theta}' \psi_2'' \psi_3 \, dz$$
$$\left. + H_c \int \bar{\theta} \psi_2'' \psi_3' \, dz + H_c \int \bar{\theta}'' \psi_2 \psi_3' \, dz + A y_p \int \bar{w}' \psi_2' \psi_3' \, dz\right]$$

$$\left[K_{5\,12} \quad K_{5\,13}\right] = \left[K_{5\,12}^{L} + A \int \bar{w}' \psi_2' \psi_4' \, dz \qquad -I_{xx} \int \bar{\theta} \psi_2'' \psi_4'' \, dz\right]$$

$$\left[k_{5\,14}\right] = \left[k_{5\,14}^{L} - I_{xx} \int \bar{v}'' \psi_2 \psi_4'' \, dz + 6 H_c \int \bar{\theta}' \psi_2' \psi_4' \, dz \right.$$
$$+ 4 H_c \int \bar{\theta}'' \psi_2' \psi_4 \, dz + 4 H_c \int \bar{\theta}' \psi_2'' \psi_4 \, dz$$
$$\left. + H_c \int \bar{\theta} \psi_2'' \psi_4' \, dz + H_c \int \bar{\theta}'' \psi_2 \psi_4' \, dz + A y_p \int \bar{w}' \psi_2' \psi_4' \, dz\right]$$

$$\left[K_{61}\right] = \left[A\int(\bar{v}' + x_p\bar{\theta}'\ {}^{w}\psi_1'\psi_2'\,dz\right]$$

$$\left[k_{62}\quad k_{63}\right] = \left[I_{yy}\int\bar{\theta}\,\psi_2''\psi_1''\,dz \qquad k_{63}{}^{L} + A\int\bar{w}'\psi_2'\psi_1'\,dz\right]$$

$$\left[K_{64}\right] = \left[\underline{-H_c\int\psi_2''\psi_1'\,dz} + I_{yy}\int\bar{u}''\psi_2\psi_1''\,dz + 6H_s\int\bar{\theta}'\psi_2'\psi_1'\,dz\right.$$
$$+ 4H_s\int\bar{\theta}''\psi_2'\psi_1\,dz + 4H_s\int\bar{\theta}'\psi_2''\psi_1\,dz$$
$$\left.+ H_s\int\bar{\theta}\,\psi_2''\psi_1'\,dz + H_s\int\bar{\theta}''\psi_2\psi_1'\,dz - A\int\bar{w}'\psi_2'\psi_1'\,dz\right]$$

$$\left[K_{65}\quad K_{66}\right] = \left[I_{yy}\int\bar{\theta}\,\psi_2''\psi_2''\,dz \qquad k_{66}{}^{L} + A\int\bar{w}'\psi_2'\psi_2'\,dz\right]$$

$$\left[K_{67}\right] = \left[\underline{-H_c\int\psi_2''\psi_2'\,dz} + I_{yy}\int\bar{u}''\psi_2\psi_2''\,dz + 6H_s\int\bar{\theta}'\psi_2'\psi_2'\,dz\right.$$
$$+ 4H_s\int\bar{\theta}''\psi_2'\psi_2\,dz + 4\int\bar{\theta}'\psi_2''\psi_2\,dz$$
$$\left.+ H_s\int\bar{\theta}\,\psi_2''\psi_2'\,dz + H_s\int\bar{\theta}''\psi_2'\psi_2'\,dz - A\int\bar{w}'\psi_2'\psi_2'\,dz\right]$$

$$\left[K_{68}\right] = \left[A\int(\bar{v}' + x_p\bar{\theta}')\ {}^{w}\psi_2'\psi_2'\,dz\right]$$

$$\left[K_{69}\quad K_{610}\right] = \left[I_{yy}\int\bar{\theta}\,\psi_2''\psi_3''\,dz \qquad K_{610}{}^{L} + A\int\bar{w}'\psi_2'\psi_3'\,dz\right]$$

$$\left[K_{611}\right] = \left[\underline{-H_c\int\psi_2''\psi_3'\,dz} + I_{yy}\int\bar{u}''\psi_2\psi_3''\,dz + 6H_s\int\bar{\theta}'\psi_2'\psi_3'\,dz\right.$$
$$+ 4H_s\int\bar{\theta}''\psi_2'\psi_3\,dz + 4H_s\int\bar{\theta}'\psi_2''\psi_3\,dz$$
$$\left.+ H_s\int\bar{\theta}\,\psi_2''\psi_3'\,dz + H_s\int\bar{\theta}''\psi_2'\psi_3'\,dz - A\int\bar{w}'\psi_2'\psi_3'\,dz\right]$$

$$\left[K_{612}\quad K_{613}\right] = \left[I_{yy}\int\bar{\theta}\,\psi_2''\psi_4''\,dz \qquad k_{613}{}^{L} + A\int\bar{w}'\psi_2'\psi_4'\,dz\right]$$

$$\left[K_{614}\right] = \left[\underline{-H_c\int\psi_2''\psi_4'\,dz} + I_{yy}\int\bar{u}''\psi_2\psi_4''\,dz + 6H_s\int\bar{\theta}'\psi_2'\psi_4'\,dz\right.$$
$$+ 4H_s\int\bar{\theta}''\psi_2'\psi_4\,dz + 4H_s\int\bar{\theta}'\psi_2''\psi_4\,dz$$
$$\left.+ H_s\int\bar{\theta}\,\psi_2''\psi_4'\,dz + H_s\int\bar{\theta}''\psi_2'\psi_4' - A\int\bar{w}'\psi_2'\psi_4'\,dz\right]$$

$$[k_{7\,1}] = \left[A \int (y_p \bar{u}' - x_p \bar{v}')\, {}^{w}\psi_1' \psi_2'\, dz + A R_p^2 \int \bar{\theta}'\, {}^{w}\psi_1' \psi_2'\, dz\right]$$

$$[k_{7\,2}] = \left[-\underline{H_s \int \psi_2'' \psi_1'\, dz} + A y_p \int \bar{w}' \psi_2' \psi_1'\, dz - (I_{xx} - I_{yy}) \int \bar{v}'' \psi_2'' \psi_1\, dz \right.$$
$$\left. + H_c \int (\bar{\theta}' \psi_2' \psi_1' + \bar{\theta}'' \psi_2' \psi_1)\, dz - K_y I_{yy} \int \bar{\theta}' \psi_2'' \psi_1'\, dz\right]$$

$$[k_{7\,3}] = \left[\underline{H_c \int \psi_2'' \psi_1'\, dz} - A x_p \int \bar{w}' \psi_2' \psi_1'\, dz - (I_{xx} - I_{yy}) \int \bar{u}'' \psi_2'' \psi_1\, dz \right.$$
$$\left. + H_s \int (\bar{\theta}' \psi_2' \psi_1' + \bar{\theta}'' \psi_2' \psi_1)\, dz - K_x I_{xx} \int \bar{\theta}' \psi_2'' \psi_1'\, dz\right]$$

$$[k_{7\,4}] = \left[\underline{I_{\omega\omega} \int \psi_2'' \psi_1''\, dz} + \underline{JG \int \psi_2' \psi_1'\, dz} + A R_p^2 \int \bar{w}' \psi_2' \psi_1'\, dz \right.$$
$$+ H_c \int (\bar{u}' \psi_2' \psi_1' + \bar{u}' \psi_2'' \psi_1)\, dz - K_y I_{yy} \int \bar{u}'' \psi_2' \psi_1'\, dz$$
$$+ H_s \int (\bar{v}' \psi_2' \psi_1' + \bar{v}' \psi_2'' \psi_1)\, dz - K_x I_{xx} \int \bar{v}'' \psi_2' \psi_1'\, dz$$
$$\left. - K_\omega I_{\omega\omega} \int (\bar{\theta}'' \psi_2' \psi_1' + \bar{\theta}' \psi_2'' \psi_1')\, dz + 2 H_\phi \int \bar{\theta}' \psi_2' \psi_1'\, dz\right]$$

$$[k_{7\,5}] = \left[\underline{-H_s \int \psi_2'' \psi_2'\, dz} + A y_p \int \bar{w}' \psi_2' \psi_2'\, dz - (I_{xx} - I_{yy}) \int \bar{v}'' \psi_2'' \psi_2\, dz \right.$$
$$\left. + H_c \int (\bar{\theta}' \psi_2' \psi_2' + \bar{\theta}'' \psi_2' \psi_2)\, dz - K_y I_{yy} \int \bar{\theta}' \psi_2'' \psi_2'\, dz\right]$$

$$[k_{7\,6}] = \left[\underline{H_c \int \psi_2'' \psi_2'\, dz} - A x_p \int \bar{w}' \psi_2' \psi_2'\, dz - (I_{xx} - I_{yy}) \int \bar{u}'' \psi_2'' \psi_2\, dz \right.$$
$$\left. + H_s \int (\bar{\theta}' \psi_2' \psi_2' + \bar{\theta}'' \psi_2' \psi_2)\, dz - K_x I_{xx} \int \bar{\theta}' \psi_2'' \psi_2'\, dz\right]$$

$$[k_{7\,7}] = \left[\underline{I_{\omega\omega} \int \psi_2'' \psi_2''\, dz} + \underline{JG \int \psi_2' \psi_2'\, dz} + A R_p^2 \int \bar{w}' \psi_2' \psi_2'\, dz \right.$$
$$+ H_c \int (\bar{u}' \psi_2' \psi_2' + \bar{u}' \psi_2'' \psi_2)\, dz - K_y I_{yy} \int \bar{u}'' \psi_2' \psi_2'\, dz$$
$$+ H_s \int (\bar{v}' \psi_2' \psi_2' + \bar{v}' \psi_2'' \psi_2)\, dz - K_x I_{xx} \int \bar{v}'' \psi_2' \psi_2'\, dz$$
$$\left. - K_\omega I_{\omega\omega} \int (\bar{\theta}'' \psi_2' \psi_2' + \bar{\theta}' \psi_2'' \psi_2')\, dz + 2 H_\phi \int \bar{\theta}' \psi_2' \psi_2'\, dz\right]$$

$$[k_{T\,8}] = \left[A \int (y_p \bar{u}' - x_p \bar{v}')\, {}^{w}\psi_2' \psi_2'\, dz + A R_p^2 \int \bar{\theta}'\, {}^{w}\psi_2' \psi_2'\, dz \right]$$

$$[k_{T\,9}] = \left[\underline{-H_s \int \psi_2'' \psi_3'\, dz} + A y_p \int \bar{w}'\, \psi_2' \psi_3'\, dz - (I_{xx} - I_{yy}) \int \bar{v}''\, \psi_2'' \psi_3\, dz \right.$$
$$\left. + H_c \int (\bar{\theta}' \psi_2' \psi_3' + \bar{\theta}''\, \psi_2' \psi_3)\, dz - K_y I_{yy} \int \bar{\theta}'\, \psi_2'' \psi_3'\, dz \right]$$

$$[k_{T\,10}] = \left[\underline{H_c \int \psi_2'' \psi_3'\, dz} - A x_p \int \bar{w}'\, \psi_2' \psi_3'\, dz - (I_{xx} - I_{yy}) \int \bar{u}''\, \psi_2'' \psi_3\, dz \right.$$
$$\left. + H_s \int (\bar{\theta}\, \psi_2' \psi_3' + \bar{\theta}''\, \psi_2' \psi_3)\, dz - K_x I_{xx} \int \bar{\theta}'\, \psi_2'' \psi_3'\, dz \right]$$

$$[k_{T\,11}] = \left[\underline{I_{\omega\omega} \int \psi_2'' \psi_3''\, dz} + \underline{JG \int \psi_2' \psi_3'\, dz} + A R_p^2 \int \bar{w}'\, \psi_2' \psi_3'\, dz \right.$$
$$+ H_c \int (\bar{u}'\, \psi_2' \psi_3' + \bar{u}'\, \psi_2'' \psi_3)\, dz - K_y I_{yy} \int \bar{u}''\, \psi_2' \psi_3'\, dz$$
$$+ H_s \int (\bar{v}' \psi_2' \psi_3' + \bar{v}' \psi_2'' \psi_3)\, dz - K_x I_{xx} \int \bar{v}''\, \psi_2' \psi_3'\, dz$$
$$\left. - K_\omega I_{\omega\omega} \int (\bar{\theta}'' \psi_2' \psi_3' + \bar{\theta}'\, \psi_2'' \psi_3)\, dz + 2 H_\phi \int \bar{\theta}'\, \psi_2' \psi_3'\, dz \right]$$

$$[k_{T\,12}] = \left[\underline{-H_s \int \psi_2'' \psi_4'\, dz} + A y_p \int \bar{w}'\, \psi_2' \psi_4'\, dz - (I_{xx} - I_{yy}) \int \bar{v}''\, \psi_2'' \psi_4\, dz \right.$$
$$\left. + H_c \int (\bar{\theta}' \psi_2' \psi_4' + \bar{\theta}''\, \psi_2' \psi_4)\, dz - K_y I_{yy} \int \bar{\theta}'\, \psi_2'' \psi_4'\, dz \right]$$

$$[k_{T\,13}] = \left[\underline{H_c \int \psi_2'' \psi_4'\, dz} - A x_p \int \bar{w}'\, \psi_2' \psi_4'\, dz - (I_{xx} - I_{yy}) \int \bar{u}''\, \psi_2'' \psi_4\, dz \right.$$
$$\left. + H_s \int (\bar{\theta}'\, \psi_2' \psi_4' + \bar{\theta}''\, \psi_2' \psi_4)\, dz - K_x I_{xx} \int \bar{\theta}'\, \psi_2'' \psi_4'\, dz \right]$$

$$[k_{T\,14}] = \left[\underline{I_{\omega\omega} \int \psi_2'' \psi_4''\, dz} + \underline{JG \int \psi_2' \psi_4'\, dz} + A R_p^2 \int \bar{w}'\, \psi_2' \psi_4'\, dz \right.$$
$$+ H_c \int (\bar{u}'\, \psi_2' \psi_4' + \bar{u}'\, \psi_2'' \psi_4)\, dz - K_y I_{yy} \int \bar{u}''\, \psi_2' \psi_4'\, dz$$
$$+ H_s \int (\bar{v}' \psi_2' \psi_4' + \bar{v}'\, \psi_2'' \psi_4)\, dz - K_x I_{xx} \int \bar{v}''\, \psi_2' \psi_4'\, dz$$
$$\left. - K_\omega I_{\omega\omega} \int (\bar{\theta}'' \psi_2' \psi_4' + \bar{\theta}'\, \psi_2'' \psi_4')\, dz + 2 H_\phi \int \bar{\theta}' \psi_2' \psi_4'\, dz \right]$$

$$\begin{bmatrix} k_{81} & k_{82} & k_{83} & k_{84} & k_{85} & k_{86} & k_{87} \end{bmatrix} =$$

$$\begin{bmatrix} k_{81}^{L} & k_{82}^{L} & k_{83}^{L} & k_{84}^{L} & k_{85}^{L} & k_{86}^{L} & k_{87}^{L} \end{bmatrix}$$

$$\begin{bmatrix} k_{88} & k_{89} & k_{8\,10} & k_{8\,11} & k_{8\,12} & k_{8\,13} & k_{8\,14} \end{bmatrix} =$$

$$\begin{bmatrix} k_{88}^{L} & k_{89}^{L} & k_{8\,10}^{L} & k_{8\,11}^{L} & k_{8\,12}^{L} & k_{8\,13}^{L} & k_{8\,14}^{L} \end{bmatrix}$$

$$\left[k_{q1}\right] = \left[A\int(\bar{u}' + y_p\bar{\Phi}')^w\psi_1'\psi_3'\,dz\right]$$

$$\left[k_{q2}\quad k_{q3}\right] = \left[k_{q2}^{L} + A\int\bar{w}'\psi_3'\psi_1'\,dz \qquad -I_{xx}\int\bar{\Phi}\psi_3''\psi_1''\,dz\right]$$

$$\begin{aligned}\left[k_{q4}\right] = \Big[k_{q4}^{L} &- I_{xx}\int\bar{v}''\psi_3\psi_1''\,dz + 6H_c\int\bar{\Phi}'\psi_3'\psi_1'\,dz\\ &+ 4H_c\int\bar{\Phi}''\psi_3'\psi_1\,dz + 4H_c\int\bar{\Phi}'\psi_3''\psi_1\,dz\\ &+ H_c\int\bar{\Phi}\psi_3''\psi_1'\,dz + H_c\int\bar{\Phi}''\psi_3\psi_1'\,dz + A\,y_p\int\bar{w}'\psi_3'\psi_1'\,dz\Big]\end{aligned}$$

$$\left[k_{q5}\quad k_{q6}\right] = \left[k_{q5}^{L} + A\int\bar{w}'\psi_3'\psi_2'\,dz \qquad -I_{xx}\int\bar{\Phi}\psi_3''\psi_2''\,dz\right]$$

$$\begin{aligned}\left[k_{q7}\right] = \Big[k_{q7}^{L} &- I_{xx}\int\bar{v}''\psi_3\psi_2''\,dz + 6H_c\int\bar{\Phi}'\psi_3'\psi_2'\,dz\\ &+ 4H_c\int\bar{\Phi}''\psi_3'\psi_2\,dz + 4H_c\int\bar{\Phi}'\psi_3''\psi_2\,dz\\ &+ H_c\int\bar{\Phi}\psi_3''\psi_2'\,dz + H_c\int\bar{\Phi}''\psi_3\psi_2'\,dz + A\,y_p\int\bar{w}'\psi_3'\psi_2'\,dz\Big]\end{aligned}$$

$$\left[k_{q8}\right] = \left[A\int(\bar{u}' + y_p\bar{\Phi}')^w\psi_2'\psi_3'\,dz\right]$$

$$\left[k_{q9}\quad k_{q10}\right] = \left[k_{q9}^{L} + A\int\bar{w}'\psi_3'\psi_3'\,dz \qquad -I_{xx}\int\bar{\Phi}\psi_3'\psi_3''\,dz\right]$$

$$\begin{aligned}\left[k_{q11}\right] = \Big[k_{q11}^{L} &- I_{xx}\int\bar{v}''\psi_3\psi_3''\,dz + 6H_c\int\bar{\Phi}'\psi_3'\psi_3'\,dz\\ &+ 4H_c\int\bar{\Phi}''\psi_3'\psi_3\,dz + 4H_c\int\bar{\Phi}'\psi_3''\psi_3\,dz\\ &+ H_c\int\bar{\Phi}\psi_3''\psi_3'\,dz + H_c\int\bar{\Phi}''\psi_3\psi_3'\,dz + A\,y_p\int\bar{w}'\psi_3'\psi_3'\,dz\Big]\end{aligned}$$

$$\left[k_{q12}\quad k_{q13}\right] = \left[k_{q12}^{L} + A\int\bar{w}'\psi_3'\psi_4\,dz \qquad -I_{xx}\int\bar{\Phi}\psi_3''\psi_4''\,dz\right]$$

$$\begin{aligned}\left[k_{q14}\right] = \Big[k_{q14}^{L} &- I_{xx}\int\bar{v}''\psi_3\psi_4''\,dz + 6H_c\int\bar{\Phi}'\psi_3'\psi_4'\,dz\\ &+ 4H_c\int\bar{\Phi}''\psi_3'\psi_4\,dz + 4H_c\int\bar{\Phi}'\psi_3''\psi_4\,dz\\ &+ H_c\int\bar{\Phi}\psi_3''\psi_4'\,dz + H_c\int\bar{\Phi}''\psi_3\psi_4'\,dz + A\,y_p\int\bar{w}'\psi_3'\psi_4'\,dz\Big]\end{aligned}$$

$$\left[K_{10\,1}\right] = \left[A\int(\bar{v}' + x_p\bar{\theta}')\,{}^{w}\psi_1'\psi_3'\,dz\right]$$

$$\left[K_{10\,2}\quad K_{10\,3}\right] = \left[I_{yy}\int\bar{\theta}\psi_3''\psi_1''\,dz \qquad K_{10\,3}^{L} + A\int\bar{w}'\psi_3'\psi_1'\,dz\right]$$

$$\left[K_{10\,4}\right] = \left[-H_c\underline{\int\psi_3''\psi_1'\,dz} + I_{yy}\int\bar{u}''\psi_3\psi_1''\,dz + 6H_s\int\bar{\theta}'\psi_3'\psi_1'\,dz \right.$$
$$+ 4H_s\int\bar{\theta}''\psi_3'\psi_1\,dz + 4H_s\int\bar{\theta}'\psi_3''\psi_1\,dz$$
$$\left. + H_s\int\bar{\theta}\psi_3''\psi_1'\,dz + H_s\int\bar{\theta}''\psi_3'\psi_1'\,dz - A\int\bar{w}'\psi_3'\psi_1'\,dz\right]$$

$$\left[K_{10\,5}\quad K_{10\,6}\right] = \left[I_{yy}\int\bar{\theta}\psi_3''\psi_2''\,dz \qquad K_{10\,6}^{L} + A\int\bar{w}'\psi_3'\psi_2'\,dz\right]$$

$$\left[K_{10\,7}\right] = \left[-H_c\underline{\int\psi_3''\psi_2'\,dz} + I_{yy}\int\bar{u}''\psi_3\psi_2''\,dz + 6H_s\int\bar{\theta}'\psi_3'\psi_2'\,dz \right.$$
$$+ 4H_s\int\bar{\theta}''\psi_3'\psi_2\,dz + 4H_s\int\bar{\theta}'\psi_3''\psi_2\,dz$$
$$\left. + H_s\int\bar{\theta}\psi_3''\psi_2'\,dz + H_s\int\bar{\theta}''\psi_3'\psi_2'\,dz - A\int\bar{w}'\psi_3'\psi_2'\,dz\right]$$

$$\left[K_{10\,8}\right] = \left[A\int(\bar{v}' + x_p\bar{\theta}')\,{}^{w}\psi_2'\psi_3'\,dz\right]$$

$$\left[K_{10\,9}\quad K_{10\,10}\right] = \left[I_{yy}\int\bar{\theta}\psi_3''\psi_3''\,dz \qquad K_{10\,10}^{L} + A\int\bar{w}'\psi_3'\psi_3'\,dz\right]$$

$$\left[K_{10\,11}\right] = \left[-H_c\underline{\int\psi_3''\psi_3'\,dz} + I_{yy}\int\bar{u}''\psi_3\psi_3''\,dz + 6H_s\int\bar{\theta}'\psi_3'\psi_3'\,dz \right.$$
$$+ 4H_s\int\bar{\theta}''\psi_3'\psi_3\,dz + 4H_s\int\bar{\theta}'\psi_3''\psi_3\,dz$$
$$\left. + H_s\int\bar{\theta}\psi_3''\psi_3'\,dz + H_s\int\bar{\theta}''\psi_3'\psi_3'\,dz - A\int\bar{w}'\psi_3'\psi_3'\,dz\right]$$

$$\left[K_{10\,12}\quad K_{10\,13}\right] = \left[I_{yy}\int\bar{\theta}\psi_3''\psi_4''\,dz \qquad K_{10\,13}^{L} + A\int\bar{w}'\psi_3'\psi_4'\,dz\right]$$

$$\left[K_{10\,14}\right] = \left[-H_c\underline{\int\psi_3''\psi_4'\,dz} + I_{yy}\int\bar{u}''\psi_3\psi_4''\,dz + 6H_s\int\bar{\theta}'\psi_3'\psi_4'\,dz \right.$$
$$+ 4H_s\int\bar{\theta}''\psi_3'\psi_4\,dz + 4H_s\int\bar{\theta}'\psi_3''\psi_4\,dz$$
$$\left. + H_s\int\bar{\theta}\psi_3''\psi_4'\,dz + H_s\int\bar{\theta}''\psi_3'\psi_4'\,dz - A\int\bar{w}'\psi_3'\psi_4'\,dz\right]$$

$$[K_{11\,1}] = \left[A\int(y_p\bar{u}' - x_p\bar{v}')\,{}^{w}\psi_1'\psi_3'\,dz + A R_p^2\int\bar{\theta}'\,{}^{w}\psi_1'\psi_3'\,dz\right]$$

$$[K_{11\,2}] = \left[-H_s\int\psi_3''\psi_1'\,dz + A y_p\int\bar{w}'\psi_3'\psi_1'\,dz - (I_{xx}-I_{yy})\int\bar{v}''\psi_3''\psi_1\,dz + H_c\int(\bar{\theta}'\psi_3'\psi_1' + \bar{\theta}''\psi_3'\psi_1)\,dz - K_y I_{yy}\int\bar{\theta}'\psi_3''\psi_1'\,dz\right]$$

$$[K_{11\,3}] = \left[H_c\int\psi_3''\psi_1'\,dz - A x_p\int\bar{w}'\psi_3'\psi_1'\,dz - (I_{xx}-I_{yy})\int\bar{u}''\psi_3''\psi_1\,dz + H_s\int(\bar{\theta}'\psi_3'\psi_1' + \bar{\theta}''\psi_3'\psi_1)\,dz - K_x I_{xx}\int\bar{\theta}'\psi_3''\psi_1'\,dz\right]$$

$$[K_{11\,4}] = \left[I_{\omega\omega}\int\psi_3''\psi_1''\,dz + JG\int\psi_3'\psi_1'\,dz + A R_p^2\int\bar{w}'\psi_3'\psi_1'\,dz + H_c\int(\bar{u}'\psi_3'\psi_1' + \bar{u}'\psi_3''\psi_1)\,dz - K_y I_{yy}\int\bar{u}''\psi_3'\psi_1'\,dz + H_s\int(\bar{v}'\psi_3'\psi_1' + \bar{v}'\psi_3''\psi_1)\,dz - K_x I_{xx}\int\bar{v}''\psi_3'\psi_1'\,dz - K_\omega I_{\omega\omega}\int(\bar{\theta}''\psi_3'\psi_1' + \bar{\theta}'\psi_3''\psi_1')\,dz + 2H_\phi\int\bar{\theta}'\psi_3'\psi_1'\,dz\right]$$

$$[K_{11\,5}] = \left[-H_s\int\psi_3''\psi_2'\,dz + A y_p\int\bar{w}'\psi_3'\psi_2'\,dz - (I_{xx}-I_{yy})\int\bar{v}''\psi_3''\psi_2\,dz + H_c\int(\bar{\theta}'\psi_3'\psi_2' + \bar{\theta}''\psi_3'\psi_2)\,dz - K_y I_{yy}\int\bar{\theta}'\psi_3''\psi_2'\,dz\right]$$

$$[K_{11\,6}] = \left[H_c\int\psi_3''\psi_2'\,dz - A x_p\int\bar{w}'\psi_3'\psi_2'\,dz - (I_{xx}-I_{yy})\int\bar{u}''\psi_3''\psi_2\,dz + H_s\int(\bar{\theta}'\psi_3'\psi_2' + \bar{\theta}''\psi_3'\psi_2)\,dz - K_x I_{xx}\int\bar{\theta}'\psi_3''\psi_2'\,dz\right]$$

$$[K_{11\,7}] = \left[I_{\omega\omega}\int\psi_3''\psi_2''\,dz + JG\int\psi_3'\psi_2'\,dz + A R_p^2\int\bar{w}'\psi_3'\psi_2'\,dz + H_c\int(\bar{u}'\psi_3'\psi_2' + \bar{u}'\psi_3''\psi_2)\,dz - K_y I_{yy}\int\bar{u}''\psi_3'\psi_2'\,dz + H_s\int(\bar{v}'\psi_3'\psi_2' + \bar{v}'\psi_3''\psi_2)\,dz - K_x I_{xx}\int\bar{v}''\psi_3'\psi_2'\,dz - K_\omega I_{\omega\omega}\int(\bar{\theta}''\psi_3'\psi_2' + \bar{\theta}'\psi_3''\psi_2')\,dz + 2H_\phi\int\bar{\theta}'\psi_3'\psi_2'\,dz\right]$$

$$\left[K_{11\,8}\right] = \left[A\int(y_p\bar{u}' - x_p\bar{v}')\,{}^{w}\psi_2'\psi_3'\,dz + A R_p^2\int\bar{\phi}'\,{}^{w}\psi_2'\psi_3'\,dz\right]$$

$$\left[K_{11\,9}\right] = \left[-\underline{H_s\int\psi_3''\psi_3'\,dz} + A y_p\int\bar{w}'\psi_3'\psi_3'\,dz - (I_{xx}-I_{yy})\int\bar{v}''\psi_3'\psi_3\,dz + H_c\int(\bar{\phi}'\psi_3'\psi_3' + \bar{\phi}''\psi_3'\psi_3)\,dz - K_y I_{yy}\int\bar{\phi}'\psi_3''\psi_3'\,dz\right]$$

$$\left[K_{11\,10}\right] = \left[\underline{H_c\int\psi_3''\psi_3'\,dz} - A x_p\int\bar{w}'\psi_3'\psi_3'\,dz - (I_{xx}-I_{yy})\int\bar{u}''\psi_3''\psi_3\,dz + H_s\int(\bar{\phi}'\psi_3'\psi_3' + \bar{\phi}''\psi_3'\psi_3)\,dz - K_x I_{xx}\int\bar{\phi}'\psi_3''\psi_3'\,dz\right]$$

$$\left[K_{11\,11}\right] = \left[I_{ww}\underline{\int\psi_3''\psi_3''\,dz} + \underline{JG\int\psi_3'\psi_3'\,dz} + A R_p^2\int\bar{w}'\psi_3'\psi_3'\,dz + H_c\int(\bar{u}'\psi_3'\psi_3' + \bar{u}'\psi_3''\psi_3)\,dz - K_y I_{yy}\int\bar{u}''\psi_3'\psi_3'\,dz + H_s\int(\bar{v}'\psi_3'\psi_3' + \bar{v}'\psi_3''\psi_3)\,dz - K_x I_{xx}\int\bar{v}''\psi_3'\psi_3'\,dz - K_\omega I_{www}\int(\bar{\phi}''\psi_3'\psi_3' + \bar{\phi}'\psi_3''\psi_3')\,dz + 2H_\phi\int\bar{\phi}'\psi_3'\psi_3'\,dz\right]$$

$$\left[K_{11\,12}\right] = \left[-\underline{H_s\int\psi_3''\psi_4'\,dz} + A y_p\int\bar{w}'\psi_3'\psi_4'\,dz - (I_{xx}-I_{yy})\int\bar{v}''\psi_3''\psi_4\,dz + H_c\int(\bar{\phi}'\psi_3'\psi_4' + \bar{\phi}''\psi_3'\psi_4)\,dz - K_y I_{yy}\int\bar{\phi}'\psi_3''\psi_4'\,dz\right]$$

$$\left[K_{11\,13}\right] = \left[\underline{H_c\int\psi_3''\psi_4'\,dz} - A x_p\int\bar{w}'\psi_3'\psi_4'\,dz - (I_{xx}-I_{yy})\int\bar{u}''\psi_3''\psi_4\,dz + H_s\int(\bar{\phi}'\psi_3'\psi_4' + \bar{\phi}'\psi_3''\psi_4)\,dz - K_x I_{xx}\int\bar{\phi}'\psi_3''\psi_4'\,dz\right]$$

$$\left[K_{11\,14}\right] = \left[I_{ww}\underline{\int\psi_3''\psi_4''\,dz} + \underline{JG\int\psi_3'\psi_4'\,dz} + A R_p^2\int\bar{w}'\psi_3'\psi_4'\,dz + H_c\int(\bar{u}'\psi_3'\psi_4' + \bar{u}'\psi_3''\psi_4)\,dz - K_y I_{yy}\int\bar{u}''\psi_3'\psi_4'\,dz + H_s\int(\bar{v}'\psi_3'\psi_4' + \bar{v}'\psi_3''\psi_4)\,dz - K_x I_{xx}\int\bar{v}''\psi_3'\psi_4'\,dz - K_\omega I_{www}\int(\bar{\phi}''\psi_3'\psi_4' + \bar{\phi}'\psi_3''\psi_4')\,dz + 2H_\phi\int\bar{\phi}'\psi_3'\psi_4'\,dz\right]$$

$$\left[K_{12\,1}\right] \quad \left[A\int(\bar{u}' + y_p\bar{\Phi}')\,{}^{w}\psi_1'\psi_4'\,dz\right]$$

$$\left[K_{12\,2} \quad K_{12\,3}\right] \quad \left[K_{12\,2}^{L} + A\int\bar{w}'\psi_4'\psi_1'dz \qquad -I_{xx}\int\bar{\Phi}\psi_4''\psi_1''dz\right]$$

$$\left[K_{12\,4}\right] \quad \left[K_{12\,4}^{L} - I_{xx}\int\bar{v}''\psi_4\psi_1''dz + 6H_c\int\bar{\Phi}'\psi_4'\psi_1'dz \right.$$
$$+ 4H_c\int\bar{\Phi}''\psi_4'\psi_1\,dz + 4H_c\int\bar{\Phi}'\psi_4''\psi_1\,dz$$
$$\left. + H_c\int\bar{\Phi}\psi_4''\psi_1'dz + H_c\int\bar{\Phi}''\psi_4\psi_1'dz + A\,y_p\int\bar{w}'\psi_4'\psi_1'dz\right]$$

$$\left[K_{12\,5} \quad K_{12\,6}\right] \quad \left[K_{12\,5}^{L} + A\int\bar{w}'\psi_4'\psi_2'dz \qquad -I_{xx}\int\bar{\Phi}\psi_4''\psi_2''dz\right]$$

$$\left[K_{12\,7}\right] \quad \left[K_{12\,7}^{L} - I_{xx}\int\bar{v}''\psi_4\psi_2''dz + 6H_c\int\bar{\Phi}'\psi_4'\psi_2'dz \right.$$
$$+ 4H_c\int\bar{\Phi}''\psi_4'\psi_2\,dz + 4H_c\int\bar{\Phi}'\psi_4''\psi_2\,dz$$
$$\left. + H_c\int\bar{\Phi}\psi_4''\psi_2'dz + H_c\int\bar{\Phi}''\psi_4\psi_2'dz + A\,y_p\int\bar{w}'\psi_4'\psi_2'dz\right]$$

$$\left[K_{12\,8}\right] \quad \left[A\int(\bar{u}' + y_p\bar{\Phi}')\,{}^{w}\psi_2'\psi_4'\,dz\right]$$

$$\left[K_{12\,9} \quad K_{12\,10}\right] \quad \left[K_{12\,9}^{L} + A\int\bar{w}'\psi_4'\psi_3'dz \qquad -I_{xx}\int\bar{\Phi}\psi_4''\psi_3''dz\right]$$

$$\left[K_{12\,11}\right] \quad \left[K_{12\,11}^{L} - I_{xx}\int\bar{v}''\psi_4\psi_3''dz + 6H_c\int\bar{\Phi}'\psi_4'\psi_3'dz \right.$$
$$+ 4H_c\int\bar{\Phi}''\psi_4'\psi_3\,dz + 4H_c\int\bar{\Phi}'\psi_4''\psi_3\,dz$$
$$\left. + H_c\int\bar{\Phi}\psi_4''\psi_3'dz + H_c\int\bar{\Phi}''\psi_4\psi_3'dz + A\,y_p\int\bar{w}'\psi_4'\psi_3'dz\right]$$

$$\left[K_{12\,12} \quad K_{12\,13}\right] \quad \left[K_{12\,12}^{L} + A\int\bar{w}'\psi_4'\psi_4'dz \qquad -I_{xx}\int\bar{\Phi}\psi_4''\psi_4''dz\right]$$

$$\left[K_{12\,14}\right] \quad \left[K_{12\,14}^{L} - I_{xx}\int\bar{v}''\psi_4\psi_4''dz + 6H_c\int\bar{\Phi}'\psi_4'\psi_4'dz \right.$$
$$+ 4H_c\int\bar{\Phi}''\psi_4'\psi_4\,dz + 4H_c\int\bar{\Phi}'\psi_4''\psi_4\,dz$$
$$\left. + H_c\int\bar{\Phi}\psi_4''\psi_4'dz + H_c\int\bar{\Phi}''\psi_4\psi_4'dz + A\,y_p\int\bar{w}'\psi_4'\psi_4'dz\right]$$

$$\left[K_{13,1}\right] = \left[A\int(\bar{v}' + x_0\bar{\theta}')\ {}^{w}\psi_1'\psi_4'\,dz\right]$$

$$\left[K_{13,2}\quad K_{13,3}\right] = \left[I_{yy}\int\bar{\theta}\psi_4''\psi_1''\,dz \qquad k_{13,3}{}^{L} + A\int\bar{w}'\psi_4'\psi_1'\,dz\right]$$

$$\left[K_{13,4}\right] = \left[\underline{-H_c\int\psi_4''\psi_1'\,dz} + I_{yy}\int\bar{u}''\psi_4\psi_1''\,dz + 6H_s\int\bar{\theta}'\psi_4'\psi_1'\,dz \right.$$
$$+ 4H_s\int\bar{\theta}''\psi_4'\psi_1\,dz + 4H_s\int\bar{\theta}'\psi_4''\psi_1\,dz$$
$$\left. + H_s\int\bar{\theta}\psi_4''\psi_1'\,dz + H_s\int\bar{\theta}''\psi_4'\psi_1'\,dz - A\int\bar{w}'\psi_4'\psi_1'\,dz\right]$$

$$\left[K_{13,5}\quad K_{13,6}\right] = \left[I_{yy}\int\bar{\theta}\psi_4''\psi_2''\,dz \qquad k_{13,6}{}^{L} + A\int\bar{w}'\psi_4'\psi_2'\,dz\right]$$

$$\left[K_{13,7}\right] = \left[\underline{-H_c\int\psi_4''\psi_2'\,dz} + I_{yy}\int\bar{u}''\psi_4\psi_2''\,dz + 6H_s\int\bar{\theta}'\psi_4'\psi_2'\,dz \right.$$
$$+ 4H_s\int\bar{\theta}''\psi_4'\psi_2\,dz + 4H_s\int\bar{\theta}'\psi_4''\psi_2\,dz$$
$$\left. + H_s\int\bar{\theta}\psi_4''\psi_2'\,dz + H_s\int\bar{\theta}''\psi_4'\psi_2'\,dz - A\int\bar{w}'\psi_4'\psi_2'\,dz\right]$$

$$\left[K_{13,8}\right] = \left[A\int(\bar{v}' + x_0\bar{\theta}')\ {}^{w}\psi_2'\psi_4'\,dz\right]$$

$$\left[K_{13,9}\quad K_{13,10}\right] = \left[I_{yy}\int\bar{\theta}\psi_4''\psi_3''\,dz \qquad k_{13,10}{}^{L} + A\int\bar{w}'\psi_4'\psi_3'\,dz\right]$$

$$\left[K_{13,11}\right] = \left[\underline{-H_c\int\psi_4''\psi_3'\,dz} + I_{yy}\int\bar{u}''\psi_4\psi_3''\,dz + 6H_s\int\bar{\theta}'\psi_4'\psi_3'\,dz \right.$$
$$+ 4H_s\int\bar{\theta}''\psi_4'\psi_3\,dz + 4H_s\int\bar{\theta}'\psi_4''\psi_3\,dz$$
$$\left. + H_s\int\bar{\theta}\psi_4''\psi_3'\,dz + H_s\int\bar{\theta}''\psi_4'\psi_3'\,dz - A\int\bar{w}'\psi_4'\psi_3'\,dz\right]$$

$$\left[K_{13,12}\quad K_{13,13}\right] = \left[I_{yy}\int\bar{\theta}\psi_4''\psi_4''\,dz \qquad k_{13,13}{}^{L} + A\int\bar{w}'\psi_4'\psi_4'\,dz\right]$$

$$\left[K_{13,14}\right] = \left[\underline{-H_c\int\psi_4''\psi_4'\,dz} + I_{yy}\int\bar{u}''\psi_4\psi_4''\,dz + 6H_s\int\bar{\theta}'\psi_4'\psi_4'\,dz \right.$$
$$+ 4H_s\int\bar{\theta}''\psi_4'\psi_4\,dz + 4H_s\int\bar{\theta}''\psi_4'\psi_4\,dz$$
$$\left. + H_s\int\bar{\theta}\psi_4''\psi_4'\,dz + H_s\int\bar{\theta}''\psi_4'\psi_4'\,dz - A\int\bar{w}'\psi_4'\psi_4'\,dz\right]$$

$$[K_{14,1}] = \left[A \int (y_p \bar{u}' - x_p \bar{v}') \, \psi_1' \psi_4' \, dz + A R_p^2 \int \bar{\theta}' \psi' \psi_4' \, dz \right]$$

$$[K_{14,2}] = \left[-H_s \int \psi_4'' \psi_1' \, dz + A y_p \int \bar{w}' \psi_4' \psi_1' \, dz - (I_{xx} - I_{yy}) \int \bar{v}'' \psi_4'' \psi_1 \, dz \right.$$
$$\left. + H_c \int (\bar{\theta}' \psi_4' \psi_1' + \bar{\theta}'' \psi_4' \psi_1) \, dz - K_y I_{yy} \int \bar{\theta}' \psi_4'' \psi_1' \, dz \right]$$

$$[K_{14,3}] = \left[H_c \int \psi_4'' \psi_1' \, dz - A x_p \int \bar{w}' \psi_4' \psi_1' \, dz - (I_{xx} - I_{yy}) \int \bar{u}'' \psi_4'' \psi_1 \, dz \right.$$
$$\left. + H_s \int (\bar{\theta}' \psi_4' \psi_1' + \bar{\theta}'' \psi_4' \psi_1) \, dz - K_x I_{xx} \int \bar{\theta}' \psi_4'' \psi_1' \, dz \right]$$

$$[K_{14,4}] = \left[I_{\omega\omega} \int \psi_4'' \psi_1'' \, dz + JG \int \psi_4' \psi_1' \, dz + A R_p^2 \int \bar{w}' \psi_4' \psi_1' \, dz \right.$$
$$+ H_c \int (\bar{u}' \psi_4' \psi_1' + \bar{u}' \psi_4'' \psi_1) \, dz - K_y I_{yy} \int \bar{u}'' \psi_4' \psi_1' \, dz$$
$$+ H_s \int (\bar{v}' \psi_4' \psi_1' + \bar{v}' \psi_4'' \psi_1) \, dz - K_x I_{xx} \int \bar{v}'' \psi_4' \psi_1' \, dz$$
$$\left. - K_\omega I_{\omega\omega} \int (\bar{\theta}'' \psi_4' \psi_1' + \bar{\theta}' \psi_4'' \psi_1') \, dz + 2 H_\phi \int \bar{\theta}' \psi_4' \psi_1' \, dz \right]$$

$$[K_{14,5}] = \left[-H_s \int \psi_4'' \psi_2' \, dz + A y_p \int \bar{w}' \psi_4' \psi_2' \, dz - (I_{xx} - I_{yy}) \int \bar{v}'' \psi_4'' \psi_2 \, dz \right.$$
$$\left. + H_c \int (\bar{\theta}' \psi_4' \psi_2' + \bar{\theta}'' \psi_4' \psi_2) \, dz - K_y I_{yy} \int \bar{\theta}' \psi_4'' \psi_2' \, dz \right]$$

$$[K_{14,6}] = \left[H_c \int \psi_4'' \psi_2' \, dz \quad A x_p \int \bar{w}' \psi_4' \psi_2' \, dz - (I_{xx} - I_{yy}) \int \bar{u}'' \psi_4'' \psi_2 \, dz \right.$$
$$\left. + H_s \int (\bar{\theta}' \psi_4' \psi_2' + \bar{\theta}'' \psi_4' \psi_2) \, dz - K_x I_{xx} \int \bar{\theta}' \psi_4'' \psi_2' \, dz \right]$$

$$[K_{14,7}] = \left[I_{\omega\omega} \int \psi_4'' \psi_2'' \, dz + JG \int \psi_4' \psi_2' \, dz + A R_p^2 \int \bar{w}' \psi_4' \psi_2' \, dz \right.$$
$$+ H_c \int (\bar{u}' \psi_4' \psi_2' + \bar{u}' \psi_4'' \psi_2) \, dz - K_y I_{yy} \int \bar{u}'' \psi_4' \psi_2' \, dz$$
$$+ H_s \int (\bar{v}' \psi_4' \psi_2' + \bar{v}' \psi_4'' \psi_2) \, dz - K_x I_{xx} \int \bar{v}'' \psi_4' \psi_2' \, dz$$
$$\left. - K_\omega I_{\omega\omega} \int (\bar{\theta}'' \psi_4' \psi_2' + \bar{\theta}' \psi_4'' \psi_2') \, dz + 2 H_\phi \int \bar{\theta}' \psi_4' \psi_2' \, dz \right]$$

$$[k_{14\ 8}] \quad \left[A \int (y_p \bar{u}' - x_p \bar{v}') \, {}^{w}\psi_2' \psi_4' \, dz + A R_p^2 \int \bar{\theta}' \, {}^{w}\psi_2' \psi_4' \, dz \right]$$

$$[k_{14\ 9}] \quad \left[-H_s \int \psi_4'' \psi_3' \, dz + A y_p \int \bar{w}' \psi_4' \psi_3' \, dz - (I_{xx} - I_{yy}) \int \bar{v}'' \psi_4'' \psi_3 \, dz \right.$$
$$\left. + H_c \int (\bar{\theta}' \psi_4' \psi_3' + \bar{\theta}'' \psi_4' \psi_3) \, dz - K_y I_{yy} \int \bar{\theta}' \psi_4'' \psi_3' \, dz \right]$$

$$[k_{14\ 10}] \quad \left[H_c \int \psi_4'' \psi_3' \, dz + A x_p \int \bar{w}' \psi_4' \psi_3' \, dz - (I_{xx} - I_{yy}) \int \bar{u}'' \psi_4'' \psi_3 \, dz \right.$$
$$\left. + H_s \int (\bar{\theta}' \psi_4' \psi_3' + \bar{\theta}'' \psi_4' \psi_3) \, dz - K_x I_{xx} \int \bar{\theta}' \psi_4'' \psi_3' \, dz \right]$$

$$[k_{14\ 11}] \quad \left[I_{\omega\omega} \int \psi_4'' \psi_3'' \, dz + J G \int \psi_4' \psi_3' \, dz + A R_p^2 \int \bar{w}' \psi_4' \psi_3' \, dz \right.$$
$$+ H_c \int (\bar{u}' \psi_4' \psi_3' + \bar{u}' \psi_4'' \psi_3) \, dz - K_y I_{yy} \int \bar{u}'' \psi_4' \psi_3' \, dz$$
$$+ H_s \int (\bar{v}' \psi_4' \psi_3' + \bar{v}' \psi_4'' \psi_3) \, dz - K_x I_{xx} \int \bar{v}'' \psi_4' \psi_3' \, dz$$
$$\left. - K_\omega I_{\omega\omega} \int (\bar{\theta}'' \psi_4' \psi_3' + \bar{\theta}' \psi_4'' \psi_3') \, dz + 2 H_\phi \int \bar{\theta}' \psi_4' \psi_3' \, dz \right]$$

$$[k_{14\ 12}] \quad \left[-H_s \int \psi_4'' \psi_4' \, dz + A y_p \int \bar{w}' \psi_4' \psi_4' \, dz - (I_{xx} - I_{yy}) \int \bar{v}'' \psi_4'' \psi_4 \, dz \right.$$
$$\left. + H_c \int (\bar{\theta}' \psi_4' \psi_4' + \bar{\theta}'' \psi_4' \psi_4) \, dz - K_y I_{yy} \int \bar{\theta}' \psi_4'' \psi_4' \, dz \right]$$

$$[k_{14\ 13}] \quad \left[H_c \int \psi_4'' \psi_4' \, dz - A x_p \int \bar{w}' \psi_4' \psi_4' \, dz - (I_{xx} - I_{yy}) \int \bar{u}'' \psi_4'' \psi_4 \, dz \right.$$
$$\left. + H_s \int (\bar{\theta}' \psi_4' \psi_4' + \bar{\theta}'' \psi_4' \psi_4) \, dz - K_x I_{xx} \int \bar{\theta}' \psi_4'' \psi_4' \, dz \right]$$

$$[k_{14\ 14}] \quad \left[I_{\omega\omega} \int \psi_4'' \psi_4'' \, dz + J G \int \psi_4' \psi_4' \, dz + A R_p^2 \int \bar{w}' \psi_4' \psi_4' \, dz \right.$$
$$+ H_c \int (\bar{u}' \psi_4' \psi_4' + \bar{u}' \psi_4'' \psi_4) \, dz - K_y I_{yy} \int \bar{u}'' \psi_4' \psi_4' \, dz$$
$$+ H_s \int (\bar{v}' \psi_4' \psi_4' + \bar{v}' \psi_4'' \psi_4) \, dz - K_x I_{xx} \int \bar{v}'' \psi_4' \psi_4' \, dz$$
$$\left. - K_\omega I_{\omega\omega} \int (\bar{\theta}'' \psi_4' \psi_4' + \bar{\theta}' \psi_4'' \psi_4') \, dz + 2 H_\phi \int \bar{\theta}' \psi_4' \psi_4' \, dz \right]$$

BIBLIOGRAPHY

1. Bert, C. W., and Francis, P. H., "Composite Material Mechanics : Structural Mechanics", AIAA Journal, Volume 12, Sept 1974, pp. 1173-1186.

2. Vlasov, V. Z., "Novyi metod rascheta prizmaticheskikh balok iz tongostennykh profilei na sovmestnoe deistvie osevoi sily, izgiba i krucheniya" (A new method designing thin-walled prismatical shells for combined action of an axial force, bending and torsion) Vestnik VIA RKKA im. V.V. Kuibysheva 20 (2), 1936.

3. Vlasov, V. Z., Thin-Walled Elastic Rods (in Russian), Gos. Izdvo Stroit. Lit., Moscow-Leningard, 1940.

4. Vlasov, V. Z., Thin-walled Elastic Beams, Office of Technical Services, U.S. Department of Commerce, Washington 25, DC, TT-61-11400, 1961.

5. Bauld, N. R., and Tzeng, L. S., "A Vlasov Theory for Fiber-reinforced Beams with Thin-Walled Open Cross Sections", Int. J. Solids Structures, Volume 20, No. 3, 1984, pp. 277-294.

6. Love, A. E. H., A Treatise on the Mathematical Theory of Elasticity, Fourth Edition, Cambridge University Press, New York, 1944, pp. 3, 19, 365.

7. Michell, A. G. M., "Elastic Stability of Long Beams Under Transverse Forces", Philosophical Magazine, Volume 48, 1899, pp. 298.

8. Prandtl, L., Kipperscheinungen. "Ein Fall von Instabilem Gleichgewicht" Dissertion, Nurnberg, 1899.

9. Timoshenko, S., "Ob ustoichivosti ploskoi formy izgiba dvutavrovoi balki (On the stability in plane bending of an I-beam)" Izvestiya St. Petersburg Politekhnicheskogo instituta IV-V, 1905-1906.

10. v. Bach, C., "Versuche uber die tatsachliche Widerstandsfahigkeit von Balken", V.D.I-Zeitschrift, Volume 53, No. 41, 1909; Volume 54, No. 10, 1910.

11. Eggenschwyler, A., "Uber die Festigkeitsberechnung von Schiebetoren", Dissertion ETH-Zurich, 1921.

12. Maillart, R., "Zur Frage der Biegung", Schweizerische Bauzeitung, Volume 77, 1921, pp. 195-197.

13. Weber, C., "Ubertragung des Drehmomentes in Balken mit doppelflanschigem Querschnitt", Zeitschrift fur Angewandte Mathematik und Mechanik, Volume 6, 85, 1926.

14. Duncan, W. J., "The Torsion and Flexure of Cylinders and Tubes", Aero. Res. Comm. Lond. Rep. Mem., 1444, 1932.

15. Bernshtein, S. A., "Opytnoe issledovanie raboty verkhnego poyasa otkrytogo mosta" (Experimental study of the behavior of the upper chord of an open bridge) In: Sbornik "Issledovanie napryazhenii i deformatsii pri staticheskoi rabote mosta", No. 60, Transpechat', 1927.

16. Wagner, H., "Verdrehung und Knickung von offenen Profilen, Festschrift", Funfundzwanzig Jahre Technische Hoshschule Danzig, pp. 329, Kaferman, Danzig, 1929. (Translated in National Advisory Committee for Aeronautics, Tech. Memo. 807, 1936.)

17. Ostenfeld, A., Meddelse No. 5 Politecknisk Laeranstalt Laboratorium for Bygningsstatik, Kopenhagen, 1931.

18. Bleich, F., and Bleich, H., "Bending Torsion and Buckling of Bars Composed of Thin Walls", Preliminary Publication, 2nd Congress of Internatinal Association for Bridge and Structural Engineering, (English edition, pp. 871), Berlin, 1936.

19. Kappus, R., "Drillknicken Zentrisch Gedrueckter Staebe mit offenem Profil im elastischen Bereich" (Torsion and Flexure Buckling of open section elastic bars due to concentrated load), Lufo 14 9, 444-457, 1937. (Translated in National Advisory Committee for Aeronautics Tech. Memo. 851, 1938.)

20. Lundquist, E. E., and Fligg, C. M., "A Theory for Primary Failure for Straight Centrally Loaded Columns", Tech. Rept. 582, National Advisory Committee for Aeronautics, 1937.

21. Nowinski, J. L., "Theory of Thin-Walled Bars", Applied Mechanics Review, Volume 12, No. 4, April 1959, pp. 219.

22. Dzanelidze, G. J., "Variational Formulation of the Vlasov Theory of Thin-Walled Rods", (in Russian), Prikl. Math. Mekh., 7, 6, pp. 455-462, 1943.

23. Timoshenko, S., "Theory of Bending, Torsion and Buckling of Thin-Walled Members of Open Cross-section", J. Franklin Inst., Volume 239, No. 3, pp. 201-219; No. 4, pp. 249-268; No. 5, pp. 343-361, March 1945.

24. Gjelsvik, A., The Theory of Thin Walled Beams, Wiley, New York, 1981.

25. Kachanov, L. M., Buckling of Thin-walled Rods, University of Waterloo Press, 1983.

26. Murray, N. W., Introduction To The Theory Of Thin-Walled Structures, Oxford Engineering Series, Oxford University Press, New York, 1984.

27. Chwalla, E., "Die Kipp-Stabilitat Geader Trager mit Doppelt Symmetrischem I-Querschnitt", Forsch. Gebiete Stahlbaues, No. 2, Berlin, 1939.

28. Goodier, J. N., "The Buckling of Compressed Bars by Torsion and Flexure", Cornell University Engineering Experiment Station, Bulletin 27, 1941.

29. Goodier, J. N., "Flexural Torsional Buckling of Bars of Open Section Under Bending, Eccentric Thrust or Torsional Loads", Cornell University Engineering Experiment Station, Bulletin 27, 1942.

30. Kindem, S.E., "Biegung Drehung und Knickung Gerader Stabe mit offenem Profil im elastischen Bereich", Tapirs Forlag, Trondheim, 1949.

31. Timoshenko, S. P., History of Strength of Materials, McGraw-Hill, New York, 1953.

32. Umansky, A. A., Bending and Torsion Of Thin-Walled Aircraft Structures (in Russian), Oborongiz, Moscow, 1939.

33. Umansky, A. A., "Normal stress in torsion of aircraft wing", (in Russian) Tekhn. Vozd. Flota, No. 12, 1940.

34. Barta, T. A., "On the Torsional-Flexural Buckling of Thin-walled Elastic Bars with Monosymmetric open cross-section", In : Thin-walled Structures, Chilver, A. H., Ed., John Wiley & Sons, New York, 1967.

35. Lee, G. C., "A Survey of the Literature on the Lateral Instability of Beams", Welding Research Council Bulletin, No. 63 (Aug), 1960.

36. Timoshenko, S. P., and Woinowsky-Krieger, S., Theory of Plates and Shells, McGraw-Hill, New York, 1959.

37. Pister, K. S., and Dong, S. B., "Elastic Bending of Layered Plates", J. Eng. Mech. Div., ASCE, October, 1959, pp. 1-10.

38. Reissner, E., and Stavsky, Y., "Bending and Stretching of Certain Types of Heterogeneous Aeolotropic Elastic Plates", J. Appl. Mech., September, 1961, pp. 402-408.

39. Ambartsumyan, S. A., Theory of Anisotropic Plates, Technomic Publishing Co., 1973.

40. Ashton, J. E., and Whitney, J. M., Theory of Laminated Plates, Technomic Publishing Co., 1970.

41. Lekhnitskii, S. G., Theory of Elasticity of An Anisotropic Elastic Body, Holden-Day Publishers, 1963.

42. Dong, S. B., Pister, K. S., and Taylor, R. L., "On the Theory of Laminated Anisotropic Shells and Plates", Journal of Aerospace Sciences, August 1962, pp. 969-975.

43. Ambartsumyan, S. A., "Theory of Anisotropic Shells", NASA TT F-118, May 1964.

44. Jones, R. M., Mechanics of Composite Materials, McGraw-Hill, New York, 1975.

45. Davies, G. A. O., Virtual Work in Structural Analysis, Wiley, London, 1982.

46. Flugge, W., Stresses in Shells, Second Edition, Springer-Verlag, New York, 1966.

47. Timoshenko, S. P., and Gere, J. M., Theory of Elastic Stability, McGraw-Hill, New York, 1961.

48. Brush, D. O. and Almroth, B. O., Buckling of Bars, Plates, and Shells, McGraw-Hill, New York, 1975.

49. Reddy, J. N., An Introduction to the Finite Element Method, McGraw-Hill, New York, 1984.

50. Oden, J. T., Finite Elements of Non-linear Continua, McGraw-Hill, New York, 1972.

51. Weaver, W. J., and Johnson, P. R., Finite Elements for Structural Analysis, Prentice-Hall, 1984.

52. Tyahla S. T., "Failure and Crippling of Graphite-Epoxy Stiffeners Loaded in Compression", Masters Thesis, Department of Aerospace and Ocean Engineering, Virginia Polytechnic Institute and State University, 1984.

53. Chailleux, A., Hans, Y., and Verchery, G., "Experimental Study of the Buckling of Laminated Composite Columns and Plates", Int. J. Mech. Sci., Volume 17, 1975, pp. 489-498.

54. Lee, D. J., and Hewson, P. J., "The Use of Fibre-Reinforced Plastics in Thin-Walled Structures", in Stability Problems in

Engineering Structures and Composites , ed. Richards, T. H., and Stanley, P., Applied Science Publishers, Ltd., London, 1979.

55. Lentini, M., and Pereyra, V., "An Adaptive Finite Difference Solver for Nonlinear Two Point Boundary Value Problem with Mild Boundary Layers", SIAM Journal of Numerical Analysis, Volume 14, 1977, pp. 91-111.

The vita has been removed from the scanned document